NASA-CR-159552
19790016202

NASA CR-159552

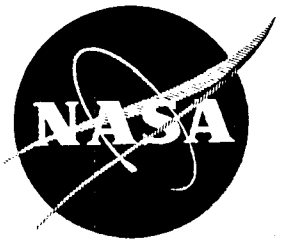

Development of Procedures for Calculating Stiffness and Damping of Elastomers in Engineering Applications

Part V. Elastomer Performance Limits and the Design and Test of an Elastomer Damper

by J. A. Tecza, M. S. Darlow, A. J. Smalley

Mechanical Technology Incorporated

prepared for
National Aeronautics and Space Administration

NASA Lewis Research Center
Contract NAS 3-18546

1. Report No.	2. Government Accession No.	3. Recipient's Catalog No.
NASA CR-159552		

4. Title and Subtitle	5. Report Date
DEVELOPMENT OF PROCEDURES FOR CALCULATING STIFFNESS AND DAMPING OF ELASTOMERS IN ENGINEERING APPLICATIONS. PART V - ELASTOMER PERFORMANCE LIMITS AND THE DESIGN AND TEST OF AN ELASTOMER DAMPER	February, 1979
	6. Performing Organization Code 79TR30

7. Author(s)	8. Performing Organization Report No.
J. A. Tecza, M. S. Darlow, A. J. Smalley	
	10. Work Unit No.

9. Performing Organization Name and Address	11. Contract or Grant No.
Mechanical Technology Incorporated 968 Albany-Shaker Road Latham, New York 12110	NAS3-18546
	13. Type of Report and Period Covered
12. Sponsoring Agency Name and Address	Contractor Report
National Aeronautics and Space Administration Washington, D. C. 20546	14. Sponsoring Agency Code

15. Supplementary Notes

Data Report

16. Abstract

Tests have been performed on elastomer specimens of the material polybutadiene to determine the performance limitations imposed by strain, temperature, and frequency. Three specimens were tested: a shear specimen, a compression specimen, and a second compression specimen in which thermocouples were embedded in the elastomer buttons. Stiffness and damping were determined from all tests, and internal temperatures were recorded for the instrumented compression specimen. Ambient temperatures investigated were 32°C, 66°C and 80°C. Strains investigated covered the range from .0005 to .08. These tests were performed using the base excitation resonant mass method. Measured results are presented together with comparisons between predictions of a thermo-viscoelastic analysis and the measured results.

Based on previously developed elastomer technology, elastomer dampers were designed to control the vibrations of a high-speed flexible rotor which dynamically simulated the power turbine and drive shaft of an advanced gas turbine engine. Dampers of polybutadiene and Viton were designed and built. The rotor was tested through two critical speeds. Vibration measurements were made and sensitivity of vibration to change in unbalance was also determined. Values for log decrement were extracted from the synchronous response curves. Comparisons were made between measured sensitivity to unbalance and log decrement and predicted values for these quantities.

17. Key Words (Suggested by Author(s))		18. Distribution Statement
Viscoelasticity Elastomers Dynamic Properties Damping Vibrations	Critical Speeds Resonance Testing Gas Turbine Strain Effects	Unclassified - Unlimited N79-24373#

19. Security Classif. (of this report)	20. Security Classif. (of this page)	21. No. of Pages	22. Price*
Unclassified	Unclassified	153	

* For sale by the National Technical Information Service, Springfield, Virginia 22161

FOREWORD

This report presents the work performed under NASA contract NAS3-18546 in the period April, 1977 to April, 1978, with Mr. Robert E. Cunningham, NASA Lewis Research Center as project manager. It is the fifth in a series of reports on the development of procedures for calculating stiffness and damping properties of elastomers in engineering applications. The program manager for MTI was Dr. A.J. Smalley. Principal investigator for the performance limits portion was Mr. M.S. Darlow. Principal investigator for the elastomer damper design was Mr. J.A. Tecza.

TABLE OF CONTENTS

SECTION		PAGE
	FOREWORD	iii
	LIST OF FIGURES	vii
	LIST OF TABLES	xi
I.	SUMMARY	1
II.	INTRODUCTION	3
III.	TEST PROGRAM - ELASTOMER PERFORMANCE LIMITS	5
	A. Test Plan	7
	B. Test Procedure	9
IV.	TEST RESULTS - ELASTOMER PERFORMANCE LIMITS	11
	A. Test Results for Instrumented Compression Specimen	12
	B. Comparison of Measured and Predicted Dynamic Characteristics	13
V.	DISCUSSION - ELASTOMER PERFORMANCE LIMITS	17
VI.	DESIGN OF ELASTOMER DAMPER FOR TEST ROTOR	21
	A. Test Rig Mathematical Model	21
	B. Support Optimization	21
	C. Response Analysis	25
	D. Elastomer Suspension Design	25
	E. Test Rig Assembly	29
	F. Summary of Design Procedure	29
VII.	TEST RESULTS - ELASTOMER MOUNTED TEST ROTOR	31
	A. Instrumentation and Test Plan	31
	B. Data Reduction Plan	31
	C. Test Results	32
	D. Frequency Spectrum and Shaft Orbits	37
VIII.	CONCLUSIONS AND RECOMMENDATIONS	39
	A. Conclusions from Performance Limits Tests	39
	B. Conclusions from Design and Testing of an Elastomer Damper	39
	C. Recommendations	40
	APPENDIX A: PROPERTIES OF POLYBUTADIENE MATERIAL NICHOLLS NEX 156G	41
	A. Introduction	41
	B. Thermal Conductivity	41
	C. Coefficient of Thermal Expansion	41
	D. Specific Heat and Tg	42
	E. Ts by Iterative Determination	42
	F. Chemical Analysis	43
	G. Summary of Properties, Nicholls NEX 156G	44
	H. Discussion	44

TABLE OF CONTENTS (Cont'd)

SECTION		PAGE
APPENDIX B:	TABULATION OF TEMPERATURE RESULTS FOR INSTRUMENTED COMPRESSION SPECIMENS.	47
APPENDIX C:	RUN LOG - TEST OF ELASTOMER MOUNTED ROTOR . . .	57
REFERENCES		61

LIST OF FIGURES

NUMBER		PAGE
1	Schematic of Elastomer Test Rig Showing All Components	63
2	View of Shake-Table-Mounted Elastomer Test Rig with Preload Cylinder and Small Mass.	64
3	Schematic of Data Acquisition for Measurement of Elastomer Dynamic Properties	65
4	Test Assembly of Four Elastomer Shear Specimens, Each 2.54 Centimeters (1.0 in.) High.	66
5	Compression Test Sample Without Instrumentation.	67
6	Location of Accelerometers and Thermocouples External to the Elastomer in the Instrumented Compression Test Specimen.	68
7	Location of Imbedded Thermocouples in Instrumented Compression Specimen	69
8	Location of Thermocouples Imbedded in Elastomer Elements for Instrumented Compression Test Specimen	70
9	Stiffness and Loss Coefficient vs. Strain. Shear Specimen, 32°C .	71
10	Stiffness and Loss Coefficient vs. Frequency. Shear Specimen, 32°C	72
11	Stiffness and Loss Coefficient vs. Strain. Shear Specimen, 66°C .	73
12	Stiffness and Loss Coefficient vs. Frequency. Shear Specimen, 66°C	74
13	Stiffness and Loss Coefficient vs. Strain. Shear Specimen, 80°C .	75
14	Stiffness and Loss Coefficient vs. Frequency. Shear Specimen, 80°C	76
15	Stiffness and Loss Coefficient vs. Strain. Compression Specimen, 32°C	77
16	Stiffness and Loss Coefficient vs. Frequency. Compression Specimen, 32°C	78
17	Stiffness and Loss Coefficient vs. Strain. Compression Specimen, 66°C	79
18	Stiffness and Loss Coefficient vs. Frequency. Compression Specimen, 66°C	80
19	Stiffness and Loss Coefficient vs. Strain. Compression Specimen, 80°C	81
20	Stiffness and Loss Coefficient vs. Frequency. Compression Specimen, 80°C	82
21	Stiffness and Damping vs. Frequency. Low Strain ($\varepsilon \simeq .001$), Shear Specimen, 32°C	83

LIST OF FIGURES (Cont'd)

NUMBER		PAGE
22	Stiffness and Damping vs. Frequency. Low Strain ($\varepsilon \simeq .0008$), Shear Specimen, 66°C	84
23	Stiffness and Damping vs. Frequency. Low Strain ($\varepsilon \simeq .0008$), Shear Specimen, 80°C	85
24	Stiffness and Loss Coefficient vs. Strain. Temperature Instrumented Compression Specimen Test Results, 32°C	86
25	Peak Temperature vs. Strain. Compression Specimen	87
26	Center Line Temperature Profiles. Compression Specimen, 200 Hz, 32°C Ambient Temperature	88
27	Center Line Temperature Profiles. Compression Specimen, 300 Hz, 32°C Ambient Temperature	89
28	Center Line Temperature Profiles. Compression Specimen, 450 Hz, 32°C Ambient Temperature	90
29	Center Line Temperature Profiles. Compression Specimen, 600 Hz, 32°C Ambient Temperature	91
30	Stiffness and Loss Coefficient vs. Strain. Comparison of Predicted and Measured Results, Shear Specimen	92
31	Stiffness and Loss Coefficient vs. Strain. Comparison of Predicted and Measured Results, Compression Specimen 32°C.	93
32	Peak Temperature vs. Strain. Comparison of Prediction and Measurement Results, Compression Specimen, 200 Hz.	94
33	Peak Temperature vs. Strain. Comparison of Prediction and Measurement Results, Compression Specimen.	95
34	Ratio of Stiffness at Finite Strain to Stiffness at .001 Strain as a Function of Dynamic Strain. Shear and Compression Specimens, 32°C, 66°C and 80°C	96
35	Loss Coefficient vs. Dynamic Strain. Shear and Compression Specimens, 32°C, 66°C, and 80°C.	97
36	Photo of Test Rotor During Assembly.	98
37	Test Rotor Schematic Diagram	99
38	Elastomer Damper Test Rig. Log Decrement as a Function of Elastomer Damping.	100
39	Damping Coefficient as a Function of Loss Coefficient.	101
40	Disc Unbalance. Sensitivity to Weight at Disc for Polybutadiene Mounts	102
41	Shaft Unbalance. Sensitivity to Weight at Shaft for Polybutadiene Mounts	103

LIST OF FIGURES (Cont'd)

NUMBER		PAGE
42	Disc Unbalance. Sensitivity to Weight on Disc for Viton-70 Mounts	104
43	Shaft Unbalance. Sensitivity to Weight on Shaft for Viton-70 Mounts	105
44	Method of Supporting Test Rig Rotor on Elastomers	106
45	Support Geometry and Button Deformation for Stiffness Calculations.	107
46	Plot of Support Stiffness vs. Button Diameter for Viton-70 at 32°C.	108
47	Plot of Support Stiffness vs. Button Diameter for Viton at 50°C	109
48	Plot of Support Stiffness vs. Button Diameter for Polybutadiene at 32°C	110
49	Plot of Support Stiffness vs. Button Diameter for Polybutadiene at 50°C	111
50	Detail View of Elastomer Cartridge During Assembly.	112
51	Elastomer Damper Rig, Pedestals, and Bearing Housing.	113
52	Partially Assembled Disc, Bearing Housing and Pedestal.	114
53	Side View of Assembled Test Rig	115
54	Front View of Assembled Test Rig.	116
55	Close-up of Turbine in Bearing Housing Showing Elastomer Cartridges at 12 noon and 4:00 Positions.	117
56	Schematic Drawing of Rotor System Showing Weight Addition Planes and Displacement Probe Locations	118
57	Installation of Unbalance Weight on the Test Rig Shaft.	119
58	Effect of Disc Unbalance With Polybutadiene Dampers	120
59	Effect of Shaft Unbalance With Polybutadiene Dampers.	121
60	Effect of Disc Unbalance With Viton Dampers	122
61	Effect of Shaft Unbalance With Viton Dampers.	123
62	Sensitivity of Test Rig to Unbalance.	124
63	Repeatability of Elastomer Mounted Rotor Running to and from Speed	125
64	Response at the Disc to Disc Unbalance for the Hard-Mounted Rotor.	126
65	Response at the Shaft to Disc Unbalance, for the Hard-Mounted Rotor.	127

LIST OF FIGURES (Cont'd)

NUMBER		PAGE
66	Effect of Using Viton Damper Cartridges at the Turbine End Only .	128
67	Spectrum Analyses of Output From Disc and Turbine Probes.	129
68	Disc Orbit Photos Through First Critical With Unbalance in Disc .	130
69	Shaft Orbit Photos Through Second Critical With Unbalance in Shaft.	131
A-1	Thermal Conductivity Versus Temperature Nicholls NEX 156G	132
A-2	Specific Heat Versus Temperature Nicholls NEX 156G D.S.C.	133
A-3	Log α_T Versus Temperature Nicholls NEX 156G	134
A-4	Corrected Complex Compression Modulus Versus Frequency. Master Curve, Nicholls NEX 156G	135

LIST OF TABLES

NUMBER		PAGE
1	Test Plan for Elastomer Performance Limits	7
2	Frequency and Strain Combinations to be Tested	8
3	Values of Strain and Actual Amplitudes	8
4	Frequency Values	9
5	Shear Modulus Coefficients	12
6	Test Rotor Mathematical Model	22
7	Damped Natural Frequency and Log Decrement as a Function of Bearing Support Stiffness and Damping	23
8	Damping Coefficients for an Elastomer with a Loss Coefficient of Unity	24
9	Comparison of Mode 2 Log Decrement for Polybutadiene and Viton-70 with Optimum Damping	24
10	Computed Values of Critical Speed and Sensitivity to Unbalance	25
11	Values of Shear Modulus G' at 2000 Radians/Second	28
12	Stiffness Values to be Used in Finding Button Diameters	28
13	Button Diameters to Achieve a 100,000 LB/IN. Radial Stiffness	29
14	Summary of Weights Used to Unbalance the Test Rig Disc and Shaft	33
15	Locations of Critical Speeds for Different Elastomer Supports	33
16	Sensitivity of Test Rig to Unbalance	34
17	Measured Values of Log Decrement for Polybutadiene and Viton	35
18	Average Values for Log Decrement and Amplification Factor	36
19	Speeds and Maximum Amplitude of Shaft Orbits	38

SECTION I

SUMMARY

A program has been undertaken to determine the effects of strain on elastomer damper performance and the implications of these effects in design, using polybutadiene as a test material. A program has also been undertaken to design and test an elastomer damper for control of flexible rotor vibration.

Strain effects were investigated in three test specimens: A shear specimen, a compression specimen, and a compression specimen with thermocouples embedded at various locations in the elastomer buttons. Strain has been shown to reduce stiffness by a factor of up to 3 over the range of strains tested, and to increase loss coefficient by a factor of 2.5. It has been conclusively shown that thermal effects are only a partial contributor to the effects of strain.

The problems of establishing a generalized deterministic predictive method accounting for strain are identified. However, steps are outlined whereby the influence of strain effects can be accounted for in design of systems in which elastomers are employed to control vibrations. A thermo-viscoelastic predictive method is shown to provide satisfactory, conservative, definitions of limiting operational amplitudes to avoid excessive internal temperatures.

Two alternative dampers are designed for controlling vibration in a high-speed (25,000 rpm) flexible rotor, one of Viton-70 and one of polybutadiene. Both designs were built and tested. Response to synchronous (unbalance) excitation at two bending criticals was measured and compared to predictions. System log decrement was also measured in two ways and again was compared to prediction. In all cases the elastomer was more effective than predicted in controlling system vibrations and the measured value of system log decrement was higher than predicted. The Viton-70 damper, which had a higher loss coefficient, was in all cases more effective in controlling system vibrations, and had a higher log decrement, than the polybutadiene damper.

SECTION II

INTRODUCTION

Damped bearing supports are seeing increasing application as a means of controlling rotationally excited vibrations in high-speed rotating machinery. Examples can be found in aircraft gas turbines, high-performance compressors, and flexible power transmission shafting. The damper most commonly used in these applications is the squeeze film damper, often in parallel with some type of mechanical flexure.

Elastomer dampers are an attractive alternative to the squeeze film damper because of their simplicity, their inherent combination of stiffness and damping, their compactness, and their lack of need for seals or oil supply. Because of these advantages they are presently being considered for low cost, limited life, engine applications and for helicopter transmission shafting.

Factors which have resisted the growth and application of elastomer dampers are the limited availability of design-oriented data on their dynamic behavior, and concern about the effects of environment including temperature, vibration amplitude and the presence of oil or other fluids. For several years a program has been pursued at MTI whose intent is to quantify dynamic performance of elastomer dampers, to provide the capability to design for desired characteristics, to evaluate the effects of environment, to demonstrate the effectiveness of elastomers in vibration control for high-speed rotating machinery, and to evaluate any problems which may be encountered in their application to rotating machinery vibration control. References 2, 3, 4, and 5 document previous efforts under this program.

Under this program a powerful test method for determining elastomer component properties has been developed entitled "The Base Excitation Resonant Mass Method". This test method employs a large electromagnetic shaker on which test specimens are mounted. The test specimens comprise a one degree of freedom spring mass damper system in which a variable mass is excited at or near the resonant frequency of that mass mounted on an elastomeric spring. Transmissibility and phase angle across the elastomer spring are measured and, in the region of resonance, allow accurate determination of both stiffness and damping.

Under past test programs the effects of excitation frequency, specimen geometry, environmental temperature, dynamic strain and material have been tested. Empirical approaches to predicting component properties have evolved and their effectiveness has been evaluated under both translatory and rotating excitation.

Clear evidence of the importance of dynamic strain has been obtained in past tests. Further, it has been tentatively concluded, for elastomers in the rubbery region, such as polybutadiene, that dynamic characteristics show a more consistent dependence on strain than on frequency. Part of the work reported herein is directed at a more intensive evaluation of the effects of strain on the dynamic characteristics of the elastomer polybutadiene, and of the implications of these effects on design. Included in this evaluation are, firstly, an attempt to delineate the contribution of self heating to changes in dynamic characteristics under large strains; secondly, an evaluation of the extent of the strain regime under which the dynamic characteristics can be considered strain independent; and thirdly, a further evaluation of strain as an effective independent variable for characterization of elastomer dampers.

To this end strain and temperature effects were investigated both under shear and compression loading. Under compression loading, two specimens were tested: one with thermocouples embedded only in the metal fixtures and the second with additional thermocouples embedded at selected points in the elastomer elements themselves. These two compression test specimens will be referred to as the uninstrumented and the instrumented specimens, respectively. For both the uninstrumented compression specimen and the shear specimen (also uninstrumented) a full combination of three ambient temperatures, ten strains and ten frequency values were investigated. For the instrumented specimen, investigations were limited to one ambient temperature. Stiffness, damping, and temperature values were recorded at each test condition.

As will be shown, under all conditions strain has a strong influence and, for the material tested, strain provides better unification of the data than frequency. Comparisons were made between the measured data and the predictions of a thermo-viscoelastic analysis. These comparisons made clear that effects other than self heating have a significant influence on the variation of dynamic stiffness and damping with dynamic strain.

In parallel with these elastomer characterization tests, previously developed technology was applied in the design and testing of an elastomer damper for control of high-speed rotor vibrations. As opposed to a vibration absorber or shock mount applications where an entire machine is elastomerically mounted, in this application the elastomeric damper serves as a flexible damped pedestal to each bearing. The elastomers are intimately connected with the dynamics of the flexible rotor bearing system and heavily influence its dynamic behavior.

The rotor bearing system chosen for this application was a rotor designed to simulate closely the dynamics of a power turbine and drive shaft of an advanced gas turbine engine (ref. 1). The rotor has two bending critical speeds in its operating speed range. In its original configuration this rotor was exceedingly difficult to balance. For this reason, and the fact that it closely simulates one of the possible applications for elastomer dampers, this rotor was considered a good critical test for the first application of elastomeric bearing mounts under this program.

The program to design and test an elastomer damper had the following objectives:

- Redesign the test rotor support system to incorporate elastomeric damped pedestals.
- Design the elastomer supports themselves to effectively control rotor response amplitude through the speed range.
- Measure the damping actually present in the rotor bearing system by running the rig through two bending critical speeds.
- Perform the tests with two types of elastomers representing materials with both high and low internal damping to cover the reasonable extremes of elastomer capability.

The project was successful in meeting these objectives, clearly demonstrating the effectiveness of elastomer mounts to control response to unbalance, and of the technology to support design of elastomeric mounts for this purpose.

The following sections of this report describe in detail both the tests to characterize further the effect of frequency, temperature, and strain (referred to as performance limits), and the program to design and test an elastomer damper for control of high-speed rotor vibration.

SECTION III

TEST PROGRAM - ELASTOMER PERFORMANCE LIMITS

The investigation of effects of strain, ambient temperature, and frequency on elastomer component properties was executed using the Base Excitation Resonant Mass test method. This test method was developed under preceding phases of the program and the details are provided in references 2, 3 and 4. For comprehensiveness, a brief description of the method will be provided here.

The Base Excitation Resonant Mass test method employs a large electromagnetic shaker to apply base excitation to a one degree-of-freedom spring-mass-damper system. The elastomer test elements form the spring and damper upon which a rigid mass is supported whose magnitude can be varied over a wide range. The response of the supported mass is a function of the input excitation and the dynamic characteristic of the spring mass damper system. Accelerometers are used to measure the shaker excitation and the response of the mass. A tracking filter, phase meter, and digital voltmeter are employed to determine the amplitude of the input excitation, the amplitude of the response component at the same frequency as the input excitation, and the phase angle between input excitation and response. Amplitude across the test specimen is a controlled, independent, variable which is measured by a capacitance probe.

A computerized data acquisition system acquires amplitude and phase information for one input accelerometer and three output accelerometers mounted on the resonant mass and from the capacitance displacement probe. In addition, temperature values are acquired via a computer controlled scanner from as many as twenty different thermocouples at various locations in the test speciment. Data is acquired over a range of frequencies for which resonant or near resonant behavior is observed. The criterion normally employed is that the phase angle should lie between 15° and 165°. A wide range of test frequencies is achieved by varying the supported mass and acquiring data satisfying this criterion for each mass tested.

Data reduction software determines the transmissibility between input excitation and response and, from this quantity and the phase angle, stiffness and damping of the elastomer test specimen are readily calculated. Other quantities calculated include the amplitude across the elastomer and the energy dissipation per unit volume. The operator is provided with an immediate printout of stiffness, damping, strain, dissipation and temperature values as each test point is completed. These quantities can be reviewed for consistency and the point rejected or preserved. Preserved data is stored on a disk and is available for a subsequent summary printout at the end of each test series.

Figure 1 provides a schematic of the Base Excitation Resonant Mass test rig. Included in this figure are a number of items not referred to in the preceding summary description. The preload air spring is a pressurized air cylinder which can apply a downward force on the elastomer specimen and is used for all compression tests to ensure that the test elements never go into tension. The axial motion mass guide spokes are used when very large masses are supported on the elastomer to ensure that motion is purely vertical and that undesirable

rocking motion does not occur. The mass support air spring is used to relieve the force applied by very large masses to the test specimen. In the present series of tests, mass values were limited to those which did not require the axial motion guide spokes or the mass support air spring. Figure 2 is a photograph of the electromagnetic shaker with part of the Base Excitation Resonant Mass test rig mounted upon it. The outer dark colored metal casing is the outside of the preload air spring and its means of attachment to the table. Protruding from the top of the casing is a small added mass; through the side of the casing may be seen part of a test specimen and to the left of the shaker may be seen a heater which provides a source of hot air for controlling the ambient temperature of the elastomer test specimen. Figure 3 is a schematic of the data acquisition system for the elastomer tests. The data acquisition items previously discussed may now be seen in more detail. In addition to the items previously discussed, this schematic shows the various ways that the operator can monitor the testing process, i.e., via oscilloscopes, the temperature indicator readout, and the teletype terminal.

Figures 4 and 5 show the elastomer test specimens employed in the present series of tests. Figure 4 shows the shear specimen consisting of a central square metal block surrounded by four similar slotted blocks. The slotted blocks are clamped to the shaker table and the central mass is attached to each slotted block via an elastomer sheet of approximately 3.15 mm (1/8 in.) thickness and 48.8 mm x 25.4 mm (1.92" x 1.0") in sheared area for each interface. Thus the central block forms the resonant mass. This mass may be added to by passing a rod through the central hole and adding mass at the top of the rod. Three output accelerometers are shown mounted on the central block together with a fourth dummy accelerometer for inertial symmetry.

Figure 5 shows the compression test specimen. In this specimen, ten cylindrical elastomer buttons are bonded to a bottom and top aluminum surface. The bottom surface is clamped to the shaker table and the top surface forms the resonant mass. Again, mass may be added by inserting a rod in a central hole. The buttons are 6.35 mm (1/4 in.) high and 12.7 mm (1/2 in.) in diameter. There are ten buttons whose centers lie on a circle. Although not shown, three accelerometers are mounted on the upper plate via the screws which may be seen. Both the uninstrumented and instrumented compression specimens were basically as shown in Figure 5. The instrumented specimen was obtained by drilling holes through appropriate points in the various elastomer buttons and inserting thermocouples therein.

Figures 6, 7 and 8 define the locations of the accelerometers and all the thermocouples. Figure 6 shows accelerometers AD (attached to the table) and A1, A2 and A3 which are attached to the resonant mass. Figure 6 also shows the six thermocouple locations external to the elastomer elements themselves in the instrumented compression test specimen (chromel-alumel thermocouples were used). Three thermocouples were located on top of the lower plate; one thermocouple was located on top of the upper plate and two thermocouples were in the upper mounting plate. Figure 7 shows the locations of the fourteen thermocouples which were embedded in, or in direct contact with, elastomer elements in the instrumented compression test specimen. The ten cylindrical buttons may be seen as circles numbered 1 through 10 in Figure 7. Thermocouples are indicated

by square boxes with the numbers 7 through 20 in them and arrows pointing to the button in which the thermocouple in question was embedded. Figure 8 shows a diametral cross section of a single button element with letters A through G to indicate thermocouple locations. Beneath this cross section are listed the thermocouple numbers which were placed in the various locations A through G. By using Figures 7 and 8, the location of any thermocouple may be pinned down to a specific button number and a specific location within that button. It is recognized that the temperatures recorded from any thermocouple may be caused in part by frictional heating due to rubbing of the thermocouple itself in its cavity. The temperature results presented are subject to this possible uncertainty.

A. Test Plan

The test plan followed for this investigation of strain, frequency, and ambient temperature effects is defined by Tables 1, 2, and 3. In Table 1 are listed the test series executed for the uninstrumented compression specimen, the instrumented compression specimen and the shear specimen. As may be seen for the shear specimen and uninstrumented compression specimen, a full combination of frequency and strain values was executed at each of the three ambient temperatures (32°C, 66°C, 80°C). For the instrumented compression specimen, the same set of strain and frequency values were executed at a single ambient temperature of 32°C.

TABLE 1

TEST PLAN FOR ELASTOMER PERFORMANCE LIMITS

I. Compression Specimen Tests (uninstrumented)

- A. For a temperature of 32°C at each combination of frequency and strain defined by Table 2, measure elastomer stiffness and damping.
- B. For a temperature of 66°C at each combination of frequency and strain defined by Table 2, measure elastomer stiffness and damping.
- C. For a temperature of 80°C at each combination of frequency and strain defined by Table 2, measure elastomer stiffness and damping.

II. Temperature Instrumented Compression Specimen

For a temperature of 32°C at each combination of frequency and strain defined by Table 2, measure elastomer stiffness, damping and temperatures.

III. Shear Specimen Tests

- A. For a temperature of 32°C at each combination of frequency and strain defined by Table 2, measure elastomer stiffness and damping.
- B. For a temperature of 66°C at each combination of frequency and strain defined by Table 2, measure elastomer stiffness and damping.
- C. For a temperature of 80°C at each combination of frequency and strain defined by Table 2, measure elastomer stiffness and damping.

Table 2 defines the combinations of strain and frequency which were executed. Strain values between 0.0005 and 0.08 were tested while frequencies between 170 Hz and 600 Hz were tested. For the majority of frequency/strain combinations, the tests were applied to both compression and shear specimens. For the highest four values of strain, some limitations were imposed by the shaker capacity and some of these combinations could not be executed for either specimen and other combinations could be executed only for the shear specimen. Table 3 defines the actual vibration amplitudes for the compression and shear specimens which were required to achieve the strain amplitudes of Table 2. As may be seen, the required amplitudes for the compression specimen were larger than for the shear specimen which explains the high strain limitation of Table 2 for the compression specimens.

TABLE 2

FREQUENCY AND STRAIN COMBINATIONS TO BE TESTED

Strain	Frequency No.									
	1	2	3	4	5	6	7	8	9	10
0.0005	C,S	C,S	C,S	C,S	C,S	C,S	C,S	C,S	C,S	C,S
0.001	C,S	C,S	C,S	C,S	C,S	C,S	C,S	C,S	C,S	C,S
0.002	C,S	C,S	C,S	C,S	C,S	C,S	C,S	C,S	C,S	C,S
0.004	C,S	C,S	C,S	C,S	C,S	C,S	C,S	C,S	C,S	C,S
0.005	C,S	C,S	C,S	C,S	C,S	C,S	C,S	C,S	C,S	C,S
0.008	C,S	C,S	C,S	C,S	C,S	C,S	C,S	C,S	C,S	C,S
0.01	C,S	C,S	C,S	C,S	C,S	C,S	C,S	C,S	C,S	S
0.02	C,S	C,S	C,S	C,S	C,S	C,S	S	S	S	
0.05	C,S	C,S	C,S	C,S	S	S				
0.08	C,S	C,S	C,S	S						

C - Compression Specimen Tests
S - Shear Specimen Tests

TABLE 3

VALUES OF STRAIN AND ACTUAL AMPLITUDES

Strain	Amplitude for Compression Specimen (microns/Mils P-P)	Amplitude for Shear Specimen (microns/Mils P-P)
0.0005	3.18/0.125	1.59/0.0625
0.001	6.35/0.25	3.18/0.125
0.002	12.70/0.5	6.35/0.25
0.004	25.40/1.0	12.70/0.5
0.005	31.75/1.25	15.88/0.625
0.008	50.80/2.0	25.40/1.0
0.01	63.50/2.5	31.75/1.25
0.02	127.0/5.0	63.50/2.5
0.05	317.5/12.5	158.8/6.25
0.08	508.0/20.0	254.0/10.0

Table 4 defines the frequency values corresponding to frequency numbers 1 through 10 for the majority of tests. In the cases where the highest frequencies could not be reached, additional frequency values were executed to give ten values in all cases.

TABLE 4

FREQUENCY VALUES

Frequency No.	Frequency Value, Hz
1	170
2	200
3	250
4	300
5	325
6	400
7	450
8	500
9	550
10	600

B. Test Procedure

The following step by step process defines the procedure followed by the operator in executing the tests for elastomer performance limits:

1. A resonant mass is selected and installed.
2. In the case of the compression tests, the elastomer sample is statically preloaded.
3. Operator enters information describing the test conditions and resonant mass.
4. The elastomer test sample cavity is enclosed and the temperature control system given time to adjust ambient temperature to the desired value.
5. With low vibration levels applied to the base of the elastomer holding fixture, frequency scans are conducted until the approximate resonant frequency of the system is found. It may be noted here that for a base-excited, single-degree of freedom spring-damper-mass system, resonance occurs at an angle smaller than 90°. The deviation from 90° is essentially determined by the amount of damping in the system.
6. While the predetermined strain in the elastomer test sample is maintained by adjustment of the shaker power input level, the vibration frequency is adjusted to obtain the nearest specified test frequency. Provided none of the acceleration and displacement signals show signs of abnormalities (distortions, or indications of nonaxial motion of the resonant mass), the operator instructs the computer to acquire data.
7. Computer acquires data in the form of amplitude and phase for each sensor and temperature for each thermocouple. The computer provides to the operator an immediate calculation of stiffness, damping and power dissipation per unit volume of elastomer along with the raw data from the sensors and thermocouples.

8. Operator reviews these data and calculated results and indicates to the computer either that the data point is acceptable or not acceptable (normally it is acceptable).
9. If acceptable, the computer stores the data on a disk file; if not acceptable, the data point is discarded.
10. The vibration frequency is changed to the next nearest test frequency (with the phase angle between 15 and 165 degrees).
11. Steps five through ten are repeated for each specified value of strain.
12. Tests, comprising steps 1 through 11, are then repeated with each of the remaining masses in turn, each mass giving a dynamic system with a different resonant frequency, permitting data to be taken at other test frequencies.
13. The ambient temperature in the test sample cavity is adjusted to the next specified value.
14. Steps 1 through 13 are repeated until data at all desired temperatures are obtained.

In addition to testing for dynamic properties, the material polybutadiene NEX 156G was tested to determine its thermal conductivity, coefficient of expansion, specific heat, chemical content, and reference temperature, T_s, for use in the method of reduced variables. Some of these properties are for use in analytical predictions described in Section IV; other properties are considered to be of value in design applications. The test methods for and results of these property tests are presented in Appendix A. The tests were performed by the Rubber and Plastics Research Association of Great Britain (RAPRA).

SECTION IV

TEST RESULTS - ELASTOMER PERFORMANCE LIMITS

The first series of results presented are for the shear test specimen and for the uninstrumented compression test specimen. Figures 9, 11, 13, 15, 17, and 19 show stiffness and loss coefficient as a function of dynamic strain for different combinations of geometry and ambient temperature, and Figures 10, 12, 14, 16, 18, and 20 show stiffness and loss coefficient as a function of frequency. For either independent variable, the complete set of results at the particular ambient temperature and geometry has been plotted. With frequency as an independent variable, a linear least squares fit has been applied to the data. With strain as an independent variable, a second order least squares curve fit has been applied to the data.

The curves with strain as an independent variable show certain distinct characteristics:

- Stiffness decreases with increasing strain
- Loss coefficient increases with increasing strain
- There is a consistent decrease in stiffness as the ambient temperature is increased.
- Loss coefficient decreases with increasing temperature
- The amount by which low strain loss coefficient falls with increasing temperature is small.
- At high temperature the reduction in loss coefficient is more pronounced.
- There is distinct clustering of the data points about the fitted curves.
- The plots for the compression test specimen are even more closely clustered about the fitted line than for the shear specimen.
- The plots as a function of strain provide, with some scatter, a uniform trend for data at all frequencies.

The plots as a function of frequency do not provide a uniform trend for the data at all strains. The scatter is very broad indicating that for this material, in this frequency range, the effects of strain are much more pronounced than the effects of frequency. In the case of stiffness the gross trend of the data is to show increasing stiffness with increasing frequency; but as previously stated, the scatter is considerable. In the case of loss coefficient the data suggests little dependence on frequency.

Based on the two sets of plots it is clear that dependence on strain is more pronounced and more consistent for the range of frequencies investigated than the dependence on frequency for the range of strains investigated.

Figures 21, 22, and 23 present plots of stiffness and damping as a function of frequency for a single low value of strain for the shear test specimen at 32°C, 66°C, and 80°C. These plots clearly show a more consistent variation with frequency to which an acceptable straight line fit on log paper may be applied. Treating the distortion in the shear specimens as pure shear, the

relationship between component properties, shear modulus, sheared area and strained dimension (thickness) may be used to extract storage moduli and loss moduli in shear. The resultant values are shown in Table 5 for temperatures of 32°C, 66°C, and 80°C. The moduli are presented as a power law function of frequency: $G' = A_1\omega^{B_1}$; $G'' = A_2\omega^{B_2}$ and the Tables give the four coefficients A_1, A_2, B_1, B_2 to be used at each temperature. These values will be subsequently used to assess, by analytical methods, the contribution of self heating to changes in elastomer properties with strain.

TABLE 5

SHEAR MODULUS COEFFICIENTS

$G' = A_1\omega^{B_1}$ Pa

$G'' = A_2\omega^{B_2}$ Pa

T	A_1	B_1	A_2	B_2
32°C	1.187×10^6	.297	5.385×10^4	.42
66°C	1.284×10^6	.241	9.112×10^4	.314
80°C	1.415×10^6	.210	3.507×10^4	.408

A. Test Results for Instrumented Compression Specimen

As previously discussed, tests were run with the instrumented compression test specimen at an ambient temperature of 32°C. The main supplementary results to be obtained from these tests were measurements of temperature distributions in the elastomer. However, the necessary measurements to determine stiffness and damping were also made and an evaluation has been made of how well the results with the instrumented compression test specimen reproduce the results without installed thermocouples. Figure 24 shows the variation of stiffness and loss coefficient with strain for the instrumented compression test specimen. The values of stiffness and loss coefficient are not an exact reproduction of the results with the uninstrumented test specimen, but lie within 10 percent of these results. Since the installation of thermocouples is by no means an insignificant modification to the buttons, and since the total assembly did involve a new set of buttons, this repeatability is considered satisfactory.

The variation of peak temperature, which occurred at button center, with strain, is shown in Figure 25. It is apparent from these plots that there is a negligible increase in temperature up to a strain of .005 and only between 2° and 8° temperature rise up to a strain of .01. At higher strains than .01, temperatures increase sharply. Peak temperature results are shown for three frequencies: 200 Hz, 450 Hz and 600 Hz. Ignoring the slight variations in ambient temperature which dominate results at low strain (below .008), it is clear that the highest frequency of 600 Hz causes the largest increase in temperature at a given strain, which would be expected since the dissipation rate is strongly dependent on frequency. Above a strain of .008, it is clear that 450 Hz shows slightly lower temperatures and the 200 Hz tests show lower temperatures yet at a given strain. Comparison of the temperature results in Figure 25 and the variation of stiffness and loss coefficient with strain in Figures 15, 17, and 19 provides perhaps the strongest indication of the fact that internal heating alone is not the cause of changes in dynamic characteristics with strain. The reduction in stiffness by 30 to 40 percent at a strain of .01 can in no way be explained by an increase in temperature of between 2° and 8°.

As a result of increased shaker capacity at lower frequencies it was, in fact, possible to reach higher ultimate temperatures at 200 Hz than at 450 Hz, and at 450 Hz than at 600 Hz. The 200 Hz ultimate temperature is so high that, in addition to change in dynamic characteristics, the potential for permanent damage due to high internal temperatures should be of concern in elastomer damper design. Methods of establishing the potential internal temperature will be discussed in conjunction with predictions presented subsequently in this report.

Figures 26, 27, 28, and 29 present centerline temperature profiles for the elastomer buttons. In general the centerline profiles maintain reasonable symmetry, with the possible exception of the 300 Hz and 450 Hz results at higher strains. Only at the lowest frequency is the expected parabolic type of temperature distribution obtained, whereas at higher frequencies there is a sharper peak to the central temperature. The specific cause of these differences is not clear. It is apparent, however, that as the midpoint temperature of the elastomer increases, the flow of heat to the faces of the button causes these faces to achieve a temperature higher than the ambient temperature. Appendix A provides a more comprehensive set of internal temperature measurements at all the thermocouple locations.

B. Comparison of Measured and Predicted Dynamic Characteristics

As part of the effort to define the contribution of self-heating to the changes in dynamic characteristics induced by dynamic strain, measured results for stiffness, loss coefficient and peak temperature have been compared with predictions based on a thermo-viscoelastic analysis. This thermo-viscoelastic analysis was developed under an earlier phase of the program and is documented in reference 4. A summary description of the approach is presented here.

The thermo-viscoelastic analysis solves, in parallel, the stress equilibrium and energy equations for the elastomer button. Both equations are treated one dimensionally, the basic assumption being that changes occur more rapidly in a direction parallel to the button centerline than radially across the button. The basis for this assumption is that the elastomer is in intimate thermal contact with the metallic fixtures at both button faces, whereas the free surface of the button is exposed only to near stationary air. The energy equation equates the local rate of heat generation in the elastomer to the rate of flow of heat away by conduction. Steady-state vibration is assumed with the rate of heat generation being the average over a vibration cycle. The stress equilibrium equation equates the axial force at adjacent axial stations through the button. The material properties (storage and loss moduli in shear) are assumed to vary axially through the button as a function of temperature only. To account for the effects of shape in compression specimens, the local stress is multiplied by an empirical factor based on test results from an earlier program phase.

Both stress equilibrium and energy equations are solved by one-dimensional finite difference methods in which the continuum equation is replaced by a discrete equivalent. Sufficient axial stations are used to ensure numerical accuracy. The system of equations is nonlinear and the most effective solution algorithm was found to be a time transient method in which the energy equation

diffuses to a steady-state solution which consists of the axial distribution of displacement and temperature. Once these distributions have been obtained, the effective stiffness and damping of the button are calculated by integrating the stress over the face area and dividing by the amplitude of motion, which is an independent parameter of the analysis.

Material properties required by the analysis are density, specific heat and conductivity for the energy equation, and storage and loss moduli in shear as a function of frequency and temperature for the stress equilibrium equation. It is an implicit assumption of the analysis that the shear moduli are a function of temperature and frequency only, and that the only effect of strain is to change the local properties as a function of the local temperature. The properties of conductivity and specific heat were determined by the Rubber and Plastics Research Association of Great Britain (RAPRA); the methods used are described in Appendix A. The average values obtained were: conductivity = .25 W/mK; specific heat = 1.58 J/gk. Storage and loss moduli in shear as a function of frequency and temperature were obtained from the low strain shear tests. Plots of stiffness and damping of the shear specimen at low strain for three ambient temperatures have already been presented. Using the relationship $G = Kh/A$ where G is the complex shear modulus, K is complex stiffness, h is the shear specimen thickness, and A is its sheared area, values for shear moduli were obtained from these test results as presented in Table 5.

The thermo-viscoelastic analysis was executed for the shear and compression specimens over a range of strains corresponding to the previously described test results and for a number of frequency values. These resultant predictions have then been compared with measured results for stiffness, loss coefficient and temperature. The results are presented in Figures 30, 31, 32, and 33.

The comparisons for the shear test specimen show that predicted stiffnes does show some strain dependence at very high strains (above .02) but that the measured drop in stiffness with strain is much more pronounced than that predicted by the analysis. This is consistent with previous observations that small measured temperature rise corresponds to significant reduction in stiffness due to strain. Thus, the predicted trends for stiffness as a function of strain from the thermo-viscoelastic analysis do not adequately reflect the observed material behavior. The predicted loss coefficient shows no observable variation with strain over the entire test range, whereas the measured loss coefficient increases by a factor between 2 and 3 over the test range of strains. Thus, again the predicted dependence of loss coefficient on strain from the thermo-viscoelastic analysis does not adequately represent the measured behavior.

Similar observations are obtained for the compression specimen. No significant reduction in stiffness is predicted over the range of strains tested whereas the measured stiffness shows over a factor of 2 reduction over this range of strains. The low strain predictions for stiffness are, in fact, lower than measured which reflects a shape factor coefficient some 30 to 40 percent higher for these button specimens than the number used in the thermo-viscoelastic analysis. However, at high strains the variation in stiffness with strain is so slight that, above a strain of .01, the predictions are higher than measured.

Again the loss coefficient shows no perceptible variation with strain over the range tested, although the measured value increases by approximately a factor of 2. The predicted low strain, loss coefficient value is close to the measured value, but the high strain predictions are significantly lower than measured. Thus, both for shear and for compression specimens, the thermo-viscoelastic analysis does not adequately reflect the observed dependence of dynamic stiffness and loss coefficient upon dynamic strain.

As previously discussed and demonstrated by measured results, the reason for the inadequacy of the thermo-viscoelastic analysis in predicting strain-dependent stiffness and damping is that thermal effects alone do not cause the changes in dynamic characteristics observed at high strains. As a further aspect of the high-strain behavior, the predicted peak temperature results from the thermo-viscoelastic analysis are compared in Figures 32 and 33 with measured peak temperature values at two frequencies, 200 Hz and 450 Hz. At strains up to .025 the measured and predicted values of peak temperature are very similar. At higher strains, the predicted values of peak temperature tend to be higher than the measured values by up to 20° to 30°. It may, therefore, be concluded that predicted temperature rise is as high or higher than measured. This conclusion reinforces the argument that the inadequacies of the thermo-viscoelastic model in predicting stiffness and damping could not be the result of under-prediction of the temperature rise.

The distinct overestimate of the temperature rise by the thermo-viscoelastic analysis offers a conservative approach to establishing amplitude limits in the design and application of elastomer components as dampers. The analysis should be used to predict peak internal temperature as a function of ambient temperature, and strain. Limiting values of strain are defined as those values causing the predicted peak internal temperature to equal the limiting temperature for the material (as quoted by the supplier, or as determined by separate test). If these corresponding amplitude values are used as absolute operating limits for the component in its intended application, then the component should be safe from short-term damage due to internal temperature generation. Note that this does not address the question of fatigue, which would be expected to impose more severe constraints on long-term operation.

SECTION V

DISCUSSION - ELASTOMER PERFORMANCE LIMITS

The elastomer performance limits task was directed at evalution of the effects of strain on the dynamic characteristics of the elastomer and the implications of these effects on design of elastomer dampers. The results have shown that over the range tested, strain is an important parameter which reduces the stiffness and increases the loss coefficient or ratio of damping to stiffness. The damping itself is reduced at high frequency but not so severely as stiffness. These observations are consistent with previous results of references 4, 5, 6, and 7.

In evaluating the significance of these observations to design, one important consideration is the relationship of strains to be expected in-service to the strains which have been tested. While it is difficult to set universal values for strain limits, double amplitude vibration of up to 125 microns (5 mils) could be anticipated at an elastomer damper under severe vibration conditions; and in a satisfactorily balanced rotor, 25 microns double amplitude might be expected. The strained dimension is expected to be in the range of 3 to 10 mm. The resultant range of strains from these numbers, which will be taken as representative, is .0025 to .04. This range falls within the range of values tested.

Review of the test results in Figures 9, 11, 13, 15, 17, and 19 shows that at the low end of the representative strain range, the stiffness and loss coefficient vary only a small amount from values at lower strain. At the upper end of this representative strain range however, the deviation from the low strain values are substantial: at least a factor of 2 decrease in stiffness and a factor of 2 increase in loss coefficient. There exists a strain region where dynamic characteristics are nearly independent of strain, but this region extends only to the low end of strain values to be expected in vibration control applications. Thus, some effective account should be taken of strain in design of rotor systems which employ elastomer dampers as components.

Accounting for strain effects in design has several implications. Firstly, it is desirable to be able to predict a range of dynamic characteristics which may be experienced over a range of possible vibration amplitudes. Secondly, it is necessary to ensure that the rotor system dynamic characteristics remain satisfactory over this range of dynamic characteristics of the damper. Thirdly, it is necessary that the elastomer survive its environment.

Addressing the need to predict, several questions present themselves: Is there an analytical model which can predict strain effects from the physics of the problem? Is there an empirical model which can be fitted to the data? How many parameters have to be independent variables in the model? Will the same model apply to different materials or different classes of material?

The prognosis for an analytical model along the lines of the thermo-viscoelastic model already tested is not good. The additional influence of strain, beyond

its thermal effect, which involves changes to the structural interaction of the elastomer material, makes a thermo-viscoelastic model alone of limited value.

Empirical models can be fitted. The curve fits in Figures 9, 11, 13, 15, 17, and 19 represent such models. But unless these models can be generalized, they are of limited use in deterministic prediction. Since the trends are in all cases similar, they encourage such a generalization in which the results are combined by normalization and presentation on a single plot.

If it is assumed that the low-strain dynamic characteristics can be predicted using available low-strain data, then the knowledge of the ratios of high-strain characteristics to low-strain characteristics would suffice to define the required high-strain dynamic characteristics. To this end the empirical curve fits as a function of strain have been used to determine the ratio of high-strain stiffness to low-strain stiffness for each geometry and each temperature tested, and the results have been plotted for all cases in Figure 34 as a function of strain. Unfortunately the results are disappointing. They show that both geometry and temperature affect the variation of the stiffness ratio with strain. In particular:

- Compression specimens show substantially more reduction in the stiffness ratio at a given strain than shear specimens.
- There is a more pronounced variation with strain in low-temperature values for stiffness ratio than high-temperature values.

In Figure 35 the loss coefficient is plotted as a function of strain for all geometries and temperatures tested. Again, both geometry and temperature significantly affect the variation of loss coefficient. In particular:

- Compression specimens show more variation in loss coefficient than shear specimens.
- There is a more pronounced variation in low-temperature loss coefficient than high-temperature loss coefficient.

Thus, this empirical approach is not seen as a promising basis for the generalized deterministic predictive model. However, Figures 34 and 35 do provide the tentative basis for establishing the uncertainty in stiffness and loss coefficient which must be accounted for at preliminary stages of design when only analytical prediction can be made. The following sequence describes possible steps in design which would use this information.

- Obtain low-strain loss and storage moduli in shear at different temperatures for each candidate material (from previous tests or published data).
- Apply geometrical relationships to establish low-strain stiffness and loss coefficient of candidate elastomer configurations and materials at temperatures of interest (using standard stress-strain relationships and shape effect).
- Define anticipated range of dynamic amplitudes and strains.
- Apply ratios read from figures 34 and 35 to establish variation in stiffness and loss coefficient to be expected over the anticipated range of dynamic amplitude; thereby determine stiffness and loss coefficient envelope.

- Perform system dynamic analysis to calculate system dynamic performance over the established envelope of stiffness and loss coefficient for each candidate.
- Narrow candidate geometry and material down to those which provide satisfactory dynamic performance over the expected envelope of dynamic characteristics.

Further selection within this set of candidates can be made on the basis of other considerations such as environmental compatibility. Desirably, several of the most promising candidates would be tested both as components for component properties and in the system for resultant system performance. In this way the uncertainty in component performance can be reduced and the final selection made on the basis of actual system performance. The steps provided above should ensure that there is a number of acceptable candidates from which to choose. As the next section of this report will show, very modular simple-to-replace elastomer dampers can be built and tested. Alternatives can be compared by system damping and an optimum thereby identified.

As indicated earlier in this discussion, in addition to satisfactory dynamic performance, the question of survival is important. One aspect of survival is to ensure acceptable internal temperatures and for this requirement, as discussed under Section IV of this report, the thermo-viscoelastic analysis previously referred to and evaluated provides an encouraging basis for conservative identification of operational amplitude limits. A second important aspect of survival is the requirement to maintain integrity and acceptable dynamic characteristics over an acceptable life. As yet, the present test program has not addressed these questions. Fatigue tests should be performed under different amplitudes of dynamic strain and at different frequencies; and tests should also be performed to determine the degree of deterioration in stiffness and damping which result from exposure to fluids such as oil and fuel which will be present in bearings and/or gas turbine engines.

The next sections of this report describe the design and test of an elastomer for control of flexible rotor vibrations. While the design procedure followed is consistent with some of the steps described in the preceding discussion, it is noted that the elastomer performance limits and elastomer design and test efforts proceeded in parallel and, as a result, not all the above thinking was followed in the elastomer damper design.

SECTION VI

DESIGN OF ELASTOMER DAMPER FOR TEST ROTOR

A. Test Rig Mathematical Model

The test rig used for this project was adapted from an earlier test rig described in reference 2. The rotor was designed to represent the power turbine of an advanced gas turbine engine and consists of a 2.22 cm (7/8 in.) x 58.4 cm (23 in.) shaft with a 26 cm (10.25 in.) diameter disc mounted at one end. A small air turbine at the opposite end drives it to a maximum speed of 30,000 rpm. Figure 36 is a photograph of this rotor during assembly. The rotor runs on one pair of angular contact ball bearings at either end, originally supported in pedestals by metallic flexures and damped with squeeze film dampers. These pedestals were put aside and a new set was designed to substitute elastomeric mounts for the older flexure-squeeze film arrangement.

The new mounts were designed by first creating a mathematical model of the rotor. This model, shown schematically in Figure 37, consists of 31 stations defining 30 discrete sections. Each section is defined by length, outer diameters for use in stiffness and mass calculations, inner diameter, elastic modulus, density and shear modulus. Additionally, discs described by concentrated mass and inertia values may be located at any station. The mathematical model of this rotor is shown in Table 6. Elastomeric pedestals were represented by radial stiffness and equivalent viscous damping coefficients. The ball bearings were likewise represented by a radial elastic stiffness and a small viscous damping coefficient. It was assumed that the bearings and pedestals had zero angular stiffness and damping.

The mathematical analysis of the elastomer damper test rig was composed of three phases. The first phase consisted of a damped critical speed analysis, which allowed the optimum support properties to be determined, and the selection of elastomers to test. The second phase consisted of performing a response analysis to compute expected unbalance response of the test rig, while the third phase involved the actual design of the elastomer supports.

B. Support Optimization

In order to find values for elastomer stiffness and damping, a damped natural frequency analysis was performed. The pedestals were assumed to have stiffnesses of 1.75×10^6, 5.25×10^6 and 1.75×10^7 N/m (10^4, 3×10^4 and 10^5 lb/in.) at both ends. Damped natural frequencies were computed for pedestal damping coefficeints of 1750, 3500 and 8750 Ns/m (10, 20, and 50 lb-sec/in.). Table 7 shows the results of these calculations. Damped natural frequencies are calculated by assuming a rotor speed and calculating the natural frequencies corresponding to that speed. They are complex and of the form $\sigma \pm j\omega$, where σ denotes system stability (negative σ implies stability) and ω denotes the frequency. The natural frequencies for Table 7 were calculated by first finding the approximate location of the natural frequencies and then using a rotational speed close to the natural frequency to be calculated. For example, referring to Table 7, with a stiffness and damping of 1.75×10^6 N/m and 1750 N-sec/m (10^4 lb/in. and 10 lb-sec/in.), respectively, the first damped natural frequency at 4,425 cpm was calculated by setting the rotor speed to about 4,000 rpm and computing the natural frequency in this range. Similarly, the speed may then be set to about 17,000 rpm to find the second frequency at 17,278 cpm, and so on. The damped natural frequencies, therefore, are approximately synchronous values.

TABLE 6

TEST ROTOR MATHEMATICAL MODEL

ROTOR DATA

STATION	MASS,LBS	POLAR M.IN	TRNSV.M.IN	LENGTH	DIA(STIFF)	DIA(MASS)	INNER DIA.	YOUNGS MOD	(SHEAR)*G	DENSITY
1	-0.	-0.	-0.	.4380E+00	.6250E+00	.1125E+01	0.	.3000E+08	.8650E+07	.2830E+00
2	-0.	-0.	-0.	.2500E+00	.7000E+00	.3000E+01	0.	.3000E+08	.8650E+07	.2830E+00
3	-0.	-0.	-0.	.1000E+01	.7000E+00	.1000E+01	0.	.3000E+08	.8650E+07	.2830E+00
4	-0.	-0.	-0.	.1062E+01	.7000E+00	.1000E+01	0.	.3000E+08	.8650E+07	.2830E+00
5	-0.	-0.	-0.	.7800E+00	.7000E+00	.1000E+01	0.	.3000E+08	.8650E+07	.2830E+00
6	-0.	-0.	-0.	.6950E+00	.8750E+00	.8750E+00	0.	.3000E+08	.8650E+07	.2830E+00
7	-0.	-0.	-0.	.1000E+01	.8750E+00	.8750E+00	0.	.3000E+08	.8650E+07	.2830E+00
8	-0.	-0.	-0.	.1000E+01	.8750E+00	.8750E+00	0.	.3000E+08	.8650E+07	.2830E+00
9	-0.	-0.	-0.	.1000E+01	.8750E+00	.8750E+00	0.	.3000E+08	.8650E+07	.2830E+00
10	-0.	-0.	-0.	.1000E+01	.8750E+00	.8750E+00	0.	.3000E+08	.8650E+07	.2830E+00
11	.6000E-01	-0.	-0.	.1000E+01	.8750E+00	.8750E+00	0.	.3000E+08	.8650E+07	.2830E+00
12	-0.	-0.	-0.	.1500E+01	.8750E+00	.8750E+00	0.	.3000E+08	.8650E+07	.2830E+00
13	-0.	-0.	-0.	.5000E+00	.8750E+00	.8750E+00	0.	.3000E+08	.8650E+07	.2830E+00
14	-0.	-0.	-0.	.1000E+01	.8750E+00	.8750E+00	0.	.3000E+08	.8650E+07	.2830E+00
15	-0.	-0.	-0.	.1000E+01	.8750E+00	.8750E+00	0.	.3000E+08	.8650E+07	.2830E+00
16	.6000E-01	-0.	-0.	.1000E+01	.8750E+00	.8750E+00	0.	.3000E+08	.8650E+07	.2830E+00
17	-0.	-0.	-0.	.1000E+01	.8750E+00	.8750E+00	0.	.3000E+08	.8650E+07	.2830E+00
18	-0.	-0.	-0.	.1000E+01	.8750E+00	.8750E+00	0.	.3000E+08	.8650E+07	.2830E+00
19	-0.	-0.	-0.	.1150E+01	.8750E+00	.8750E+00	0.	.3000E+08	.8650E+07	.2830E+00
20	-0.	-0.	-0.	.6500E+00	.1200E+01	.1200E+01	0.	.3000E+08	.8650E+07	.2830E+00
21	-0.	-0.	-0.	.4000E+00	.1250E+01	.1700E+01	0.	.3000E+08	.8650E+07	.2830E+00
22	-0.	-0.	-0.	.6750E+00	.1400E+01	.1700E+01	0.	.3000E+08	.8650E+07	.2830E+00
23	-0.	-0.	-0.	.9400E+00	.1400E+01	.1700E+01	0.	.3000E+08	.8650E+07	.2830E+00
24	-0.	-0.	-0.	.2000E+00	.1700E+01	.1700E+01	0.	.3000E+08	.8650E+07	.2830E+00
25	-0.	-0.	-0.	.2500E+00	.1400E+01	.1400E+01	.4375E+00	.3000E+08	.8650E+07	.2830E+00
26	-0.	-0.	-0.	.7000E+00	.1400E+01	.1400E+01	.8750E+00	.3000E+08	.8650E+07	.2830E+00
27	-0.	-0.	-0.	.3000E+00	.2200E+01	.2900E+01	.8750E+00	.3000E+08	.8650E+07	.2830E+00
28	-0.	-0.	-0.	.5000E+00	.3600E+01	.1000E-02	0.	.1550E+08	.4310E+07	.1630E+00
29	.1318E+02	.1914E+03	.9579E+02	.5000E+00	.1900E+01	.1000E-02	0.	.1550E+08	.4310E+07	.1630E+00
30	0.	-0.	-0.	.5000E+00	.8750E+00	.1000E-02	0.	.1550E+08	.4310E+07	.1630E+00
31	-0.	-0.	-0.	0.	0.	0.	0.	.1550E+08	.4310E+07	.1630E+00

ROTOR WEIGHT	TRANS.MOM.IN	POLAR MOM.IN	STATION 1-CG	ROTOR LENGTH
.1933574E+02	.8328863E+03	.1935124E+03	.1887895E+02	.2299000E+02

TABLE 7

DAMPED NATURAL FREQUENCY AND LOG DECREMENT AS A FUNCTION OF BEARING SUPPORT STIFFNESS AND DAMPING

Bearing Support Stiffness $\left(\frac{N}{m}/\frac{lb}{in.}\right)$	Bearing Support Damping $\left(\frac{Ns}{m}/\frac{lb\text{-}sec}{in.}\right)$	Damped Natural Frequency (cpm)			System Log Decrement		
$1.75 \times 10^6/10^4$	1750/10	4,425	17,278	23,168	1.311	.077	.023
	3500/20	4,144	17,241	23,142	2.791	.152	.044
	8750/50	-	16,997	23,017	-	.371	.089
$5.25 \times 10^6/$ 3×10^4	1750/10	7,373	17,521	23,241	.767	.086	.028
	3500/20	7,217	17,478	23,206	1.574	.168	.052
	8750/50	-	17,301	23,131	-	.186	.061
$1.75 \times 10^7/10^5$	1750/10	12,988	18,380	23,645	.100	.081	.110
	3500/20	12,948	18,382	23,430	.200	.156	.110
	8750/50	12,609	18,282	23,178	.460	.392	.132

The system log decrement, δ, is extracted from the damped natural frequency using the equation

$$\delta = -\frac{2\pi\sigma}{|\omega|} \tag{1}$$

where $|\omega|$ represents the absolute value of the frequency. The sign of the log decrement indicates stability (a positive value means a stable system, a negative value means an unstable system) and its magnitude indicates how quickly a transient disturbance will grow or die out. Additionally, the log decrement yields information concerning the sharpness of the resonance curve, since the quality or amplification factor Q is related to the log decrement by the expression:

$$Q = \frac{\pi}{\delta} \tag{2}$$

and to the modal damping ratio ζ by the equation:

$$\zeta \simeq \frac{\delta}{2\pi} \tag{3}$$

The stiffness range of 1.75×10^6 to 1.75×10^7 N/m (10^4 to 10^5 lb/in.) was established as the practical elastomer stiffness range for this size and type of rig.

The optimum stiffness choice, from Table 7 is not immediately apparent because, for higher values of damping, the low (1.75×10^6 N/m) stiffness value has the first mode critically damped, while the high (1.75×10^7 N/m) stiffness shows a better third critical log decrement. The third mode is a backward mode and will not be excited by forward whirling unbalance. The optimum stiffness is readily apparent, however, when it is recalled that, for elastomers, the stiffness K and the viscous damping, coefficient B, are related by the loss coefficient η.

$$\omega B = \eta K \tag{4}$$

Assuming, for purposes of argument, that K is not frequency dependent, and the loss coefficient is unity, we can tabulate the damping coefficients for the first two modes. The tabulation is given in Table 8.

TABLE 8

DAMPING COEFFICIENTS FOR AN ELASTOMER WITH A LOSS COEFFICIENT OF UNITY

Support Stiffness $\left(\frac{N}{m}/\frac{lb}{in.}\right)$	Frequency $\left(\frac{cycles}{minute}\right)$	Damping Coefficient $\left(\frac{N\text{-}sec}{m}/\frac{lb\text{-}sec}{in.}\right)$
$1.75 \times 10^6/10^4$	4,000	4203/24
	17,000	1051/6
$5.25 \times 10^6/3 \times 10^4$	7,000	7180/41
	17,000	2977/17
$1.75 \times 10^7/10^5$	13,000	12784/73
	18,000	9282/53

Using Table 8, it is apparent that reasonable values for the damping coefficient are only obtainable using the largest value of bearing stiffness. Additionally, from Tables 7 and 8, it appears that the problem natural frequency will be the second, occurring at a little under 20,000 rpm. If log decrement is plotted against pedestal damping, for an elastomer stiffness of 1.75×10^7 N/m (100,000 lb/in.), the curves illustrated in Figure 38 are the result. From this figure, it is apparent that an optimum value of damping exists, approximately 1.75×10^4 N-sec/m (100 lb-sec/in.), and that the corresponding log decrement is .965. Figure 39 shows how damping B varies with the loss coefficient η. For a loss coefficient of 0.8, corresponding to Viton-70 at 70°F, the damping at 20,000 rpm is 6655 N-sec/m (38 lb-sec/in.) and for a loss coefficient of 0.15, corresponding to polybutadiene at 70°F, the damping is 1261 N-sec/m (7.2 lb-sec/in.).

For this project, plans were made to test two elastomers, Viton and polybutadiene since under planned test conditions, they represent the practical extremes of elastomer capability, in terms of internal damping. Both elastomers incur a penalty, with respect to the damping, giving optimum log decrement. Table 9 presents this penalty, by comparing the expected log decrement of an elastomer damper with the optimum value of log decrement.

TABLE 9

COMPARISON OF MODE 2 LOG DECREMENT FOR POLYBUTADIENE AND VITON-70 WITH OPTIMUM DAMPING

		$B\left(\frac{N\text{-}sec}{m}\right)/\left(\frac{lb\text{-}sec}{in.}\right)$	δ
(1)	Optimum	17513/100	.965
(2)	Polybutadiene	1261/7.2	.075
(3)	Viton-70	6655/38	.31

The table shows a larger penalty with polybutadiene than with Viton but, from experience, both combinations are balanceable using multiplane balancing methods.

C. Response Analysis

To estimate the unbalance sensitivity of the elastomer-mounted rotor, a series of unbalance response calculations was performed. As seen in Figure 36, unbalance may be added in the form of threaded weights screwed into tapped holes at several locations along the rotor. Included in these locations are the large disc, two discrete locations along the shaft, and the drive turbine. Figures 40 through 43 illustrate the results of unbalance response calculations, using an unbalance of 2.54 gram centimeters (1 gram-inch) in either the disc or the shaft (stations 29 or 11, respectively, in Figure 37). These figures show the response of the disc (Station 31 of Figure 37) if weight was added to the disc, or response of the center of the shaft (Station 13) if weight was assumed to be in the shaft.

Figures 40 and 41 show the calculated response plots of amplitude against rotor speed for the test rig on polybutadiene mounts (loss coefficient $\eta \simeq .15$). Figures 42 and 43 show the response to these same unbalances, but with Viton-70 supports ($\eta \simeq .8$). These sets of curves indicate that the second critical will be the most troublesome and that the rig will be much more sensitive to unbalance when mounted on the lower loss coefficient polybutadiene supports. Table 10 gives the computed values of the rig critical speeds and the expected sensitivity to unbalance in units of microns (peak-to-peak) per gram of unbalance at the balance hole radius.

TABLE 10

COMPUTED VALUES OF CRITICAL SPEED AND SENSITIVITY TO UNBALANCE

Support Material	Loss Coefficient	Critical Speed Number	Critical Speed Value (rpm)	Sensitivity to Unbalance $\left(\frac{\text{microns P-P}}{\text{gram}}\right)/\left(\frac{\text{mils P-P}}{\text{gram}}\right)$
Polybutadiene	.15	1	9,030	917/36.1 (Disc on Disc)
	.15	2	18,894	1478/58.2 (Shaft on Shaft)
Viton-70	.8	1	8,184	254/10.0 (Disc on Disc)
	.8	2	18,570	297/11.7 (Shaft on Shaft)

D. Elastomer Suspension Design

The method chosen for designing the elastomer supports was to mount each bearing housing on three elastomer cartridges spaced 120° apart, as shown in Figure 44A. The elastomers are composed of one or more buttons glued to upper and lower platens, forming easily replaceable cartridges, shown in Figure 44B. The number, diameter and thickness of the buttons in each cartridge are chosen to satisfy the requirement of a 1.75×10^7 N/m (100,000 lb/in.) overall stiffness at 20,000 rpm under specified ambient conditions. The elastomers are preloaded, about 10 percent, by a pair of preload screws on each cartridge, such that the elastomer buttons are always in compression.

For the elastomer mounting configuration shown in Figure 44, the overall stiffness is calculated by first making the following definitions:

K_s = the elastomer button stiffness in shear

K_c = the elastomer button stiffness in compression

The support geometry is given in Figure 45A, which shows three elastomer buttons, spaced at 120° intervals, separating a bearing housing from the surrounding pedestal. When the housing is given a downward displacement of some distance X, the individual buttons are deformed in some combination of compression and shear. This is illustrated in Figure 45B for one of the buttons, where X is the total downward deflection; X_c is that component of the total deflection taken up by elastomer compression; and X_s is that component accommodated by shearing. If the individual buttons are labeled 1, 2, and 3 starting from the top, we can describe the compression and shear deflection of the individual buttons in terms of the imposed bearing housing deflection X. The deflection of the first button is simply as follows:

$$X_{1c} = X \tag{5}$$

$$X_{1s} = 0 \tag{6}$$

where X_{1c} is the compressive, or normal, deflection and X_{1s} is the shear deflection. For buttons 2 and 3, we find that:

$$X_{2c} = X_{3c} = X\cos 60° = \frac{X}{2} \tag{7}$$

$$X_{2s} = X_{3s} = X\cos 30° = \frac{\sqrt{3}}{2}X \tag{8}$$

The forces produced by these displacements are the products of the individual button spring constants (K_c for compression and K_s for shear) with the normal or shear displacements. For the first button, the forces are:

$$F_{1c} = K_c X \tag{9}$$

$$F_{1s} = 0 \tag{10}$$

where F_{1c} and F_{1s} are the compressive and shear forces, respectively. For buttons 2 and 3, the same procedure is followed.

$$F_{2c} = F_{3c} = K_c \frac{X}{2} \tag{11}$$

$$F_{2s} = F_{3s} = K_s \frac{\sqrt{3}}{2}X \tag{12}$$

The total force F_T in the direction of displacement X is the sum of the force through button 1 and the components of force in the X direction from buttons 2 and 3.

$$F_T = F_{1c} + (F_{2c} + F_{3c})\cos 60° + (F_{2s} + F_{3s})\cos 30°$$

$$= K_c X + \frac{X}{2}K_c + \frac{3}{2}X K_s \tag{13}$$

The above equation may be simplified to read:

$$F_T = 1.5\,(K_c + K_s)X \tag{14}$$

If the elastomer mount consists of cartridges with a number of individual elastomer buttons or elements, then the total force is simply the sum of the individual element forces,

$$F_T = 1.5\ N_B\ (K_c + K_s)X \tag{15}$$

where N_B is the number of buttons or elements per cartridge. The radial stiffness of the assembly, K_R, is the resultant force divided by imposed displacement.

$$K_R = \frac{F_T}{X} = 1.5\ N_B\ (K_c + K_s) \tag{16}$$

The next task is designing the individual buttons. With one required support stiffness of 1.75×10^7 N/m (100,000 lb/in.), we find from Equation (16) that

$$N_B\ (K_c + K_s) = 11.7 \times 10^6 \text{ N/m } (66{,}666 \text{ lb/in.}) \tag{17}$$

Empirical correlations for the compressive and shear stiffness of polybutadiene buttons have been developed in reference 3 and are given below,

$$K_c = 3G' \frac{\pi D^2}{4h} \left[1 + 12.33\omega^{-.29} \left(\frac{D}{4h}\right)^2\right] \tag{18}$$

$$K_s = G' \frac{\pi D^2}{4h} \tag{19}$$

where D is the diameter and h the height of a cylindrical elastomer button (meters), G' is the shear modulus (newtons per square meter) and ω is the frequency (radians per second). The shear modulus is frequency and temperature dependent and is given below for two temperatures expected to be in the range of normal operation (based on data from reference 4).

$$\text{For polybutadiene at } 32°C;\ G' = 3.686 \times 10^6\ \omega^{.2037} \text{ Pa} \tag{20}$$

$$\text{For polybutadiene at } 50°C;\ G' = 1.902 \times 10^6\ \omega^{.2627} \text{ Pa} \tag{21}$$

Equations (16), (18), and (19) can be combined to find the radial stiffness for polybutadiene buttons.

$$K_R = 4.5 N_B G' \frac{\pi D^2}{4h} \left[1.33 + 12.33\omega^{-0.29} \left(\frac{D}{4h}\right)^2\right] \tag{22}$$

In the case of Viton-70, similar test data are not available. However, if the radial stiffness correlation for polybutadiene, given in Equation (22), is assumed to apply to Viton-70, then one need only find a value for the shear modulus at the frequency of interest. The static shear modulus for 70 durometer elastomers, from reference 8, is 1.861 MPa (270 lb/in.^{2}). Results of dynamic testing of O-rings, made from Viton (ref. 5), reveal that a dynamic multiplier of 6.084 is necessary to correct the static shear modulus to an operating frequency of 2,000 radians/second (approximately 20,000 rpm) at 32°C. An additional

factor of 0.614 is also required to correct an operating temperature of 50°C at that frequency. Table 11 lists the values of shear modulus for both elastomer types at 2,000 radians per second.

TABLE 11

VALUES OF SHEAR MODULUS G' AT 2000 RADIANS/SECOND

Elastomer	Temperature (°C)	Shear Modulus MPa / $\frac{lb}{in.^2}$
Viton-70	32	11.33/1,643
Viton-70	50	6.96/1,009
Polybutadiene	32	17.31/2,511
Polybutadiene	50	14.00/2,031

Equation (22) can now be applied to the design of elastomer buttons. Figures 46 through 49 plot radial stiffness against button diameter for the case of a single button per cartridge ($N_B = 1$). Each figure consists of three curves, corresponding to elastomer thicknesses of 2.38, 3.18 and 4.76 mm (3/32, 1/8 and 3/16 of an inch). Figure 46 corresponds to Viton-70 at 32°C, Figure 47 to Viton-70 at 50°C, Figure 48 to polybutadiene at 32°C and Figure 49 to polybutadiene at 50°C. The required button diameter for any given stiffness is readily found from these curves. Table 12 gives the necessary stiffness per button to achieve the 100,000 lb/in. that is desired for the overall stiffness value.

TABLE 12

STIFFNESS VALUES TO BE USED IN FINDING BUTTON DIAMETERS

Number of Elastomer Buttons Per Cartridge	Stiffness Value to be Used in Figures 46 through 49 $\left(\frac{N}{m}/\frac{lb}{in.}\right)$
1	$1.75 \times 10^7/100,000$
2	$8.76 \times 10^6/50,000$
3	$5.84 \times 10^6/33,333$
4	$4.38 \times 10^6/25,000$

Table 13 gives the necessary button diameters, based on Table 12 and Figures 46 through 49, to achieve the 1.75×10^7 N/m (100,000 lb/in.) figure.

Preliminary layout work indicated that a 3-button per cartridge arrangement, using 1/8-inch thick elastomer stock, would go together well, therefore, this combination was selected. Also, for simplicity, it was decided to use a single diameter for Viton and polybutadiene buttons. A diameter of 15 mm (0.59 in.) was selected (see Table 13) to insure that a minimum stiffness of 1.75×10^7 N/m (100,000 lb/in.) existed at all times.

TABLE 13

BUTTON DIAMETERS TO ACHIEVE A 100,000 LB/IN. RADIAL STIFFNESS

Button Thickness (mm/in,)	Number of Buttons Per Cartridge	Button Diameter (mm/inches) For: Viton at 32°C	Viton at 50°C	Polybutadiene at 32°C	Polybutadiene at 50°C
2.38/$\frac{3}{32}$	1	14.7/.58	17.0/.67	13.2/.52	14.0/.55
	2	12.2/.48	14.0/.55	10.7/.42	11.4/.45
	3	10.7/.42	12.4/.49	9.4/.37	9.9/.39
	4	9.9/.39	11.4/.45	8.6/.34	9.1/.36
3.18/$\frac{1}{8}$	1	18.0/.71	21.6/.85	16.0/.63	17.0/.67
	2	14.7/.58	17.0/.67	13.0/.51	13.7/.54
	3	13.0/.51	15.0/.59	11.2/.44	12.2/.48
	4	11.7/.46	13.7/.54	10.2/.40	10.9/.43
4.76/$\frac{3}{16}$	1	24.4/.96	28.2/1.11	21.3/.84	22.6/.89
	2	19.6/.77	22.9/.90	16.5/.65	18.0/.71
	3	16.8/.66	20.1/.79	14.5/.57	15.5/.61
	4	15.2/.60	18.0/.71	13.0/.51	14.2/.56

E. Test Rig Assembly

Figure 50 shows a view of the elastomer cartridges as they were being assembled. On the right are two platens and three individual buttons, while the assembled cartridge can be seen on the left. Figure 51 shows the two pedestals and bearings: the disc end on the left and the turbine end on the right. Additionally, two preload screws can be seen with their calibrated washers (the washers are trimmed on assembly to get the correct preload) as well as a partially assembled elastomer cartridge. Figure 52 shows the disc end bearing housing assembled within its pedestal. Note that solid steel blocks have been inserted instead of the elastomer cartridges. These blocks allow comparisons in unbalance response to be made between hard-mounted and elastomer-mounted rotors.

Figure 53 shows a side view of the test rig as it was finally mounted and instrumented in the test cell. The disc is inside a vacuum box on the left and the drive turbine is on the right. Figure 54 shows the rig from the front, with the vacuum bases in the foreground. Finally, Figure 55 shows a detailed view of the turbine-end bearing housing and pedestal. Two elastomer cartridges are visible in the 12 and 4 O'clock positions. The two noncontacting probes measure the motion of the housing relative to the pedestal, and the two visible flexible tubes are the bearing oil feed and drain lines.

F. Summary of Design Procedure

The preceding section shows that the design of elastomer dampers for a rotor system involves a number of discrete steps. The following is a summary of the procedure followed, which forms a guideline for designing elastomer dampers to control vibrations of a particular rotor-bearing system.

1. Review elastomer materials available in the light of required parameters and operating environment (temperatures, lubricant compatibility and so forth).

2. Construct a rotordynamics model of the shaft system in its bearings.
3. Compute the damped natural frequencies and logarithmic decrements of the shaft system for a range of support coefficients, within the elastomer material limits.
4. Choose optimum support properties in terms of elastomer stiffness and loss coefficient.
5. Confirm this choice of parameters by performing an unbalance response analysis to obtain bearing loads, steady-state orbits, etc.
6. Select candidate materials and configurations for the damper. Perform tests to confirm properties and suitability for the expected operating environment, if such data are not already available.
7. Layout possible configurations for the most promising elastomer. Select dimensions to give stiffness and damping properties as close as possible to optimum values for each material. Evaluate the performance of the chosen configurations (using, for example, unbalance response analysis). Include strain effects as discussed in Section V.
8. If the results of step 7 are satisfactory, choose one or more configuration and design the damper in detail. If the results of step 7 are not satisfactory, then repeat steps 6 and/or 7 until acceptable combinations are found. Desirably, more than one viable candidate would be selected, built and evaluated by test.
9. Build and test the dampers to experimentally verify their predicted performance, and made final selections.

SECTION VII

TEST RESULTS - ELASTOMER MOUNTED TEST ROTOR

A. Instrumentation and Test Plan

The instrumentation used for these tests consisted of:

Probes - Bently Nevada, noncontacting
Proximitors - Bently Nevada
Phase reference - MTI Fotonic Sensor™
Tracking Analyzer - Vibration Instruments Co. Model 235DS
Plotter - Hewlett Packard 7046A XYY' Recorder
Tape Recorder - SANGAMO SABRE VI
Computer Balance - Digital Equipment Corp. PDP 11/34 with MTI COMMAND™ Balancing Software
Oscilloscope - Tektronix 502
Counter - Hewlett Packard 5323A
FFT - Nicolet 440A Mini-Ubiquitous with Tektronix Model 4662 Interactive Digital Plotter
Temperature - Omega 2166A Digital Thermocouple Meter

The test procedure was as follows:

1. Install Polybutadiene damper cartridges at both locations (turbine end and disk end).
2. Balance the rotor using MTI COMMAND™ balancing software.
3. Create an unbalanced condition in the disk in four discrete steps.
4. Create an unbalanced condition in the shaft in four separate steps after the unbalance was removed from the disc.
5. Remove shaft unbalance and install Viton-70 damper cartridges in place of the polybutadiene cartriges.
6. Rerun with disc unbalances.
7. Repeat shaft unbalance runs.
8. Replace Viton dampers with solid steel blocks and run with disc unbalance.
9. Replace turbine end steel block with Viton damper and run with a limited number of unbalances.
10. Record data from selected runs on magnetic tape.
11. Plot displacement amplitude against rotor speed for test runs.
12. Photograph disc and shaft orbits for selected runs.

B. Data Reduction Plan

The plan for reducing elastomer damper test rig data involves calculation of sensitivity to unbalance weights and of modal damping values and comparing these values with predictions. The sensitivity, S, to unbalance weights is defined as:

$$S = \frac{\text{Modal Response}}{\text{Unbalance Magnitude}} \qquad \left[\frac{\text{Mils P-P}}{\text{gram}}\right] \qquad (23)$$

The sensitivity for a particular mode will, of course, depend on both the location of the unbalance weight and the measurement probe. It is a valuable piece of information in that it gives a good feeling of the amount of response elicited by an unbalance weight and, therefore, of the difficulty to be expected in balancing a particular mode (at that location).

Damping information was extracted from the test runs by making use of the width of the resonance curve at the half-power points and also the rate of change of the phase angle through the resonant speed. With the half-power point method, the resonant speed, f_n (for a particular critical speed), is located by finding the peak of the resonance curve at that speed and noting the frequency at which it occurs. The half-power points are these two locations on the resonance curve where the amplitude is equal to the peak amplitude divided by the square root of two. Δf is then defined as the difference in frequency between the two half-power points. With this information, the log decrement, δ, may be found with the equation:

$$\delta \simeq \pi \frac{\Delta f}{f_n} \tag{24}$$

The second method takes advantage of the fact that the logarithmic decrement is inversely proportional to the rate of change of the phase angle through the resonant speed. Equation 25 expresses the relationship between the log decrement, the resonant frequency, and the rate of change of phase through the resonant speed:

$$\delta \simeq \frac{360}{\left(\frac{d\theta}{df}\right) f_n} \tag{25}$$

where the frequency can be in any units and the phase angle is in degrees. Using either equation, the quality or amplification factor, Q, may be calculated with the equation:

$$Q \simeq \frac{\pi}{\delta} \tag{26}$$

C. Test Results

The initial or baseline balancing was done with polybutadiene dampers using MTI's in-house COMMAND^{TM} balancing program. Because the first critical speed could not be initially negotiated, influence coefficients were first calculated at 7,000 rpm for the first three correction weight runs. Correction weights were only placed in the disc plane.

Influence coefficients were then calculated at 11,500 rpm and one additional correction weight was installed. The next correction weight run calculated a weight of 0.058 grams, which was too small to install.

The vibration level was low throughout the speed range, less than 25 microns (.001 inch or 1 mil) peak to peak.

Test runs were made with unbalance weights in either the disc (plane 1 of Figure 56) or in the shaft (plane 3 of Figure 56).

Table 14 shows the magnitudes of the unbalance weights used. In the disc, four separate and distinct weights were used alternately in the same holes, but the small hole size on the shaft required simultaneous use of from one to four weights in adjacent holes to obtain the necessary unbalance. The shaft unbalance weight shown in Table 14 is the equivalent weight that one weight would have if only one hole were used (i.e., the vector sum of the unbalance weights).

TABLE 14

SUMMARY OF WEIGHTS USED TO UNBALANCE THE TEST RIG DISC AND SHAFT

Unbalance in Disc (grams)	Unbalance in Shaft (grams)
.2	.183
.3	.353
.4	.583
.5	.621

Figure 57 shows the installation of one of the shaft unbalance weights. The log of all the test runs is shown in Appendix C.

Table 15 shows the location of the first two forward whirling critical speeds of the test rig with the two different damper materials. The critical speeds are higher with the Viton damper than with the polybutadiene dampers. In contrast to the design analysis, this indicates the Viton damper to be stiffer than the polybutadiene. The most plausible explanation is the fact that polybutadiene shear moduli used in the design (Equation 20) were based on tests of a previous material batch. Moduli for the present batch, given in Table 5, are only 60 percent of the values in Equation 20. Changes in carbon black had, in fact, been made between batches.

TABLE 15

LOCATIONS OF CRITICAL SPEEDS FOR DIFFERENT ELASTOMER SUPPORTS

Elastomer	First Critical Speed	Second Critical Speed
Polybutadiene	10,200	20,500
Viton-70	12,050	24,000

Figures 58 through 61 show the rig's response to the unbalances introduced in the different planes with the two different damper materials. Note that the location of the critical speeds drops in frequency with increasing unbalance, indicating a small strain-softening effect in the elastomer mounts, as observed in elastomer component tests documented elsewhere in this report. At highest strain, the drop in resonant frequency is approximately eight percent, indicating at least sixteen percent loss in stiffness and probably more. Peak amplitudes at the damper were approximately 10 to 20 microns (0.4 to 0.8 mils), which means a dynamic strain of .003 to .007 in a 3.2 mm button. Figure 34

indicates that such a strain could cause 9 to 32 percent loss in stiffness in a compression specimen. Thus the test results for vibration control testing of an elastomer damper are consistent with the earlier component test results for strain effects.

The influence of unbalance weight on peak amplitude is shown in Figure 62. The slopes, which are equal to the unbalance sensitivities, are approximately the same for Viton and for polybutadiene in this application; this is a qualitative discrepancy from the predicted behavior with these materials as presented in Section VI. There is some reduction in sensitivity with increasing amplitude which would be consistent with the increase in log decrement with increasing strain observed in earlier sections. Table 16 compares the observed and predicted sensitivity to unbalance. In all cases the rotor is less sensitive than predicted, indicating that the system damping achieved by the elastomer dampers exceeds expectations of the present system dynamic model. Two reasons are hypothesized. First, the computer model assumed purely radial stiffness and damping, with no moment restraint. In fact, the elastomer cartridges and double row ball bearings probably provide a considerable amount of moment stiffness and damping in addition to the radial values. Second, the elastomers ran at average temperatures of 27°C and 16°C at the disc and turbine end, respectively, (as opposed to the design temperature of 50°C), contributing both to greater stiffness and damping than was originally expected.

TABLE 16

SENSITIVITY OF TEST RIG TO UNBALANCE

Elastomer	Location of Unbalance Weight and Probe	Observed Sensitivity to Unbalance microns P-P / mils P-P gram / gram	Predicted Sensitivity to Unbalance microns P-P / mils P-P gram / gram
Polybutadiene	Disc	259/10.2	917/36.1
Polybutadiene	Shaft	84/3.3	1478/58.2
Viton-70	Disc	246/9.7	254/10.0
Viton-70	Shaft	69/2.7	297/11.7

Table 17 shows the calculated values of the log decrement for polybutadiene and Viton using both the half-power point and the rate of change of slope methods and the discrepancies between the two methods. The agreement was generally good.

The average log decrements and Q values are shown in Table 18. The predicted values for the logarithmic decrement δ in mode two are: $\delta_{poly} = .057$ and $\delta_{Viton} = .298$ (see Figures 36 and 37 and Table 6)

The repeatability of the test rig during acceleration and deceleration is shown in Figure 63. This figure was obtained with the damper material (polybutadiene) at approximately equilibrium temperature with 0.4 gram unbalance in the disc. This plot is a good representation of the rig's repeatability. The only significant deviations observed occurred when there were large temperature differences in the elastomers between the initial run-up to speed and the coast-down, which were avoided during testing by running the rotor to speed at least once before a test sequence began.

TABLE 17

MEASURED VALUES OF LOG DECREMENT FOR POLYBUTADIENE AND VITON

Material	Unbalance Magnitude (grams)	Weight Location	Critical	δ_{hp} Log Dec (half-power)	δ_s Log Dec (phase)	$\frac{\delta_s}{\delta_{hp}}$
Polybutadiene	.2	Disc	1	.426	.442	1.038
	.3	Disc	1	.485	.512	1.055
	.4	Disc	1	.496	.507	1.023
	.5	Disc	1	.531	.540	1.017
	.183	Shaft	2	*	*	-
	.353	Shaft	2	.272	.282	1.037
	.583	Shaft	2	.241	.246	1.022
	.621	Shaft	2	.230	.277	1.203
Viton	.2	Disc	1	.935	.857	.917
	.3	Disc	1	.859	.894	1.041
	.4	Disc	1	.831	.852	1.026
	.5	Disc	1	.842	.814	.967
	.183	Shaft	2	.852**	.526	.618
	.353	Shaft	2	.715	.814	1.138
	.583	Shaft	2	.605	.688	1.104
	.621	Shaft	2	.571	***	-
Steel	None	-	1	.171	-	-
	.2	Disc	1	.124		

* Signal level too low
** Approximate values, could not reach second half-power points
***Difficulty with taped data

TABLE 18

AVERAGE VALUES FOR LOG DECREMENT AND AMPLIFICATION FACTOR

Material	Critical	Log Decrement by Half-Power Point		Log Decrement by Slope of Phase		Amplification Factor	
		Mean	Std.Dev.	Mean	Std.Dev.	Q Half-Pwr.	Q Phase
Polybutadiene	1	.485	.044	.500	.042	6.48	6.28
	2	.248	.022	.268	.020	12.7	11.7
Viton	1	.867	.047	.854	.033	3.62	3.68
	2	.686	.127	.669	.144	4.58	4.70
Steel	1	.148	-	-	-	21.3	-

After the elastomer damper data were taken, solid steel blocks were substituted in place of the elastomers. See Figure 52 for the pedestal with steel blocks in place of the elastomer cartridges. With the steel blocks installed, the rig had only one resonance in the speed range, at approximately 19,000 rpm, and greatly increased response amplitude.

Figures 64 and 65 show response at disc and shaft, respectively, when an unbalance weight is added to the disc. The data were not taped or digitally acquired so the phase change is unknown, but the response appears to be nonlinear. The log decrement values are included in Tables 17 and 18, but confidence in these numbers is limited because of the support nonlinearity. It was noticed during these runs that the shaft was not as free to rotate with the steel blocks installed as it was with the elastomer dampers. The increased resistance is the result of a small amount of binding in the bearings caused by misalignment of the pedestals and shaft. The relatively soft elastomer mounts tolerated this misalignment but the stiff steel blocks could not.

Figure 66 shows the rig response with Viton dampers in the turbine end and steel blocks at the disc end. This arrangement simulates the use of elastomeric supports at the cold end of a gas turbine power shaft. The response amplitude is between the values observed with elastomers at both ends and with steel blocks at both ends. Thus, there are damping benefits to be gained with elastomers at the cold end only.

D. Frequency Spectrum and Shaft Orbits

The amplitude data for the plots in this section were handled in two distinct ways. If the probe output was not taped, then the plots were made "on-line", directly from the probe output, which was put through a tracking filter to extract the synchronous component. Appendix C is a complete run log and shows which runs were tape recorded. The tape recorded signals were analyzed by feeding them into a spectrum analyzer and using the analyzer to create a "peakhold" average spectrum for each run, which was plotted using a digital plotter. This method is valid when the synchronous component of the signal is larger, at all speeds, than any other signal component, so the analyzer is effectively acting as a tracking filter. This was the case for the elastomer rig, and two sample instantaneous spectra are shown in Figure 67. The upper spectrum shows the frequency content of the disc probe and the lower spectrum the content of a probe at the turbine. For both cases, the rotor speed is 6,000 rpm, well away from the first critical speed where the synchronous component is greatly amplified. The disc probe shows a large signal at running speed and very little elsewhere. The turbine probe shows very low vibration and, indeed, was not considered in the data analysis because of its low amplitude for both modes. However, the output of this probe is interesting because it shows very small peaks at multiples of running speed. These peaks are the result of forced vibration due to the impact of the compressed air jets on the machined "buckets" of this impulse air turbine. Traces of these spikes can be seen in the disc spectrum as well, but, at all frequencies, were exceeded by the amplitude of the synchronous component.

Figure 68 shows the orbit of the disc at three different speeds: below, at and above the first critical speed of the rig when a 0.5 gram unbalance weight was installed in the disc (Plane 1 of Figure 56). Figure 69 shows the orbit of the shaft center at three speeds which are below, at, and above the second

critical speed. The unbalance for this case was 0.621 grams in the shaft (Plane 3 of Figure 56). The maximum amplitudes of the orbits for both figures are given in Table 19.

TABLE 19

SPEEDS AND MAXIMUM AMPLITUDE OF SHAFT ORBITS

Probe Location	Shaft Speed (rpm)	Maximum Amplitude (microns/mils p-p)
Disc	9,000	56/2.2
Disc	10,950	94/3.7
Disc	12,000	33/1.3
Shaft	21,000	51/2.0
Shaft	23,000	79/3.1
Shaft	26,500	46/1.8

These photographs are presented to illustrate the fact that the orbits are essentially circular; therefore, the elastomer support can be considered isotropic.

The small irregularities in the orbits are due to a phenomenon called "electrical runout", in which small irregularities in surface finish or variations in electrical conductivity of the rotor are seen by the inductive type displacement pickup as if they were vibration signals. Since they are fixed to the rotor surface, these small "ripples" in the orbit make phase changes easily visible. This is seen in Figure 69 where a small bump appears at the top of the orbit in Figure 69a. In Figure 69b, the bump appears at some midway point (apparently smaller since the orbit has enlarged but the "electrical runout" signal has not). This bump appears at the bottom, in Figure 69c. These correspond to speeds below, at and above the second critical speed, respectively. Note also that a total phase change of about 180° has occurred while traversing the resonance.

SECTION VIII

CONCLUSIONS AND RECOMMENDATIONS

A. Conclusions From Performance Limits Tests

For polybutadiene over the range of frequencies, temperatures and strains tested, the following conclusions are drawn. It should be noted that the ranges of frequency and strain tested are likely to encompass the demands of a large body of high-speed rotating machinery applications and that the high temperature and strain values reach the likely capacity of the material tested.

- Strain strongly influences component stiffness and damping
- Stiffness reduces by up to a factor of 3 over the range of strains tested; loss coefficient increases by a factor of up to 2.5.
- Strain has a stronger influence than frequency on the dynamic characteristics.
- Variation of dynamic characteristics with strain as an independent variable is more uniform than the variation with frequency.
- Internal temperature rise does not alone cause the variation in dynamic characteristics which is observed.
- Damage resulting from internal temperature rise could be caused by high strain and should be accounted for in imposing limiting operational amplitudes.
- Prediction of a previously developed thermo-viscoelastic analysis which considers strain dependence due only to thermally induced changes in internal properties does not predict the strong observed strain dependence of stiffness and damping.
- The thermo-viscoelastic analysis provides a conservative prediction of internal peak temperatures which can be satisfactorily used in establishing amplitude limits.

B. Conclusions From Design and Testing of an Elastomer Damper

Elastomer bearing mounts have successfully controlled synchronous whirl amplitude for a flexible rotor which traverses two bending critical speeds. These mounts were designed in the form of inexpensive, easily replaced cartridges which allowed two elastomer types (representing high and low loss coefficient types) to be tested. The cartridge mounting system also allowed solid steel blocks to be substituted for the elastomers in order to create a hard-mounted condition. It is to be noted that this evaluation of an elastomer damper was pursued in parallel with the elastomer performance limits tests.

Balancing the test rig on elastomer dampers was straightforward and presented no unique problems, and unbalance response was acceptably linear for the range of conditions tested. The system damping provided by these elastomers was well in excess of predictions. In addition, it was observed that elastomeric mounts are tolerant of small misalignments.

C. Recommendations

Based on the preceding conclusions, the following recommendations are made:

- Elastomer component design analysis should account for effects of strain and temperature.
- Both changes in dynamic characteristics and internal temperature rise should be accounted for.
- Elastomer material and component tests should be designed to encompass the expected range of strains and temperatures.
- Further component testing should be undertaken with different materials to identify consistency with or deviations from present conclusions.
- Future component tests should investigate long-term performance limits in a vibration environment.
- The effect of other environmental factors on dynamic performance, in particular, the presence of oil and fuel, should be investigated.
- The ability of elastomers to control vibrations in rig with significant nonsynchronous components should be evaluated.
- The rotor system dynamic model for the gas turbine dynamic simulator should be modified to include angular support stiffness and damping in an effort to reflect in the predictions the unexpectedly high level of system damping measured for the elastomeric dampers.
- Applications design and tests of elastomer dampers should be performed; for example, in a helicopter gas turbine engine and a cruise missile engine.

APPENDIX A

PROPERTIES OF POLYBUTADIENE MATERIAL NICHOLLS NEX 156G

Reproduced in part from a report by

Rubber and Plastics Research Association
of Great Britain, Author Paul Howgate

A. Introduction

This report covers work done at RAPRA to determine the following properties of Nicholls NEX 156G Polybutadiene.

(a) Thermal conductivity 20°C to 100°C
(b) Coefficient of expansion 20°C to 90°C
(c) Specific heat 50°C to 100°C and Tg
(d) T_S by iterative determination for use in the "method of reduced variables"
(e) Chemical analysis of Polymer, Black content, volatiles and non volatiles

Each section of the work is reported in turn below.

B. Thermal Conductivity

Thermal conductivity over the temperature range 20°C (ambient) to 100°C was determined using an apparatus developed by RAPRA. A full description of the apparatus and the measurement technique is given in reference A-1.

The graph of thermal conductivity versus temperature, Figure A-1, is given at the end of this report

C. Coefficient of Thermal Expansion

Coefficient of thermal expansion was measured by heating a strip sheet sample, 2" x 6", in a water bath over the range 20°C to 90°C. Three vertical and three horizontal sets of lines were marked on the sample and the distance between those lines measured at approximately 10°C intervals of temperature. Graphs of change in length versus temperature were plotted and the best straight line constructed through the points. Values of coefficient of expansion given by the following expression:

$$\text{coefficient of expansion} = \frac{\Delta \ell}{\ell \ \Delta T}$$

where $\Delta \ell$ is the change in length for the corresponding change in temperature ΔT; ℓ is the original length between the marked lines

were evaluated for the six graphs. Each set of horizontal and vertical data was averaged and the results are given below.

Coefficient of expansion Nicholls NEX 156G

"Horizontal" direction	2.4×10^{-5} per °C
"Vertical" direction	2.1×10^{-5} per °C

estimated error, and typical scatter in the raw data provides an error figure of ± 4°C. Since the difference between the two directions is some 14 percent, anistropy exists within the moulded sheet used. However, since no indication of direction was given on the sheets supplied, no further conclusions can be drawn.

D. Specific Heat and Tg

Specific heat over the temperature range 50°C to 100°C and the glass transition temperature Tg were determined using the Perkin Elmer differential scanning calorimeter. Details of the equipment and techniques of tests are given in reference A-2. Values of specific heat are given in Figure A-2 at the end of this report.

The glass transition temperature Tg proved too difficult to measure accurately by this method. The inflections occurring at the four scan rates used were too small and ill-defined to provide a sensible value for Tg. The best defined transition occurred in the range 180°K to 270°K but further extrapolation of this data is unwise. An explanation of this effect is given in the discussion at the end of this report.

E. Ts by Iterative Determination

Ts the "reference" temperature is defined by the WLF equation:

$$(\log)_{10}\ \alpha_T = \frac{C_1(T-Ts)}{C_2+T-Ts} \qquad \text{(A-1)}$$

where C_1 and C_2 are constants

T is the temperature of test
Ts is the reference temperature
α_T is the "shift factor" in Hz

This equation can be used to determine the shift of dynamic mechanical data at a particular temperature to align with data at a different temperature to produce a master curve of reduced frequency at a single temperature. Whilst this method has been used with some success to provide data at frequencies a few decades outside the testing range of a particular piece of equipment, the main advantage is the convenient presentation of the data as a single curve of any one parameter.

The iterative technique necessary to produce the shift factors and hence the master curve has been outlined by a number of authors (refs. A-3, A-4, and A-5). There are two basic methods of deriving shift factor values. Both require dynamic mechanical data to be plotted versus frequency (strain rate) at various temperatures, and a by eye shift of the graphs to align to a smooth curve.

The first method then requires a guess to be made at Ts, usually based upon knowledge of Tg, and the shift factor from Ts plotted versus temperature. A graph of calculated shift factor from the equation,

$$(\log)_{10}\ \alpha_T = \frac{8.86\ (T-Ts)}{101.6+T-Ts} \qquad (A-2)$$

is plotted versus temperature T and compared with the measured shift factor curve. Ts is varied iteratively until a good fit between calculated and observed is obtained.

The second method is more useful where high filler loadings are present (ref. A-5). Ts is chosen either as in the first method or as some convenient temperature. Shift factor from the data is again plotted and compared with calculated values from the equation:

$$(\log)_{10}\ \alpha_T = \frac{C_1(T-Ts)}{C_2+T-Ts} \qquad (A-1)$$

where C_1 and C_2 (and if necessary Ts) are evaluated for best fit by iterative numerical techniques.

Data on the chemical analysis (see section F) showed the carbon black level for Nicholls NEX 156G to be high and the first method did not provide an adequate fit. The second method provided values of C_1, C_2 and Ts for this material as shown by the equation below:

$$(\log)_{10}\ \alpha_T = \frac{7.48\ (T-268.1)}{90.7+T-268.1} \qquad (A-3)$$

hence, $C_1 = 7.48$, $C_2 = 90.7$, and $Ts = 268.1°K$

Data presented in Figures A-3 and A-4 show $\log\alpha_T$ versus temperature, and corrected complex modulus versus frequency at Ts.

The data was produced using RAPRA's Keelavite servohydraulic dynamic test facility under the conditions set out below.

Dynamic test conditions Nicholls NEX 156G

Frequency range	0.003 Hz to 30 Hz
Control mode	displacement
dynamic amplitude	±0.05 compression strain
static prestrain	+.15
temperature range	+30°C to -30°C, approximately
structuring	+0.1 20 cycles at 40°C before commencement of testing
sample dimensions	2.54 cms diameter of 0.65 cms high

Modulus figures are dynamic shape factor corrected and transposed to reduce values of Ts (ref. A-4)

F. Chemical Analysis

The chemical analysis of Nicholls NEX 156G involved four steps

(a) An acetone extraction of the "volatile" materials giving the percentage volatiles

(b) Infra-red spectrum analysis of the polymer pyrolisate to give polymer type

(c) Nitrogen furnace extraction of polymer and volatiles to give percentage polymer content
(d) Muffle furnace extraction of carbon black to give percentage of carbon black and residual ash (non-volatiles).

The percentage composition of Nicholls NEX 156G is given in the table below:

Polymer content	48.0%
Carbon black content	35.9%
Non volatiles	6.9%
Volatiles	9.2%

Polymer type identified as Polybutadiene.

G. Summary of Properties, Nicholls NEX 156G

Thermal conductivity average 20° to 100°C		0.25 W/mK
Coefficient of thermal expansion average		2.2×10^{-5} per °C
Specific heat average 50°C to 100°C		1.58 J/gK
WLF equation values	C_1	7.48
	C_2	90.7
	T_s	268.1

For dynamic characteristics refer to Figure A-4

Chemical analysis	polymer type	Polybutadiene
	polymer content	48.0%
	carbon black content	35.9%
	non volatiles	6.9%
	volatiles	9.2%

H. Discussion

The problems encountered with measurement of Tg and the shift factor fit by varying Ts alone are both symptomatic of a high black content material as borne out by the chemical analysis. Thermal conductivity is high as is the value of damping factor, tan δ, in the rubbery region, also implying a high black loading. These factors combine to produce a flattening of the classical WLF equation curve versus temperature by virtue of the "diluting" effect of carbon black on polymer mechanical properties. This diluting effect logically shows up as a smoothing of the inflections of the calorimeter trace when determining Tg and hence explains the difficulty experienced. The $\log_{\alpha_T}$ versus temperature fit with the observed data is extremely good once the correct values of C_1 and C_2 are evaluated. The scatter produced on the dynamic data by the method of reduced variables is quite small and certainly within tolerance for the method. RAPRA has found good correlation with data at high frequencies (up to 10 KHz) obtained by this method and practice, for lightly filled (up to 50 parts per hundred rubber(pphr) carbon black) elastomers. It is therefore unwise to extrapolate these data for high tolerance applications.

Shift factor, or more correctly its derivative, does give additional information relating to the temperature sensitivity of the material. A high derivative shift factor expressed in degrees centigrade per decade of frequency is an advantage in practical applications particularly where the shape of the dynamic properties versus frequency curve is important. This parameter can

be obtained from the slope of the $\log_{a_T}$ curve versus temperature. The lower the slope (negative) the higher the temperature - frequency insensitivity.

From the thermal expansion data Nicholls NEX 156G appears to be prone to moulding anistropy and hence the moulding technique for high tolerance products should be chosen with care.

Assuming the volatiles content to be primarily oil, some reduction in the amount of carbon black used (with a consequent cost increase) could be achieved at the same stiffness level.

Dynamic strain dependency of properties has not been covered in this report and whilst the effect is likely to be significant with this level of carbon black its importance depends upon the ultimate application.

APPENDIX B

TABULATION OF TEMPERATURE RESULTS FOR INSTRUMENTED COMPRESSION SPECIMENS

Amplitude Number

Thermocouple Number	1	2	3	4	5	6	7	8	9	10	11
1	30.8	30.7	30.6	30.6	30.6	30.6	30.7	30.9	31.4	33.1	37.2
2	31.4	31.3	31.3	31.3	31.1	31.1	31.1	31.2	31.3	31.9	32.6
3	30.7	30.6	30.5	30.5	30.5	30.5	30.7	30.9	31.3	33.3	37.9
4	31.3	31.2	31.3	31.2	31.1	31.2	31.1	31.1	31.3	31.8	32.6
5	30.6	30.6	30.4	30.3	30.4	30.5	30.6	30.7	31.3	33.4	38.5
6	31.4	31.4	31.2	31.3	31.2	31.2	31.1	31.3	31.4	32.0	32.8
7	31.0	30.9	30.9	30.9	31.0	31.3	31.6	32.5	34.0	43.5	58.5
8	31.0	30.9	30.8	31.1	31.2	32.0	32.7	34.6	37.9	59.8	88.9
9	31.4	31.3	31.3	31.3	31.4	31.8	32.1	33.0	34.7	45.4	61.0
10	30.3	30.2	30.3	30.2	30.3	30.7	31.1	32.6	34.9	49.3	75.8
11	31.2	31.1	31.2	31.3	31.5	32.2	32.9	34.6	37.8	58.0	89.5
12	30.6	30.6	30.6	30.7	30.9	31.5	32.1	33.6	36.5	53.7	77.7
13	31.3	31.3	31.3	31.3	31.3	31.6	31.9	32.5	33.7	40.9	50.9
14	30.7	30.6	30.6	30.8	31.0	31.6	32.4	34.3	37.6	58.0	82.8
15	30.8	30.7	30.6	30.7	30.9	31.3	31.7	32.8	34.8	46.6	65.0
16	31.2	31.2	31.1	31.1	31.2	31.6	32.0	32.8	34.5	44.4	56.9
17	30.9	30.9	30.9	31.1	31.2	32.1	33.0	35.0	38.6	61.3	93.4
18	30.5	30.5	30.4	30.6	30.9	31.7	32.5	34.7	38.5	61.7	93.3
19	23.2	23.2	23.0	23.1	23.1	23.0	23.0	23.5	24.0	24.1	23.5
20	30.7	30.7	30.6	30.9	31.1	31.7	32.3	33.9	36.9	55.7	81.8

Table B-1 Recorded Temperature as a Function of Thermocouple No. and Amplitude No. (see Figs. 7 and 8, Table 3 for definitions). Instrument Compression Specimen, Frequency = 170 Hz.

Amplitude Number

Thermocouple Number	1	2	3	4	5	6	7	8	9	10	11
1	31.2	31.2	31.4	31.5	31.6	31.6	31.9	32.1	32.6	39.8	47.0
2	31.5	31.6	31.9	31.9	32.0	32.1	32.2	32.3	32.4	32.5	33.6
3	31.0	31.1	31.2	31.3	31.4	31.6	31.8	32.1	32.5	40.0	47.3
4	31.5	31.7	31.8	31.9	32.0	32.0	32.2	32.3	32.4	32.4	33.6
5	30.9	31.0	31.1	31.3	31.3	31.5	31.7	31.9	32.5	40.2	47.7
6	31.6	31.5	31.8	31.9	32.1	32.1	32.2	32.3	32.5	32.6	33.7
7	31.3	31.4	31.5	31.7	31.9	32.4	32.9	33.8	35.7	51.6	67.2
8	31.1	31.3	31.5	31.8	32.0	33.0	33.9	35.8	39.5	68.4	95.9
9	31.6	31.7	31.8	32.1	32.3	32.8	33.3	34.2	36.1	50.2	64.2
10	30.4	30.5	30.8	31.1	31.3	31.9	32.7	33.7	36.6	60.0	80.8
11	31.5	31.7	31.8	32.2	32.5	33.4	34.3	36.2	39.8	68.6	96.5
12	31.0	31.1	31.3	31.6	31.7	32.4	33.1	34.5	37.3	62.1	85.7
13	31.6	31.7	31.8	32.0	32.2	32.6	33.0	33.8	35.1	44.0	53.2
14	31.0	31.1	31.4	31.7	31.9	33.0	34.0	35.9	39.8	66.3	90.6
15	31.2	31.3	31.5	31.7	31.9	32.5	33.0	34.3	36.6	56.0	73.6
16	31.4	31.6	31.7	32.0	32.1	32.7	33.2	34.2	36.1	48.5	60.3
17	31.3	31.4	31.6	32.1	32.4	33.5	34.5	36.8	41.0	71.9	102.2
18	31.0	31.1	31.4	31.7	32.0	33.2	34.2	36.4	40.7	71.4	101.4
19	23.7	23.7	23.6	23.8	23.8	23.8	23.8	23.7	23.7	23.2	23.1
20	31.3	31.4	31.6	32.0	32.1	32.9	33.6	35.1	38.1	63.6	87.4

Table B-2 Recorded Temperature as a Function of Thermocouple No. and Amplitude No. (see Figs. 7 and 8, Table 3 for definitions). Instrument Compression Specimen, Frequency = 200 Hz.

Thermocouple Number	Amplitude Number										
	1	2	3	4	5	6	7	8	9	10	11
1	32.3	32.2	32.3	32.3	32.3	32.4	32.6	32.9	33.5	46.4	50.7
2	32.8	32.9	32.9	32.9	32.9	32.8	32.9	33.0	33.0	33.3	34.4
3	32.2	32.2	32.2	32.3	32.3	32.3	32.5	32.9	33.5	46.5	51.2
4	32.8	32.8	32.9	32.9	32.8	32.8	32.8	32.9	33.0	33.3	34.3
5	32.1	32.1	32.1	32.1	32.2	32.3	32.5	32.9	33.4	46.7	51.3
6	32.8	32.9	32.9	32.9	32.9	32.9	33.0	32.9	33.1	33.4	34.6
7	32.5	32.5	32.6	32.7	32.8	33.4	34.0	35.3	37.5	58.9	74.3
8	32.4	32.4	32.5	32.9	33.1	34.4	35.6	38.4	43.0	75.6	108.6
9	32.8	32.9	32.9	33.1	33.3	33.9	34.5	35.9	38.1	53.8	70.6
10	31.6	31.9	31.8	32.1	32.2	33.1	33.8	35.6	38.7	65.2	88.9
11	32.7	32.7	32.8	33.2	33.5	34.7	35.7	38.2	42.3	75.1	107.8
12	32.1	32.2	32.2	32.6	32.7	33.6	34.5	36.5	39.7	68.4	93.5
13	32.8	32.8	32.9	33.0	33.1	33.5	33.8	34.7	36.0	46.1	56.6
14	32.2	32.2	32.3	32.7	32.9	34.0	35.1	37.6	41.4	73.1	100.8
15	32.3	32.3	32.5	32.6	32.8	33.4	34.1	35.5	37.9	63.0	81.1
16	32.7	32.7	32.8	32.9	33.1	33.6	34.1	35.3	37.2	51.7	65.4
17	32.5	32.5	32.7	33.0	33.3	34.7	36.0	38.9	43.5	80.4	116.8
18	32.2	32.2	32.3	32.7	33.0	34.4	35.6	38.7	43.4	79.4	115.9
19	23.9	24.1	24.1	24.1	24.2	24.1	24.2	24.2	24.1	22.9	23.7
20	32.5	32.5	32.6	32.8	33.1	34.1	35.1	37.4	41.0	69.6	99.5

Table B-3 Recorded Temperature as a Function of Thermocouple No. and Amplitude No. (see Figs. 7 and 8, Table 3 for definitions). Instrument Compression Specimen, Frequency = 250 Hz.

Amplitude Number

Thermocouple Number	1	2	3	4	5	6	7	8	9	10	11
1	32.8	32.5	32.3	32.2	32.2	32.3	32.5	32.8	33.3	50.3	54.2
2	32.9	32.9	32.8	32.8	32.7	32.7	32.7	32.7	32.8	34.2	35.3
3	32.6	32.3	32.3	32.2	32.2	32.2	32.4	32.8	33.3	50.4	54.5
4	32.9	32.8	32.8	32.8	32.6	32.6	32.6	32.6	32.6	34.2	35.2
5	32.5	32.3	32.1	32.1	32.1	32.1	32.4	32.7	33.2	50.6	55.0
6	32.9	32.9	32.8	32.8	32.8	32.7	32.7	32.8	32.8	34.4	35.6
7	32.9	32.6	32.6	32.7	32.8	33.4	34.2	35.6	38.2	64.7	82.6
8	32.6	32.5	32.5	33.0	33.3	34.6	36.1	39.3	44.6	85.0	125.1
9	32.9	32.9	32.9	33.1	33.2	33.9	34.6	36.1	38.8	58.7	79.0
10	32.0	31.6	31.7	32.0	32.4	33.0	33.9	36.0	39.4	70.8	96.3
11	32.9	32.8	32.8	33.2	33.6	34.8	36.0	38,8	43.5	82.4	119.2
12	32.5	32.3	32.2	32.6	32.8	33.6	34.6	36.6	40.3	72.6	96.7
13	32.9	32.9	32.8	33.0	33.1	33.4	33.7	34.6	36.1	47.9	58.3
14	32.4	32.2	32.2	32.7	33.0	34.1	35.2	37.9	42.3	79.1	108.5
15	32.6	32.4	32.4	32.6	32.8	33.4	34.1	35.7	38.3	67.9	87.0
16	32.8	32.6	32.7	32.9	33.0	33.6	34.1	35.3	37.5	54.8	69.4
17	32.7	32.6	32.6	33.0	33.5	34.9	36.3	39.5	44.9	88.9	130.5
18	32.3	32.3	32.3	32.8	33.2	34.6	36.0	39.3	44.8	88.0	129.9
19	24.1	24.1	24.0	24.0	24.0	23.8	23.7	23.6	23.6	24.0	23.6
20	32.6	32.5	32.6	32.9	33.2	34.3	35.4	38.0	42.4	79.1	117.0

Table B-4 Recorded Temperature as a Function of Thermocouple No. and Amplitude No. (see Figs. 7 and 8, Table 3 for definitions). Instrument Compression Specimen, Frequency = 300 Hz.

Thermocouple Number	Amplitude Number										
	1	2	3	4	5	6	7	8	9	10	11
1	31.3	31.3	31.2	31.1	31.2	31.4	31.6	31.8	32.4	54.0	54.9
2	31.9	31.9	31.8	31.7	31.7	31.6	31.7	31.7	31.8	34.8	35.6
3	31.2	31.2	31.1	31.0	31.1	31.2	31.4	31.7	32.5	54.1	55.3
4	31.9	31.8	31.8	31.7	31.7	31.6	31.7	31.7	31.8	34.7	35.7
5	31.2	31.1	31.0	31.0	31.0	31.2	31.4	31.7	32.5	54.1	56.0
6	32.0	31.9	31.8	31.8	31.8	31.7	31.6	31.8	32.0	35.0	36.0
7	31.5	31.5	31.5	31.6	31.8	32.6	33.2	34.9	37.9	68.9	80.7
8	31.4	31.4	31.5	32.0	32.3	34.0	35.4	39.0	45.4	90.3	96.6
9	31.9	31.9	31.9	32.1	32.2	33.1	33.8	35.5	38.7	61.5	62.8
10	30.8	30.7	30.7	31.1	31.3	32.4	33.3	35.6	39.4	73.6	65.4
11	31.8	31.7	31.8	32.2	32.5	34.1	35.3	38.4	43.8	86.3	68.8
12	31.2	31.2	31.2	31.5	31.8	32.9	33.8	36.1	39.9	75.1	59.0
13	31.9	31.8	31.8	31.9	32.0	32.5	32.9	33.8	35.3	48.9	41.4
14	31.3	31.1	31.2	31.6	31.9	33.3	34.5	37.4	42.4	83.0	56.7
15	31.4	31.3	31.3	31.5	31.6	32.5	33.2	35.0	38.0	71.8	57.5
16	31.8	31.7	31.7	31.9	32.0	32.6	33.2	34.7	37.0	56.8	42.2
17	31.5	31.5	31.6	32.1	32.5	34.2	35.6	39.2	45.4	94.9	54.6
18	31.1	31.1	31.2	31.7	32.1	33.8	35.3	39.0	45.4	94.0	51.1
19	23.3	23.3	23.2	23.3	23.2	23.2	23.2	23.3	23.2	23.2	22.9
20	31.5	31.5	31.6	31.9	32.3	33.6	34.7	37.6	42.9	84.8	45.0

Table B-5 Recorded Temperature as a Function of Thermocouple No. and Amplitude No. (see Figs. 7 and 8, Table 3 for definitions). Instrument Compression Specimen, Frequency = 325 Hz.

Amplitude Number

Thermocouple Number	1	2	3	4	5	6	7	8	9	10	11
1										51.0	
2										34.9	
3	23.4	23.4	23.9	24.2	24.5	24.3	24.0		23.8	51.0	
4	30.5	30.7	31.1	31.5	31.9	32.4	33.3		34.2	35.0	
5										51.4	
6										35.4	
7	30.6	30.8	31.3	31.9	32.6	33.9	35.7		41.5	69.0	
8	30.3	30.5	31.1	32.1	33.0	35.5	38.3		50.0	97.8	
9	30.6	30.9	31.4	32.1	32.7	34.2	36.0		42.2	65.3	
10	29.9	30.2	30.4	31.4	32.1	34.0	36.1		44.4	67.3	
11										78.6	
12	30.4	30.7	31.2	32.0	32.6	34.6	36.5		44.8	63.9	
13	30.7	31.0	31.4	32.1	32.6	33.8	35.3		39.8	45.0	
14	30.1	30.5	31.1	32.1	32.9	35.3	37.8		48.7	87.4	
15										72.2	
16										59.4	
17										112.0	
18	30.3	30.6	31.2	32.5	33.3	36.2	39.2		52.0	115.5	
19										23.1	
20	30.6	30.9	31.4	32.3	33.1	35.2	37.6		46.9	110.9	

Table B-6 Recorded Temperature as a Function of Thermocouple No. and Amplitude No. (see Figs. 7 and 8, Table 3 for definitions). Instrument Compression Specimen, Frequency = 400 Hz.

Thermocouple Number	Amplitude Number										
	1	2	3	4	5	6	7	8	9	10	11
1	35.0	33.6	33.0	32.7	32.7	32.8	33.2	33.6	34.6	52.1	
2	33.2	33.0	32.9	33.0	33.0	33.0	33.1	33.2	33.4	35.7	
3	34.8	33.4	32.9	32.7	32.6	32.8	33.1	33.6	34.7	52.4	
4	33.1	33.0	32.9	32.9	32.9	33.0	33.0	33.1	33.3	35.6	
5	34.5	33.3	32.8	32.6	32.6	32.6	33.1	33.6	34.8	52.5	
6	33.1	33.0	33.0	33.0	33.0	33.0	33.1	33.1	33.4	35.9	
7	34.6	33.5	33.1	33.3	33.5	34.5	35.4	37.6	41.7	70.8	
8	33.7	33.1	32.9	33.6	34.0	36.3	38.3	42.9	51.4	83.8	
9	33.4	33.1	33.1	33.5	33.7	34.9	35.8	38.2	42.2	56.6	
10	32.7	32.3	32.1	32.7	33.0	34.5	35.9	39.0	44.6	64.0	
11	34.0	33.4	33.3	34.0	34.4	36.6	38.4	42.8	50.4	66.2	
12	34.0	33.2	32.9	33.2	33.5	35.1	36.4	39.6	44.8	60.1	
13	33.3	33.1	33.1	33.3	33.5	34.2	34.9	36.5	39.0	42.7	
14	33.3	32.8	32.7	33.2	33.5	35.4	36.9	41.0	47.8	54.9	
15	34.2	33.0	33.0	33.3	33.5	34.7	35.8	38.4	42.8	54.6	
16	33.2	33.2	33.0	33.3	33.5	34.5	35.5	37.6	41.2	41.7	
17	33.8	32.9	33.2	33.9	34.3	36.8	38.8	43.9	52.2	51.0	
18	33.3	32.8	32.8	33.6	34.0	36.5	38.5	43.6	52.0	47.9	
19	25.1	25.1	25.1	25.0	25.1	25.1	25.1	25.1	25.1	23.7	
20	33.2	33.3	32.8	33.4	33.8	35.4	36.9	40.5	47.1	42.4	

Table B-7 Recorded Temperature as a Function of Thermocouple No. and Amplitude No. (see Figs. 7 and 8, Table 3 for definitions). Instrument Compression Specimen, Frequency = 450 Hz.

Amplitude Number

Thermocouple Number	1	2	3	4	5	6	7	8	9	10	11
1											
2											
3	24.5	24.4	24.2	24.0	23.9	23.8	23.6		24.3		
4	34.7	34.6	34.5	34.5	34.4	34.4	34.5		35.4		
5											
6											
7	34.4	34.3	34.4	34.6	34.9	35.9	37.0		44.5		
8	33.9	33.9	34.0	34.7	35.4	37.8	40.1		54.2		
9	34.6	34.6	34.7	35.0	35.4	36.5	37.6		44.5		
10	32.9	32.7	32.7	33.2	33.4	35.1	36.6		45.9		
11											
12	34.0	33.9	33.9	34.4	34.6	36.2	37.7		46.3		
13	34.8	34.8	34.8	34.9	35.1	35.9	36.6		41.3		
14	33.6	33.6	33.7	34.4	34.8	36.9	38.8		49.8		
15											
16											
17											
18	33.9	33.9	34.1	34.9	35.5	37.9	40.3		53.3		
19											
20	34.6	34.5	34.6	35.1	35.5	37.3	39.0		49.5		

Table B-8 Recorded Temperature as a Function of Thermocouple No. and Amplitude No. (see Figs. 7 and 8, Table 3 for definitions). Instrument Compression Specimen, Frequency = 500 Hz.

Amplitude Number

Thermocouple Number	1	2	3	4	5	6	7	8	9	10	11
1	31.5	31.2	31.1	31.0	31.1	31.4	32.0	32.7			
2	31.7	31.6	31.6	31.4	31.6	31.8	31.9	32.0			
3	31.4	31.1	30.9	30.9	31.0	31.3	32.0	32.6			
4	31.6	31.5	31.4	31.4	31.5	31.8	31.9	32.0			
5	31.3	31.0	30.8	30.8	30.9	31.3	32.0	32.8			
6	31.6	31.6	31.6	31.4	31.6	31.9	31.9	32.0			
7	31.6	31.3	31.3	31.7	32.2	33.9	35.6	38.8			
8	31.3	31.2	31.3	32.4	33.4	38.0	41.7	49.5			
9	31.6	31.6	31.7	32.2	32.6	35.0	36.6	40.4			
10	30.6	30.7	30.7	31.4	31.9	34.4	36.2	39.8			
11	31.5	31.6	31.6	32.5	33.3	36.7	39.2	44.3			
12	31.2	31.1	31.1	31.6	32.0	33.6	35.0	38.6			
13	31.6	31.6	31.6	31.8	31.9	32.9	33.4	34.8			
14	31.1	31.0	31.2	31.8	32.3	34.4	35.9	41.1			
15	31.3	31.2	31.2	31.5	31.9	33.2	34.4	37.5			
16	31.5	31.4	31.5	31.7	32.1	33.2	34.0	36.4			
17	31.4	31.4	31.4	32.4	33.2	36.1	38.5	45.4			
18	31.0	31.0	31.1	32.2	33.0	35.9	38.2	45.5			
19	23.1	23.0	23.0	23.4	24.2	23.6	23.3	23.3			
20	31.3	31.3	31.4	32.3	33.1	36.9	40.0	48.3			

Table B-9 Recorded Temperature as a Function of Thermocouple No. and Amplitude No. (see Figs. 7 and 8, Table 3 for definitions). Instrument Compression Specimen, Frequency = 550 Hz.

Amplitude Number

Thermocouple Number	1	2	3	4	5	6	7	8	9	10	11
1	31.5	31.4	31.5	31.7	32.0	32.5	33.3	33.9	34.1		
2	31.8	31.7	31.8	32.1	32.3	32.4	32.7	33.0	33.2		
3	31.4	31.3	31.4	31.7	32.0	32.4	33.3	34.0	34.2		
4	31.8	31.3	31.8	32.0	32.2	32.4	32.6	32.9	33.2		
5	31.3	31.3	31.4	31.6	32.0	32.5	33.2	33.9	34.3		
6	31.8	31.7	31.9	32.1	32.2	32.5	32.7	33.0	33.2		
7	31.6	31.5	31.8	32.5	33.1	35.2	36.8	39.1	43.1		
8	31.4	31.5	31.8	33.3	34.4	38.7	41.4	45.8	55.2		
9	31.9	31.8	32.0	32.8	33.5	35.6	37.0	39.1	43.7		
10	31.0	31.0	31.4	32.5	33.3	36.0	38.0	41.2	48.0		
11	31.8	31.6	32.2	33.5	34.6	38.6	41.1	45.8	55.1		
12	31.3	31.3	31.7	32.5	33.2	35.6	37.6	42.1	49.3		
13	31.8	31.7	32.0	32.6	33.0	34.3	35.3	37.7	41.4		
14	31.1	31.1	31.5	32.6	33.4	35.7	38.4	44.5	53.0		
15	31.5	31.4	31.7	32.5	33.1	34.6	36.5	40.4	45.7		
16	31.7	31.6	31.9	32.5	33.0	34.4	35.8	39.2	43.9		
17	31.6	31.6	32.0	33.3	34.3	37.2	40.1	47.5	57.5		
18	31.3	31.3	31.7	33.1	34.0	36.9	39.6	47.2	57.3		
19	25.2	25.2	25.2	25.3	25.4	25.2	25.2	25.1	25.1		
20	31.5	31.5	31.9	32.9	33.7	36.2	38.1	42.6	49.6		

Table B-10 Recorded Temperature as a Function of Thermocouple No. and Amplitude No. (see Figs. 7 and 8, Table 3 for definitions). Instrument Compression Specimen, Frequency = 600 Hz.

APPENDIX C

RUN LOG - TEST OF ELASTOMER MOUNTED ROTOR

Run #	Unbalance	Comments
P1	N.A.*	First run, no tape, plots or balance attempt.
P2	N.A.	Probes 1 and 7 plotted at 7,500 rpm got high vibration.
P3	N.A.	Balance run at 7,000 rpm, plane 1; .8, 1.5, .34 gm wts in holes 11, 12, 13 calculated.
P4	N.A.	P3 weights in; plotted probes 1 and 7.
P5	N.A.	Balance run at 7,000 rpm; .275 gm in hole 7, plane 1.
P6	N.A.	P5 weights in; plotted probes 1 and 7.
P7	N.A.	Balance run at 7,000 rpm; .20 gm hole 5, plane 1.
P8	N.A.	P7 weights in; plotted probes 1 and 7.
P9	N.A.	Installed larger vacuum pump; run to 23,157 rpm.
P10	N.A.	Balance run at 11,500 rpm; .172 gm hole 34, plane 1.
P11	N.A.	P10 weights in; balance run at 11,500 rpm; calculated weight of .058 gm plane 1, too small to install.
P12	N.A.	P10 weights in; plotted probes 1 and 7; ran to 23,073 rpm.
P13	N.A.	Official base case (taped).
P14	.2 gm at 0°, plane 1	
P15	.3 gm at 0°, plane 1	Maximum speed = 22,230 rpm.
P16	.4 gm at 0°, plane 1	
P17	.5 gm at 0°, plane 1	Maximum speed = 22,274 rpm.

*Not Available

RUN LOG - TEST OF ELASTOMER MOUNTED ROTOR (Cont'd)

Run #	Unbalance	Comments
P18	.19 gm at hole 11, plane 3.	Very little response.
P19	.19 gm at hole 11, plane 3. .20 gm at hole 11, plane 4	Maximum speed = 21,645 rpm.
P20	Same as P19	Air leak repaired
P21	.19 gm at holes 11 & 12, plane 3. .20 & .19 gm at holes 11 & 12, plane 4	Maximum speed = 24,162 rpm
P22	N.A.	Base Case rerun n_{max} = 24,518 rpm
P23	.1873, .183, .1821, .1921 gm at holes 11, 12, 1, 2, plane 3	n_{max} = 23,400 rpm
P24	.1873, .183, .1821 gm at holes 11, 12, 1, plane 3	n_{max} = 22,250 rpm
P25	.183, .1821 gm at holes 12 and 1, plane 3	n_{max} = 22,600 rpm
P26	.183 gm at hole 12, plane 3	n_{max} = 22,730 rpm
P27	.2 gm at 0°, plane 1	n_{max} = 22,600 rpm
P28	.3 gm at 0°, plane 1	n_{max} = 22,700 rpm
V1	N.A.	n_{max} = 24,000 rpm, base case
V2	.2 gm at 0°, plane 1	
V3	.3 gm at 0°, plane 1	
V4	.4 gm at 0°, plane 1	Amp set wrong, not taped
V5	.5 gm at 0°, plane 1	Amp set wrong, not taped
V5'	Same as V5	
V4'	Same as V4	

RUN LOG - TEST OF ELASTOMER MOUNTED ROTOR (Cont'd)

Run #	Unbalance	Comments
V6	N.A.	n_{max} = 24,000 rpm, base case
V7	.1873 gm at hole 11, plane 3	n_{max} = 24,475 rpm
V8	.1873, .183 gm at holes 11 and 12, plane 3	n_{max} = 24,450 rpm
V9	.1873, .183, .1826 gm at holes 11, 12, and 1, plane 3	n_{max} - 24,700 rpm
V10	.1873, .183, .1826, .1921 gm at holes 11, 12, 1, and 2, plane 3	Not taped
V11	.5 gm at 0°, plane 1	Viton dampers reinstalled in different locations this run to warm them.
V12	.1873, .183, .1821, .1921 gm at holes 11, 12, 1, 2, plane 3	n_{max} = 27,350 rpm this run after steel block runs.
V13	N.A.	Base case. n_{max} = 27,200 rpm
S1	N.A.	Base case blocks loosened. n_{max} = 22,900 rpm.
S2	N.A.	Base case blocks loosened. n_{max} = 25,000 rpm.
S3	.2 gm at 0°, plane 1	n_{max} = 23,500 rpm, past 2 criticals.
S4	.4 gm at 0°, plane 1	Past 2 criticals.
SS1	N.A.	Could not pass critical.
VS1	N.A.	Viton in turbine end. Steel in disk end.
VS2	N.A.	Repeat of run VS1.
VS3	.4 gm at 0°, plane 1	Could not pass critical.
VS4	.2 gm at 0°, plane 1	Passed thru one critical.

REFERENCES

1. Cundiff, R.A., Badgley, R.H., "Pneumomechanical Critical Speed Control for Gas Turbine Engine Shafts", USAF Report AFAPl-TR-101, AD 772805.

2. Chiang, T., Tessarzik, J.M., and Badgley, R.H., "Development of Procedures for Calculating Stiffness and Damping Properties of Elastomers in Engineering Applications, Part I: Verification of Basic Methods", NASA Report CR-120905, March 1972. Prepared by MTI for NASA-Lewis Research Center under Contract NAS3-15334.

3. Gupta, P.K., Tessarzik, J.M., and Cziglenyi, L., "Development of Procedures for Calculating Stiffness and Damping Properties of Elastomers in Engineering Applications, Part II: Elastomer Characteristics at Constant Temperature", NASA Report CR-134704. Prepared by MTI for NASA-Lewis Research Center under Contract NAS3-15334, April 1974.

4. Smalley, A.J., and Tessarzik, J.M., "Development of Procedures for Calculating Stiffness and Damping Properties of Elastomers in Engineering Applications, Part III: The Effects of Temperature, Dissipation Level and Geometry", NASA Report CR-134939. Prepared by MTI for NASA-Lewis Research Center under Contract NAS3-15334, and Contract NAS3-18546, November 1975.

5. Darlow, M.S., and Smalley, A.J., "Development of Procedures for Calculating Stiffness and Damping Properties of Elastomers in Engineering Applications, Part IV: Testing of Elastomers Under a Rotating Load", NASA Report CR-135355. Prepared by MTI for NASA-Lewis Research Center under Contract NAS3-18546, November 1977.

6. Smalley, A.J., Darlow, M.S., and Mehta, R.K., "Stiffness and Damping of Elastomeric O-Ring Bearing Mounts", NASA Report CR-135328. Prepared by MTI for NASA-Lewis Research Center under Contract NAS3-19751, November 1977.

7. Smalley, A.J., Darlow, M.S., and Mehta, R.K., "The Dynamic Characteristics of O-Rings", ASME Trans., Journal of Mechanical Design, Vol. 100, No. 1, January 1978, pp. 132-138.

8. Payne, A.R., and Scott, J.R., "Engineering Design with Rubber", London: MacLaren & Sons, Ltd., 1960.

A-1 Hands, D., Horsfall, F., "A Thermal Conductivity Apparatus for Solid and Molten Polymers", Journal of Physics E: Scientific Instruments, Vol. 8, 1975.

A-2 Thompson, M.D., "Differential Scanning Calorimetry", RAPRA Bulletin, September, 1972, pp. 271-76.

A-3 Nakajima, N., Bowerman, H.H., and Collins, E.A., "Viscoelastic Behaviour of Butadiene-Acrylonitrile Copolymers Filled with Carbon Black," B.F. Goodrich Chemical Company.

REFERENCES (Cont'd)

A-4 Payne, A.R., Scott, J.R., "Engineering Design with Rubber", MacLaren 1960, pp. 24-26.

A-5 Williams, M.L., Landel, R.F., Ferry, J.D., (1955) J Am. Chem. Soc. 77 3701.

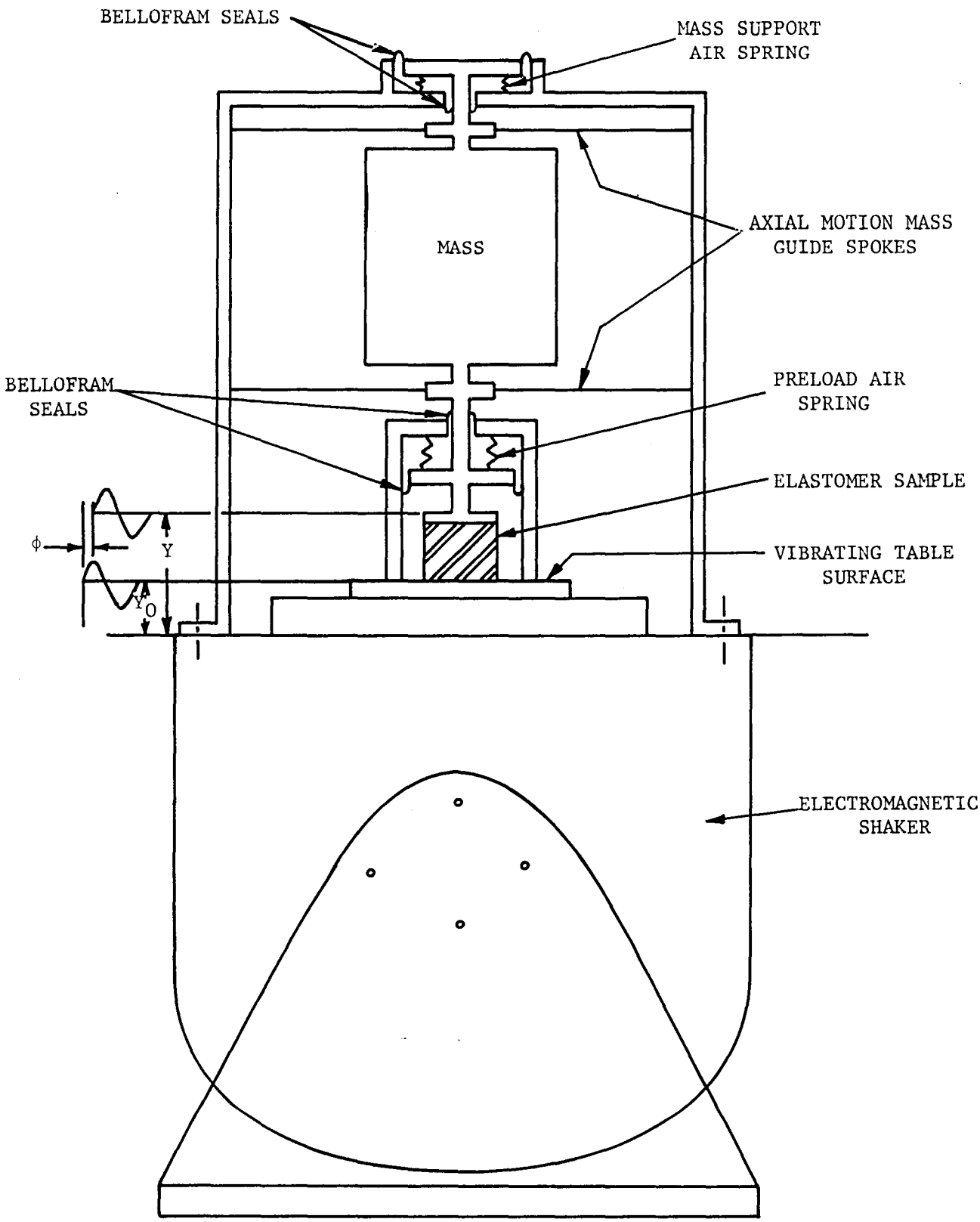

Fig. 1 Schematic of Elastomer Test Rig Showing All Components

791161

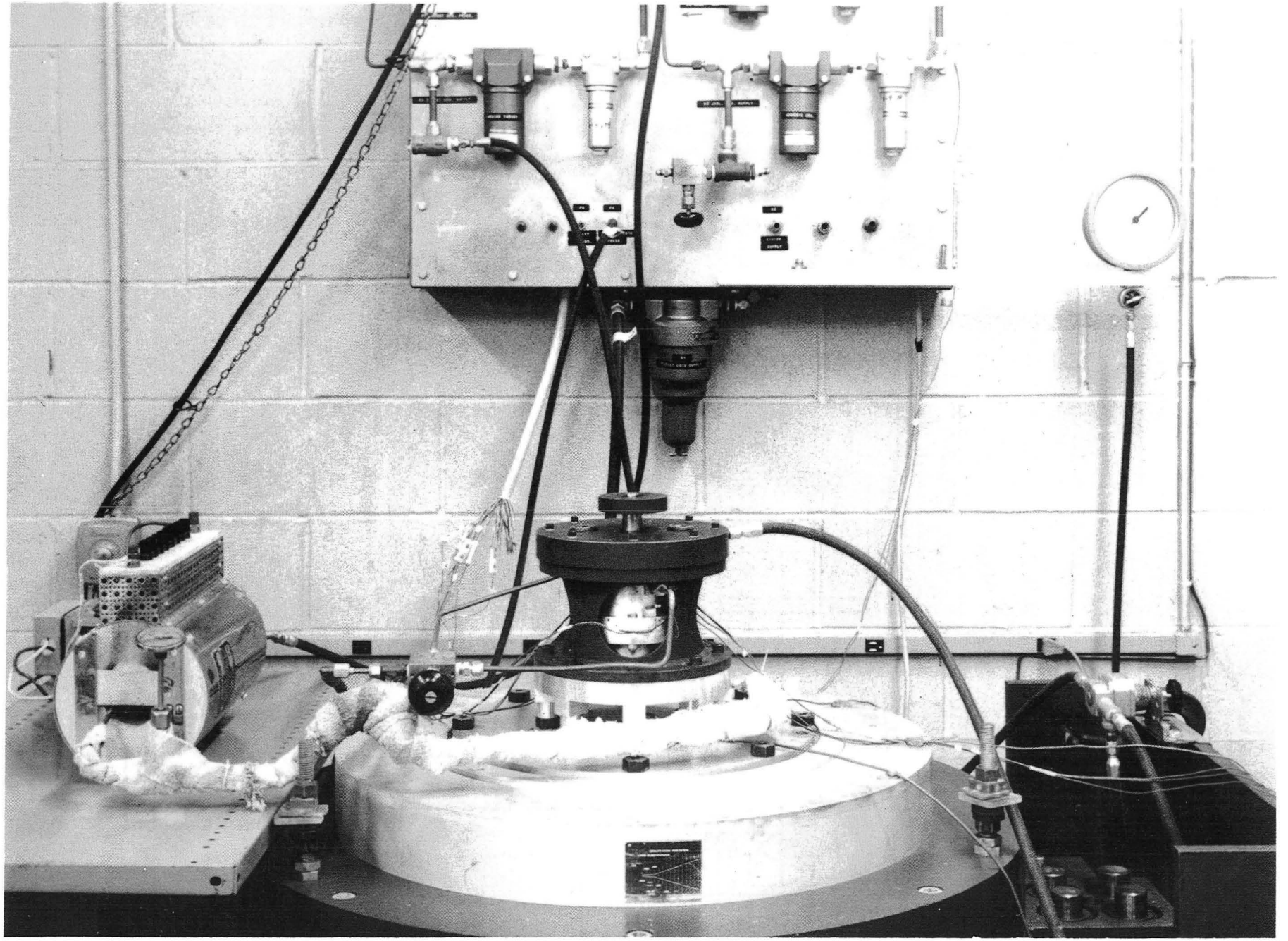

Fig. 2 View of Shake-Table-Mounted Elastomer Test Rig with Preload Cylinder and Small Mass

MTI-16654

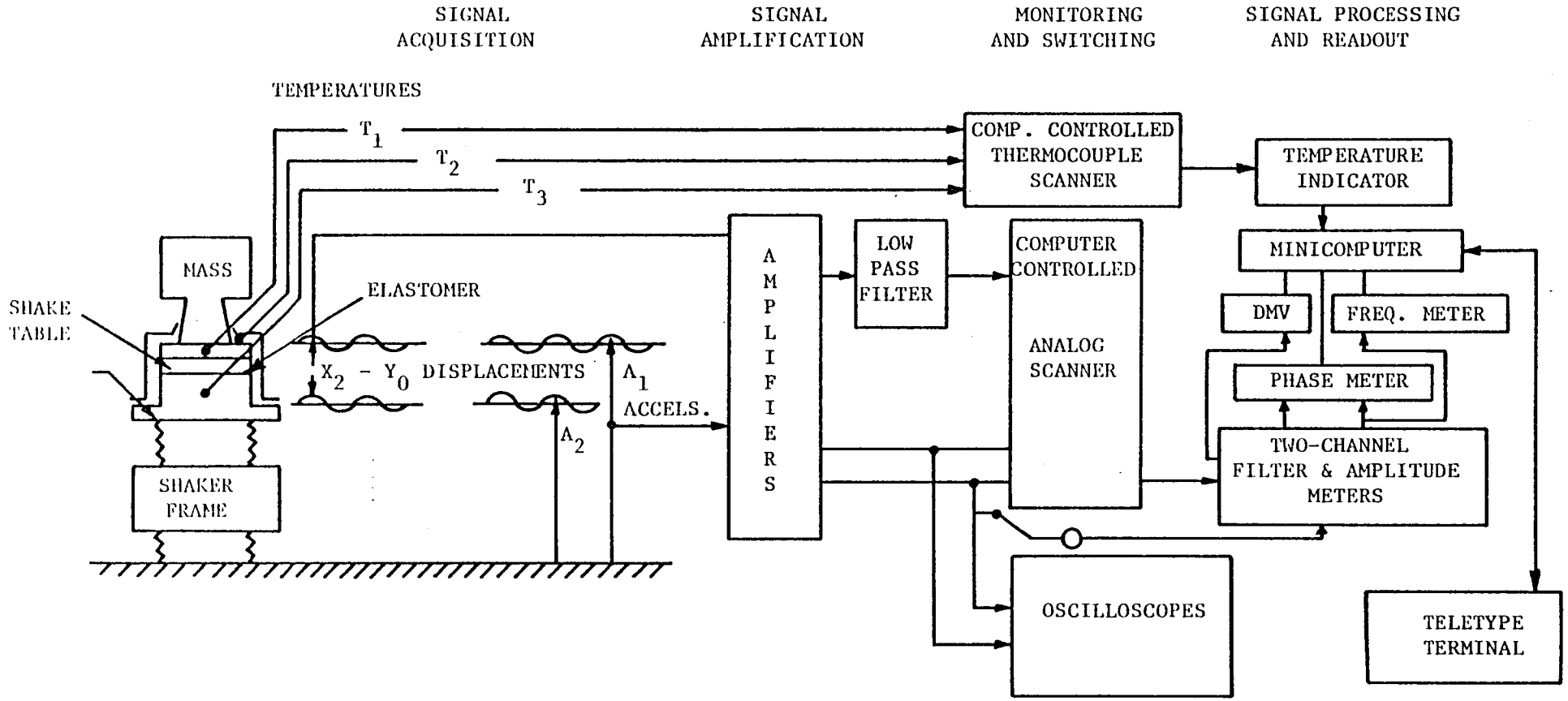

DATA ACQUISITION PROBES

T_1 - TEMPERATURE OF METAL, ELASTOMER MASS

T_2 - TEMPERATURE OF TEST ENCLOSURE AMBIENT

T_3 - TEMPERATURE OF METAL, ELASTOMER-SHAKE TABLE

$Y - Y_0$ - DISPLACEMENT MASS RELATIVE TO SHAKE TABLE

A_1 - ACCELERATION OF MASS

A_2 - ACCELERATION OF SHAKE TABLE

791162

Fig. 3 Schematic of Data Acquisition for Measurement of Elastomer Dynamic Properties

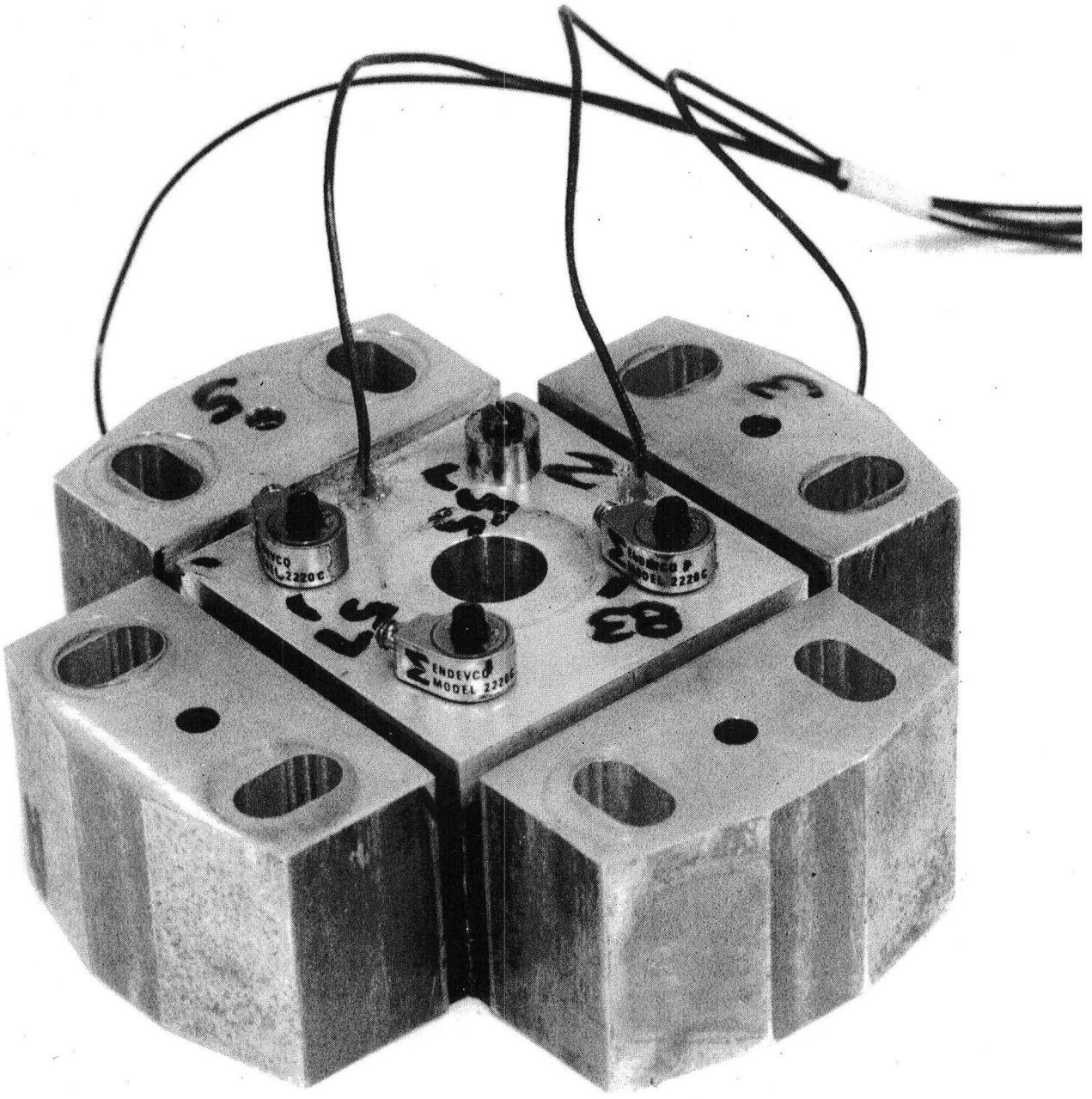

Fig. 4 Test Assembly of Four Elastomer Shear Specimens, Each 2.54 Centimeters (1.0 in.) High

MTI-16656

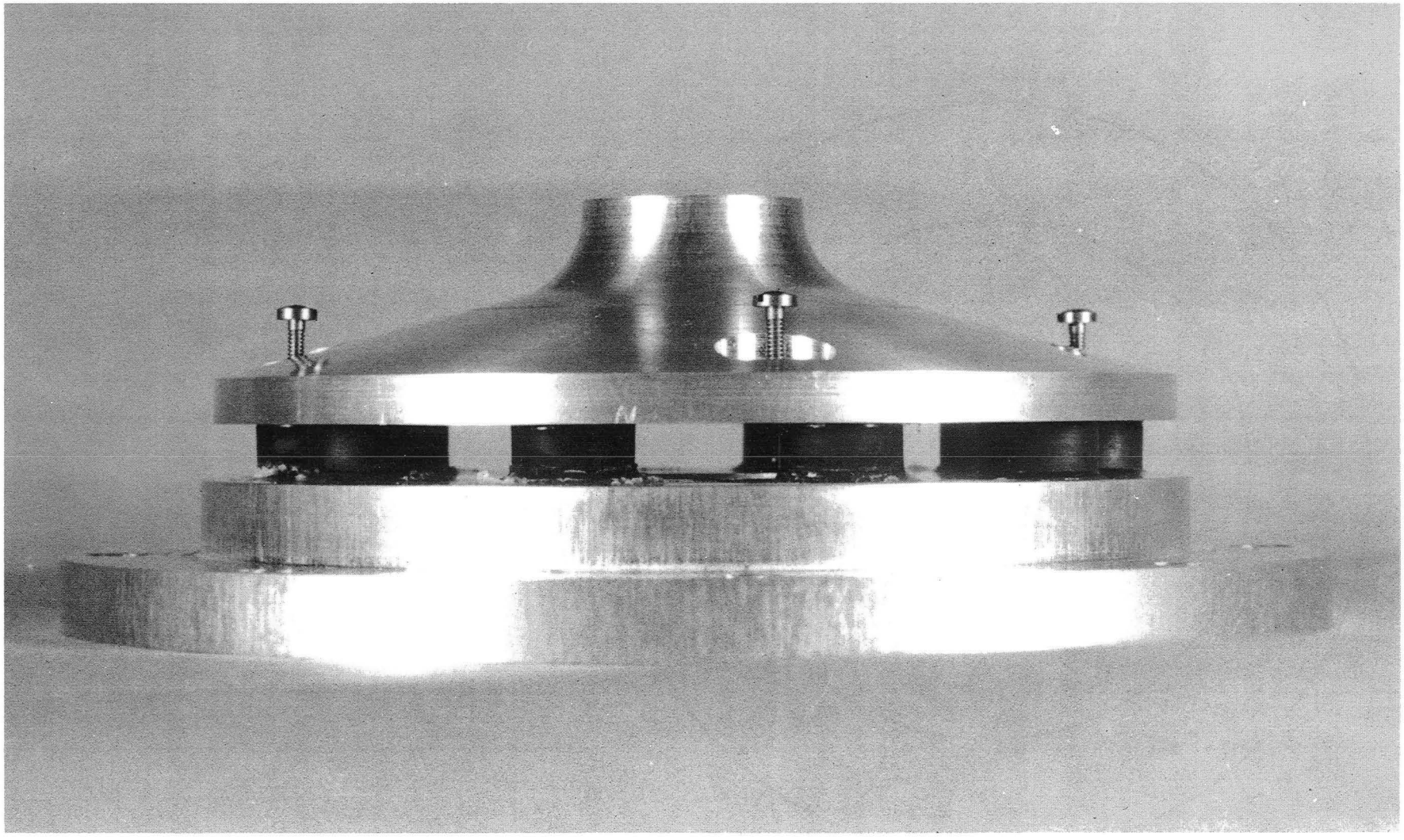

Fig. 5 Compression Test Sample Without Instrumentation

MTI-16658

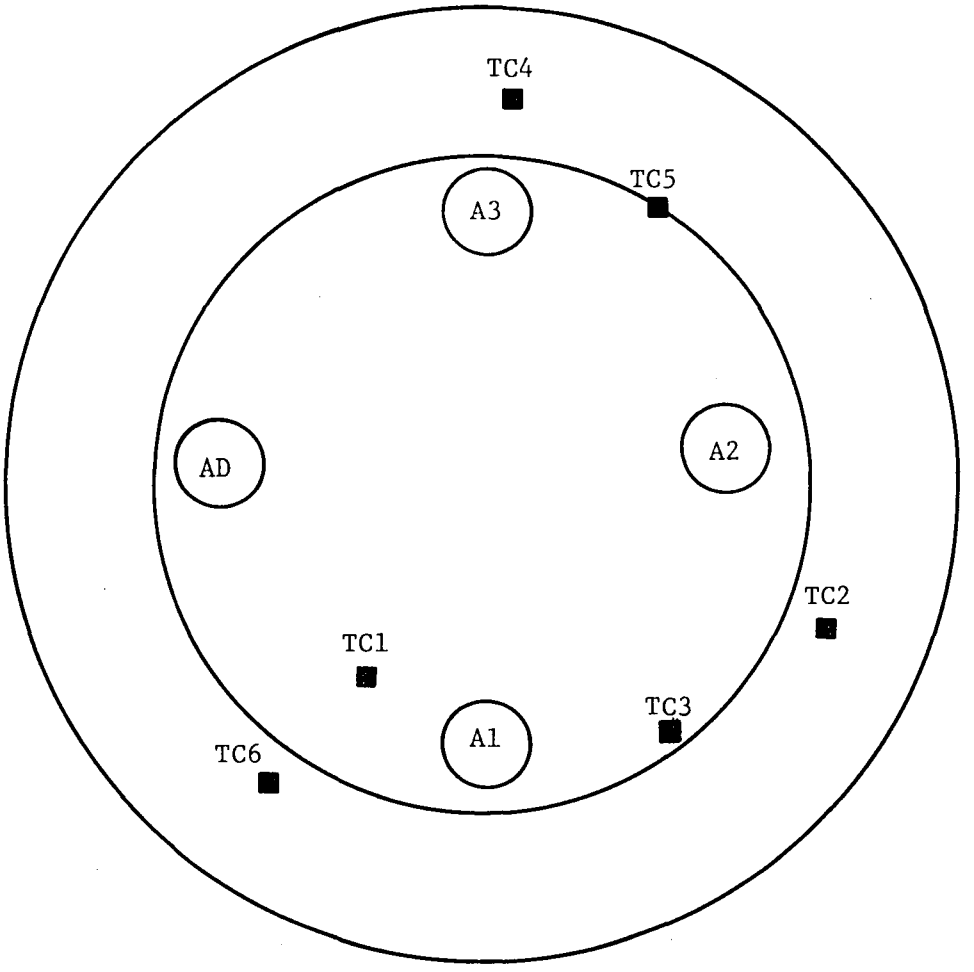

TC1 ON TOP OF UPPER MOUNTING PLATE
TC3 IN UPPER MOUNTING PLATE
TC5 IN UPPER MOUNTING PLATE
TC2 ON TOP OF LOWER MOUNTING PLATE
TC4 ON TOP OF LOWER MOUNTING PLATE
TC6 ON TOP OF INNER MOUNTING PLATE

Fig. 6 Location of Accelerometers and Thermocouples External to the Elastomer in the Instrumented Compression Test Specimen

791163

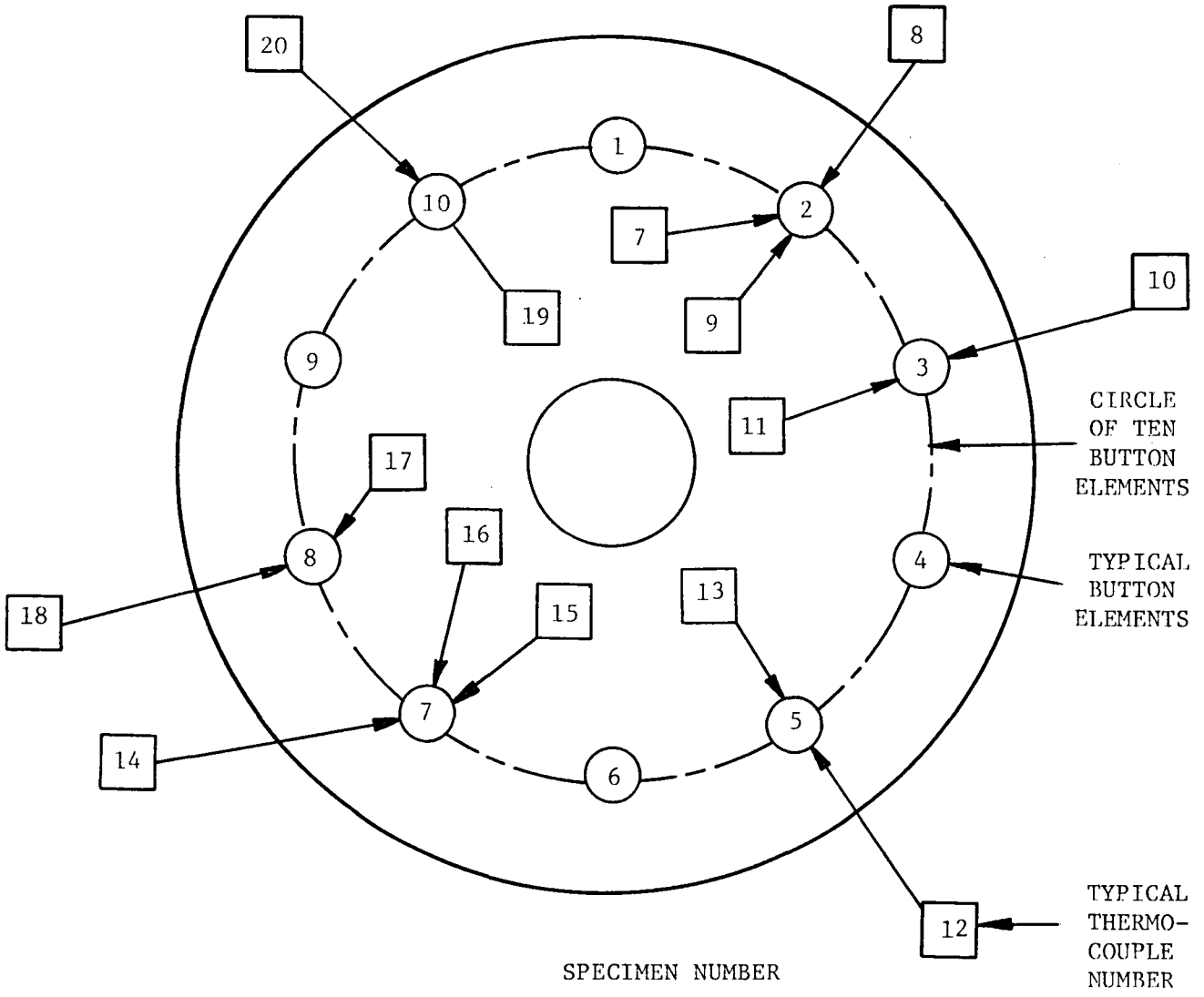

Fig. 7 Location of Imbedded Thermocouples in Instrumented Compression Specimen

791164

THERMOCOUPLE LAYOUT

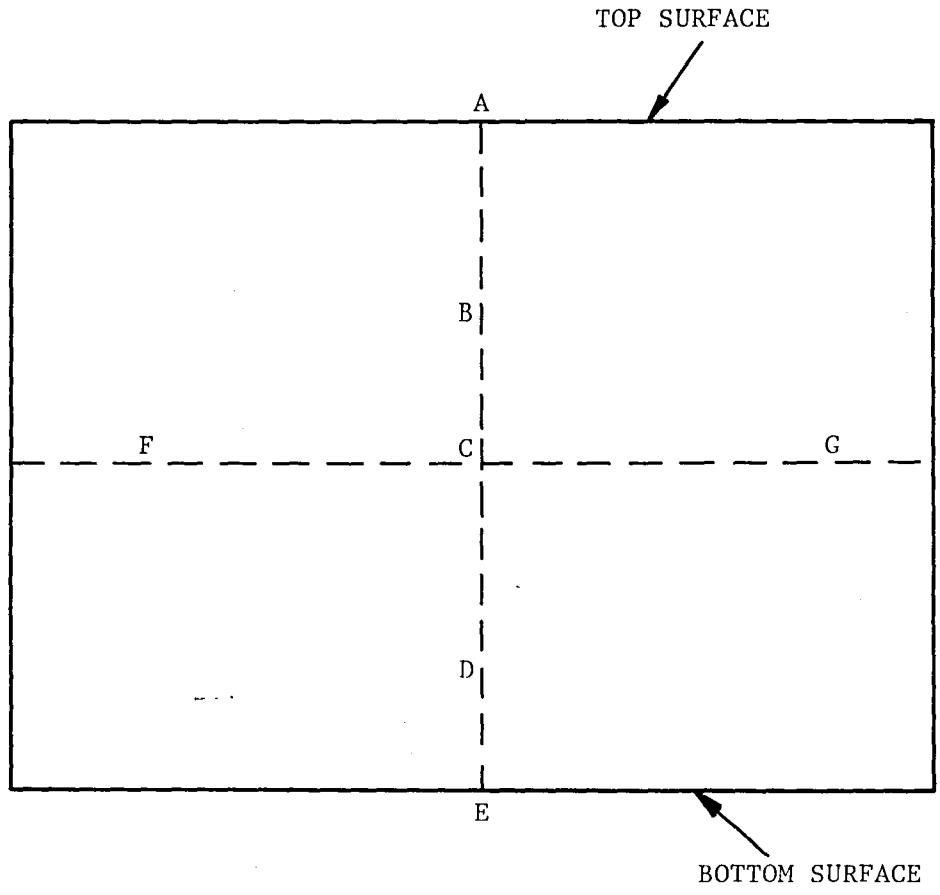

POSITION	THERMOCOUPLE #
A	7, 15
B	12, 19
C	8, 14
D	13, 20
E	9, 16
F	11, 17
G	10, 18

Fig. 8 Location of Thermocouples Imbedded in Elastomer Elements for Instrumented Compression Test Specimen

791165

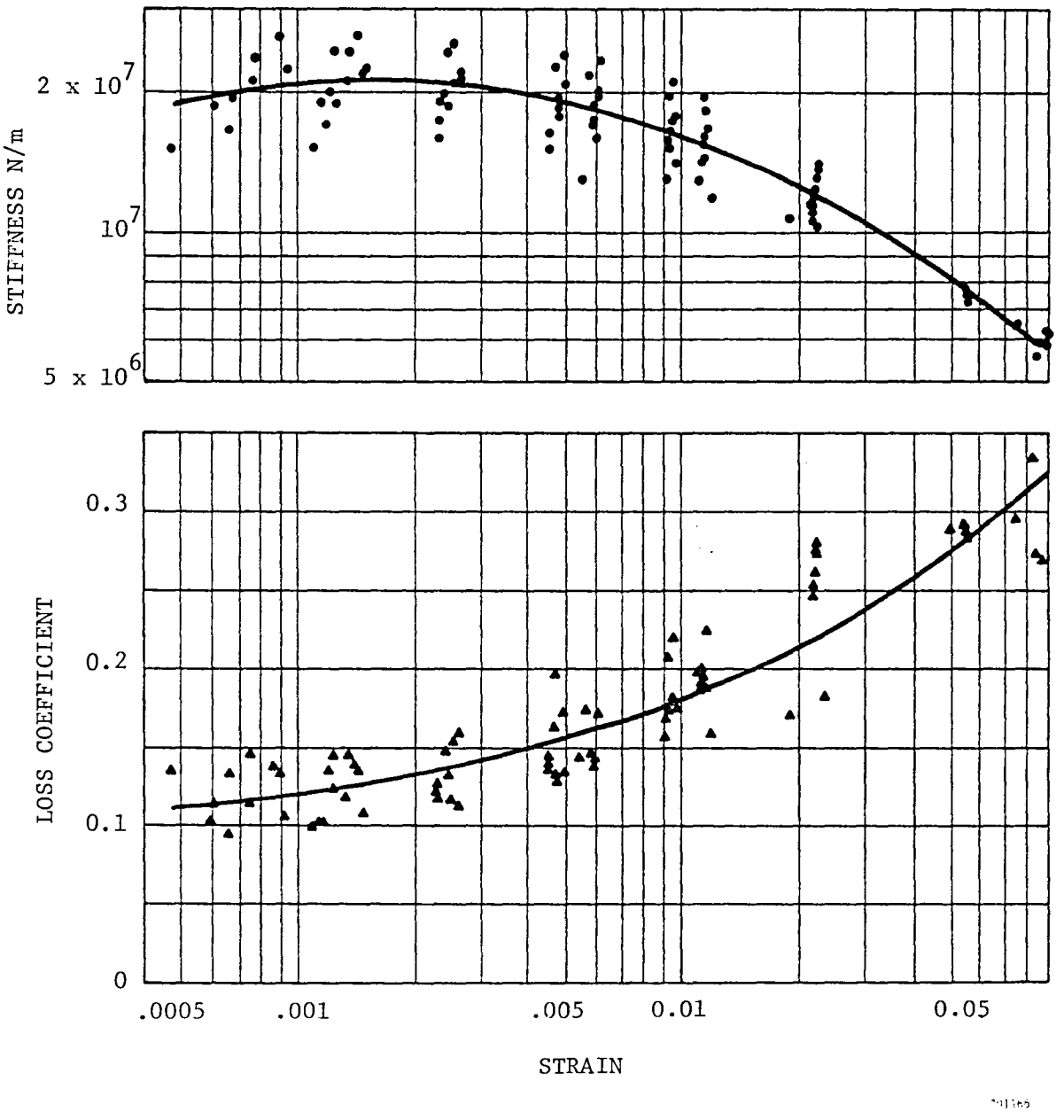

Fig. 9 Stiffness and Loss Coefficient vs. Strain. Shear Specimen, 32°C

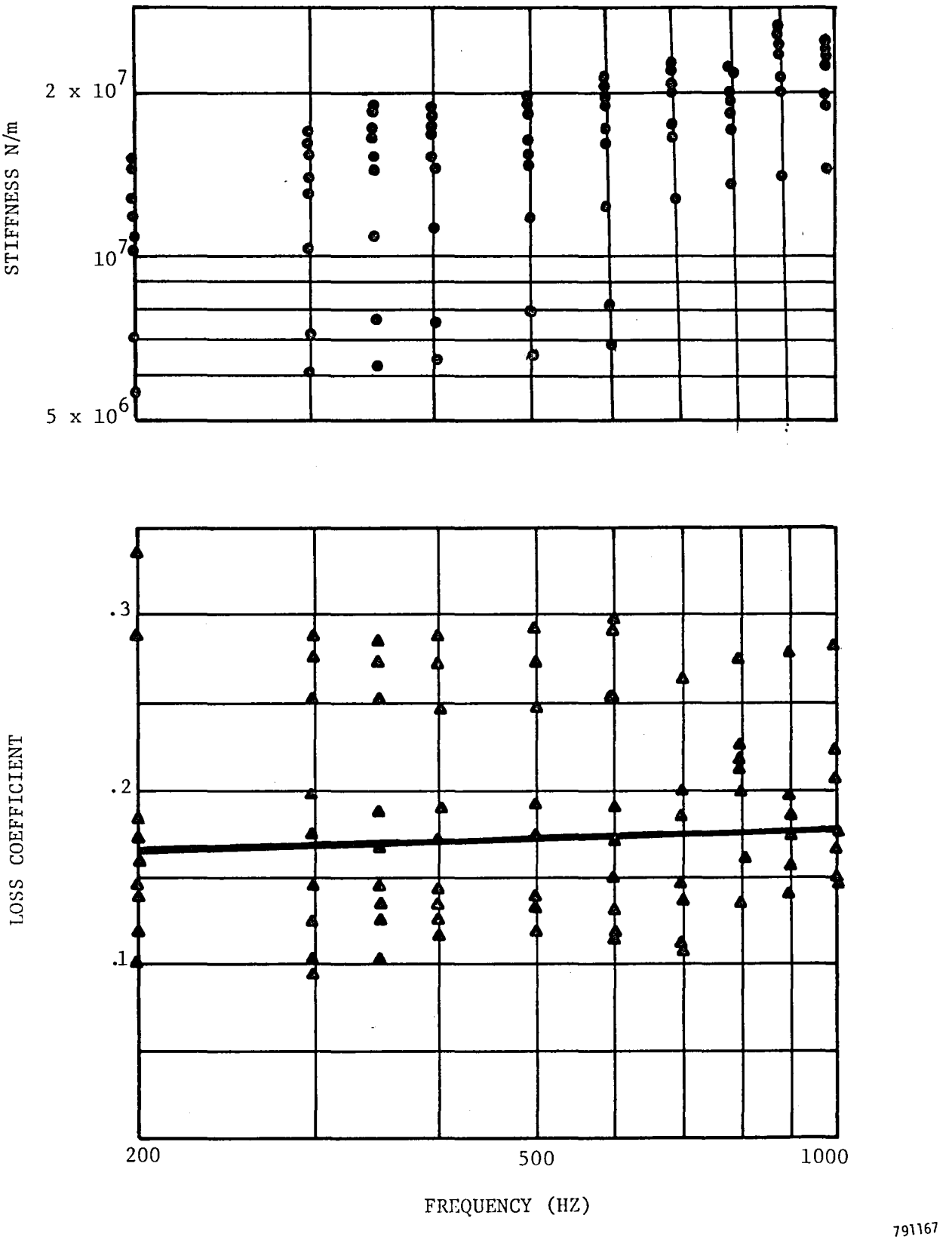

Fig. 10 Stiffness and Loss Coefficient vs. Frequency. Shear Specimen, 32°C.

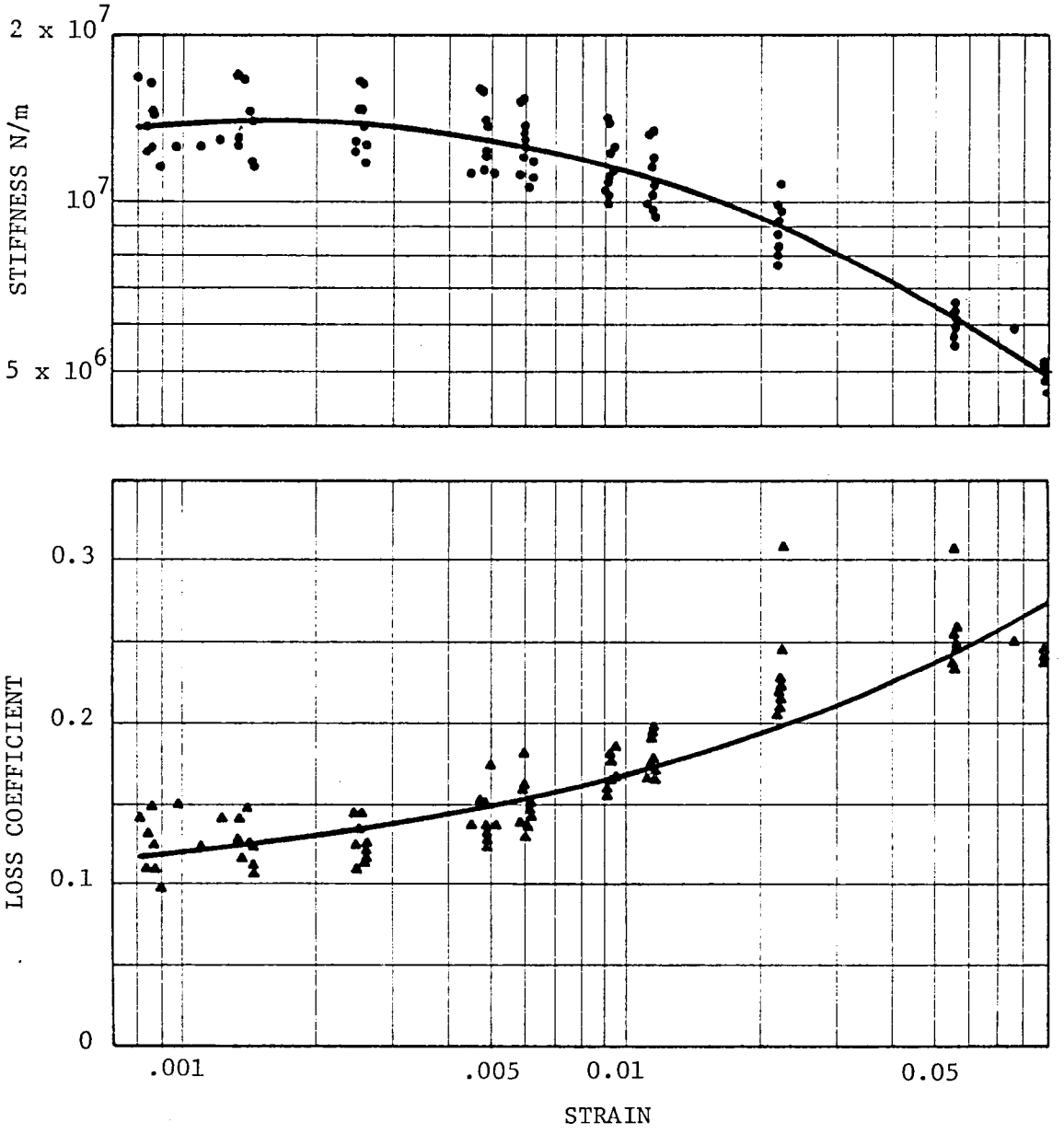

Fig. 11 Stiffness and Loss Coefficient vs. Strain. Shear Specimen, 66°C.

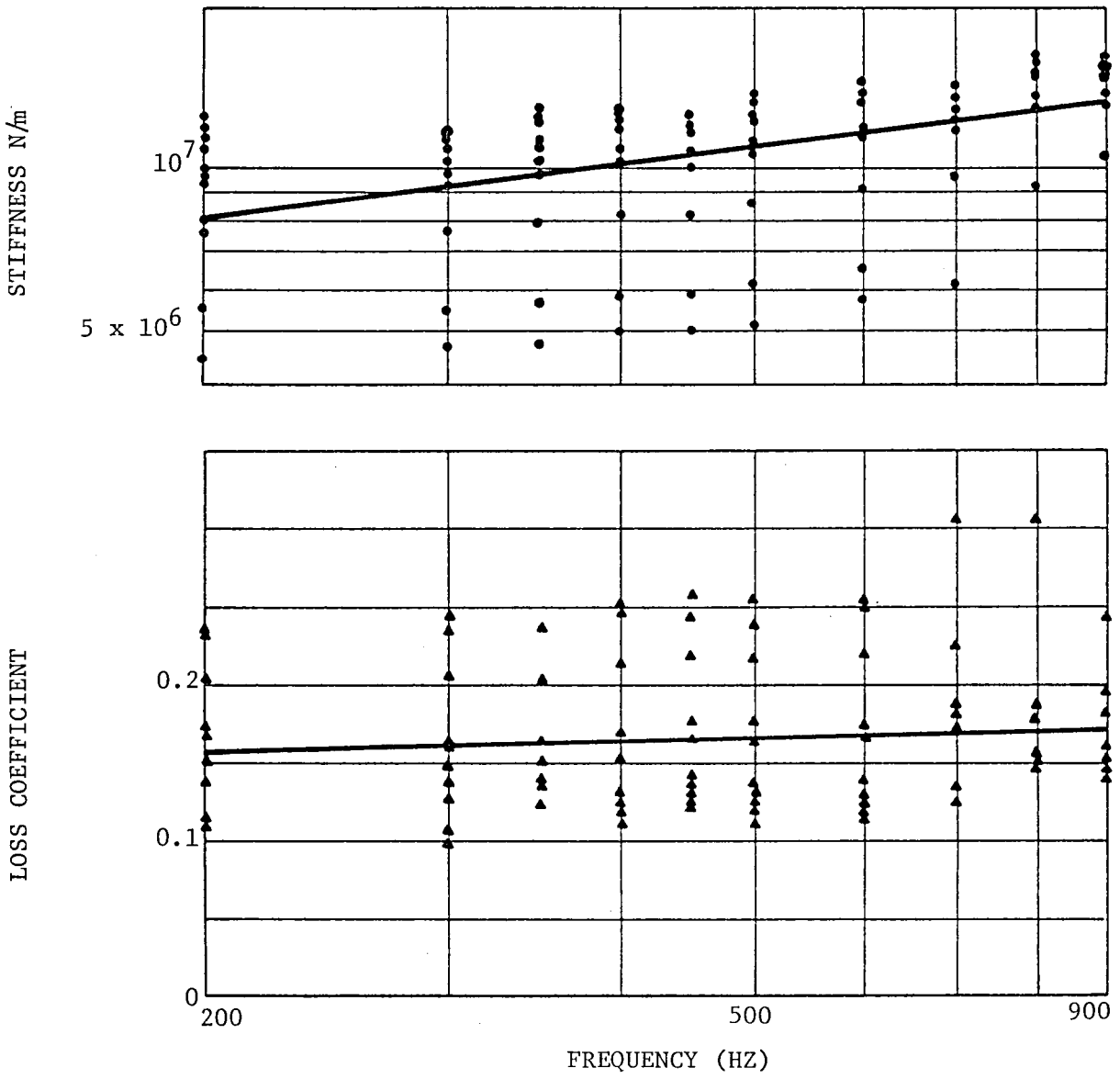

Fig. 12 Stiffness and Loss Coefficient vs. Frequency. Shear Specimen, 66°C.

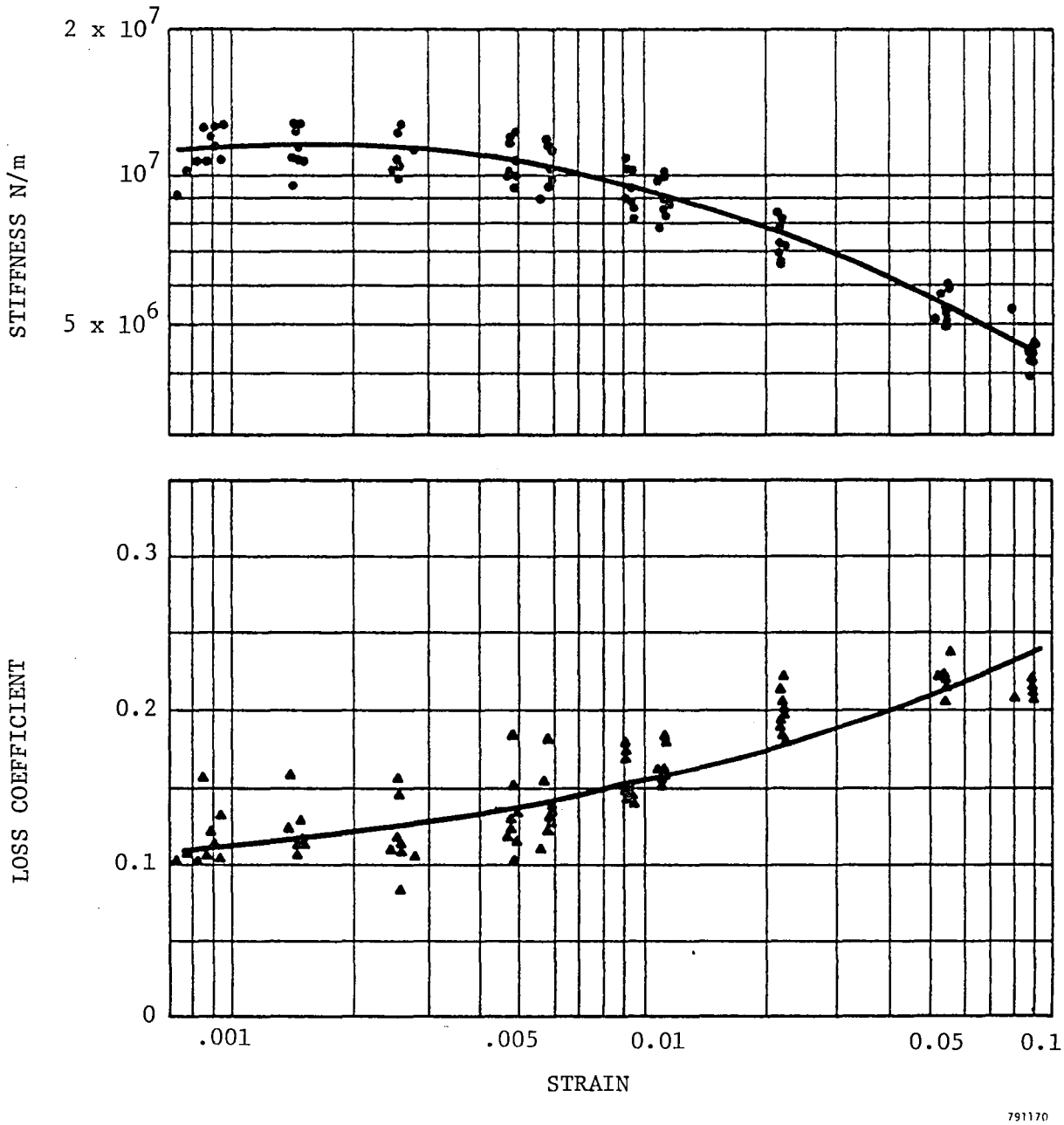

Fig. 13 Stiffness and Loss Coefficient vs. Strain. Shear Specimen, 80°C.

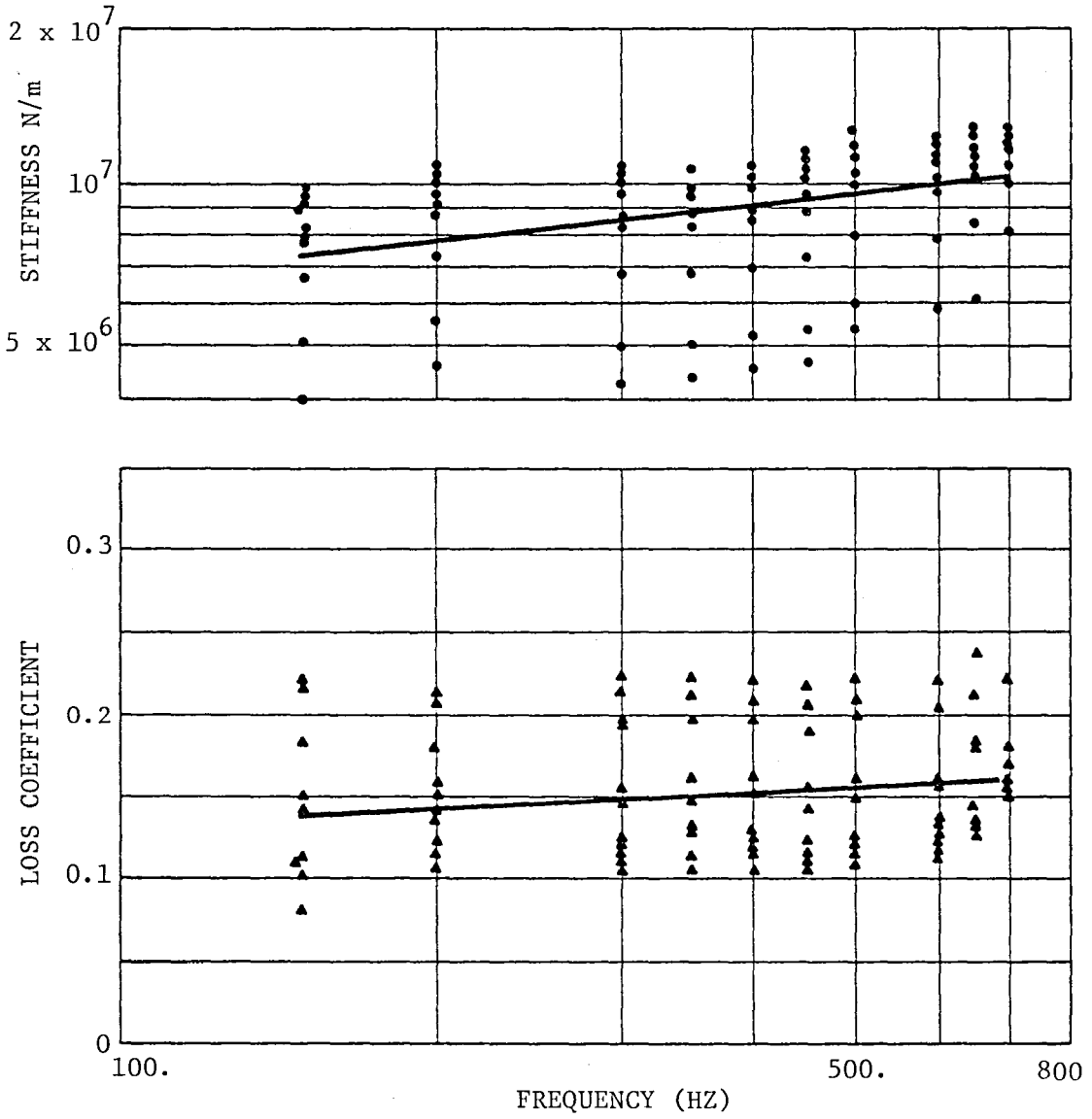

Fig. 14 Stiffness and Loss Coefficient vs. Frequency. Shear Specimen, 80°C.

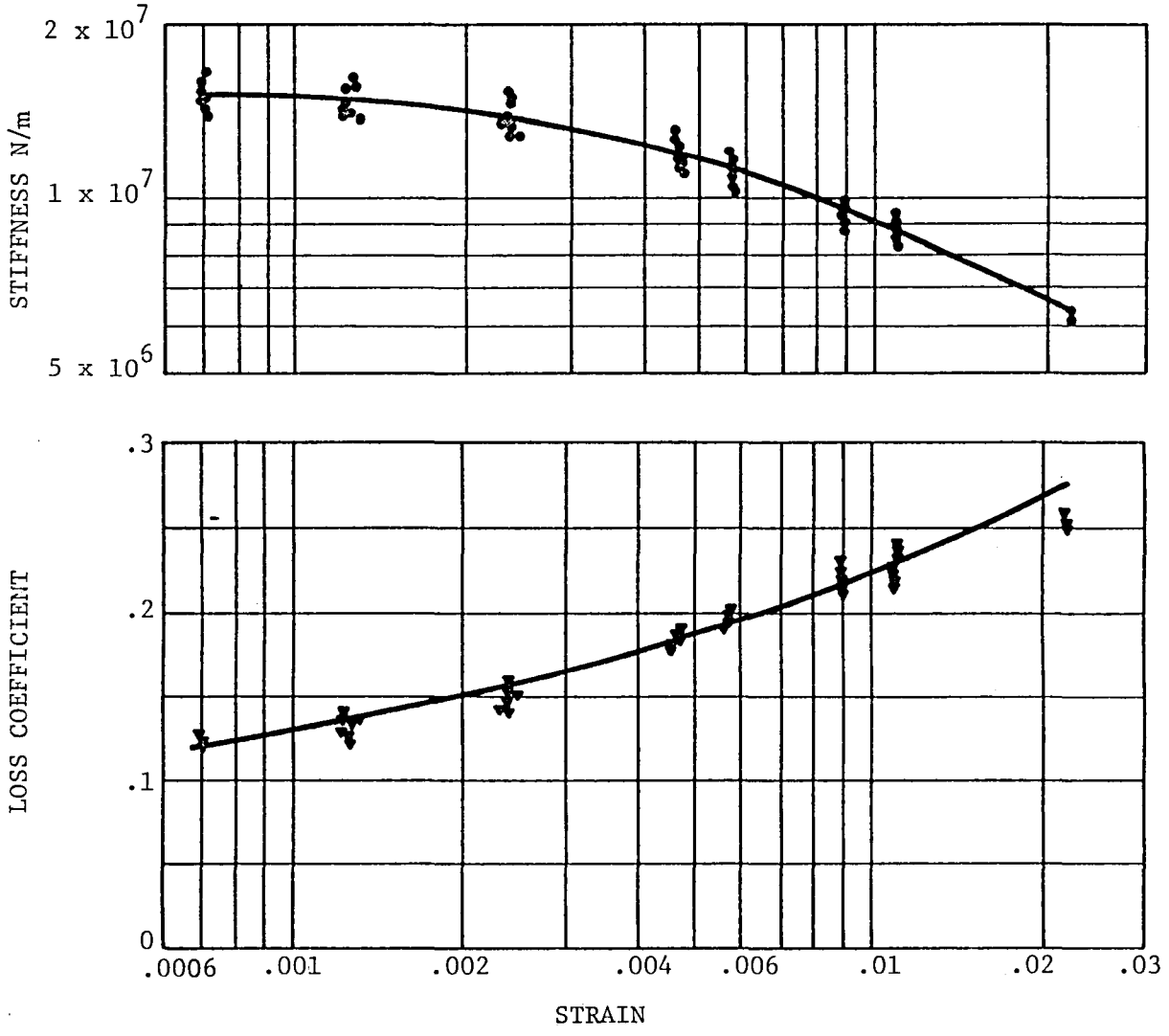

Fig. 15 Stiffness and Loss Coefficient vs. Strain. Compression Specimen, 32°C.

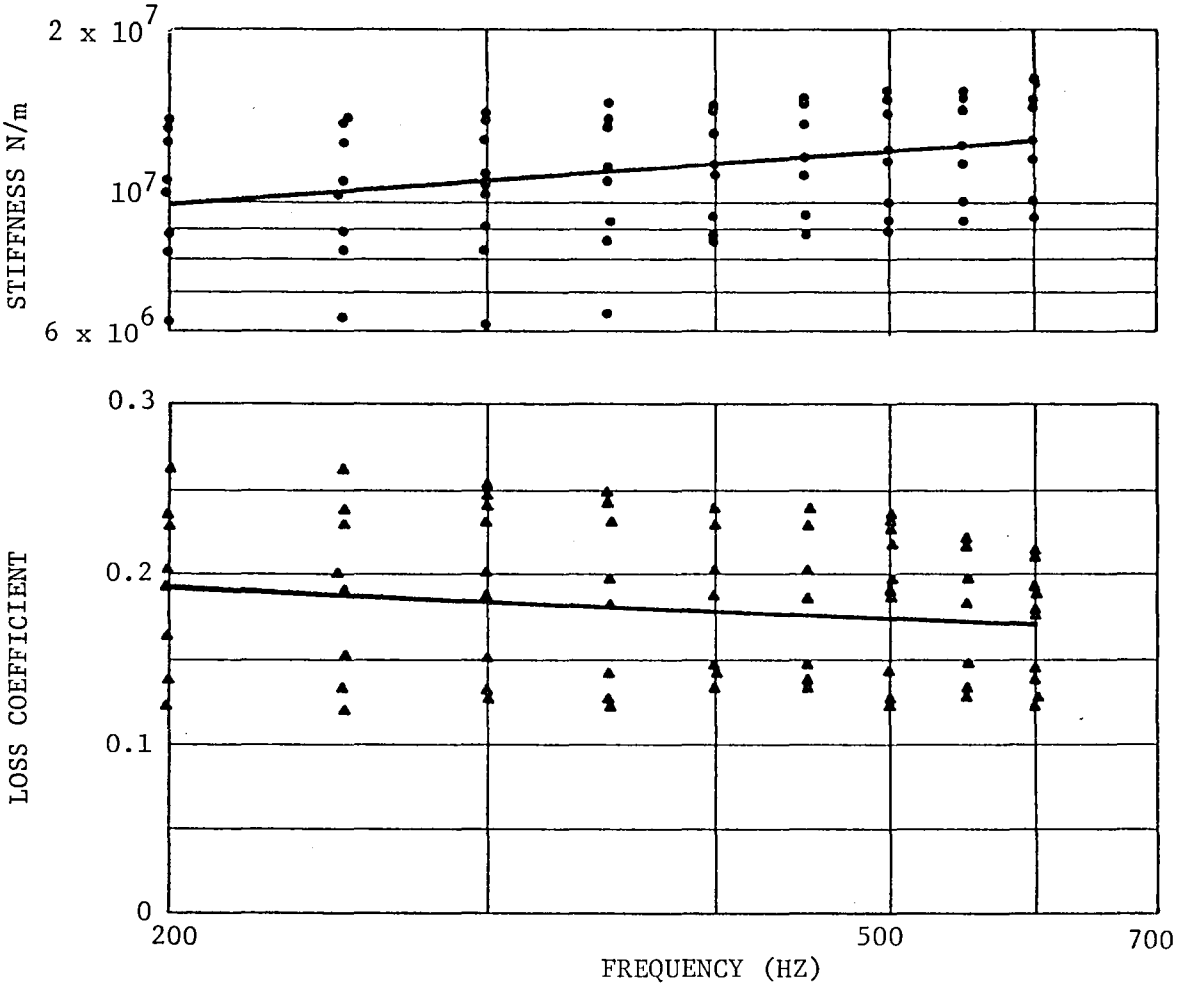

Fig. 16 Stiffness and Loss Coefficient vs. Frequency. Compression Specimen, 32°C.

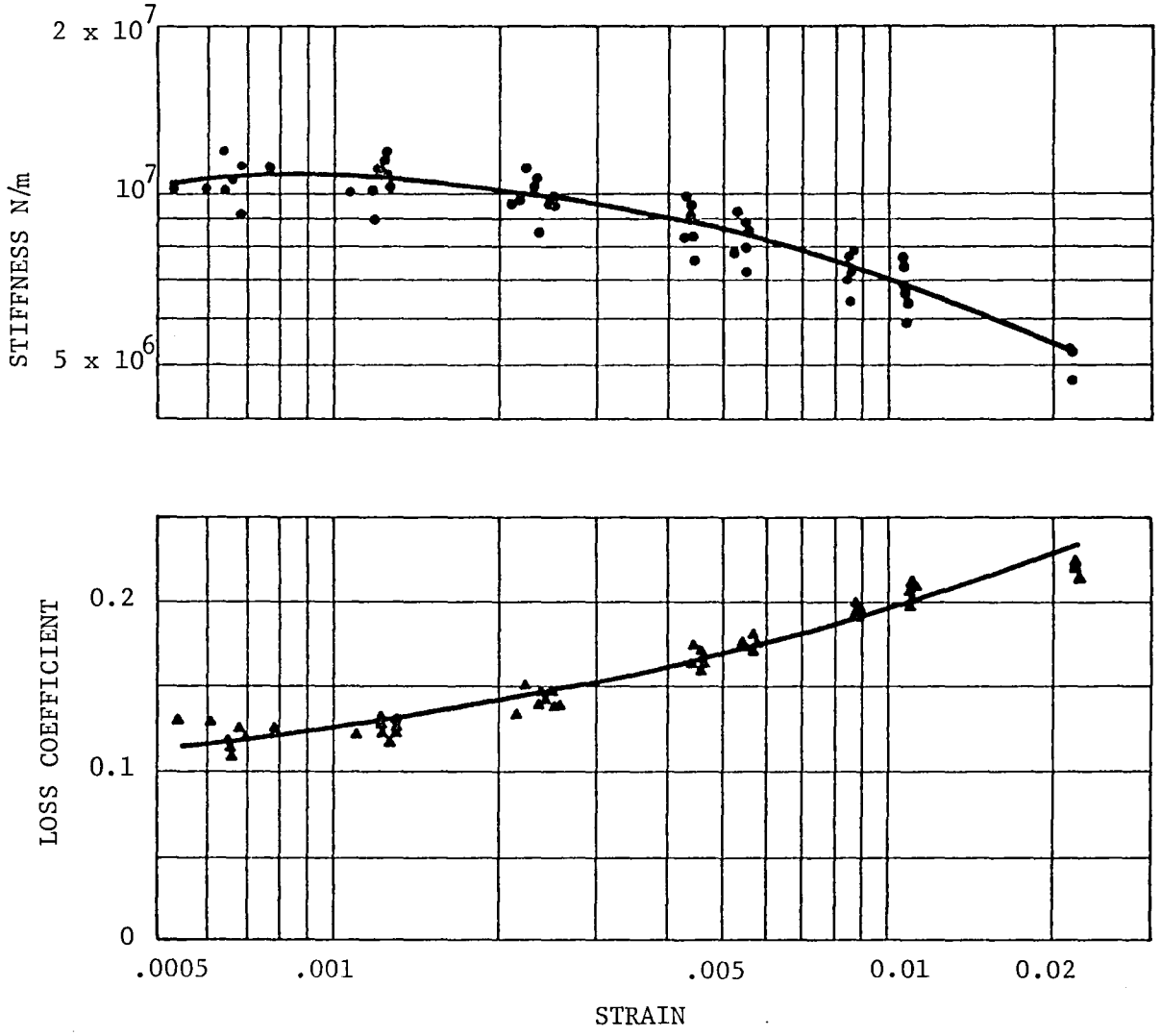

Fig. 17 Stiffness and Loss Coefficient vs. Strain.
Compression Specimen, 66°C.

791174

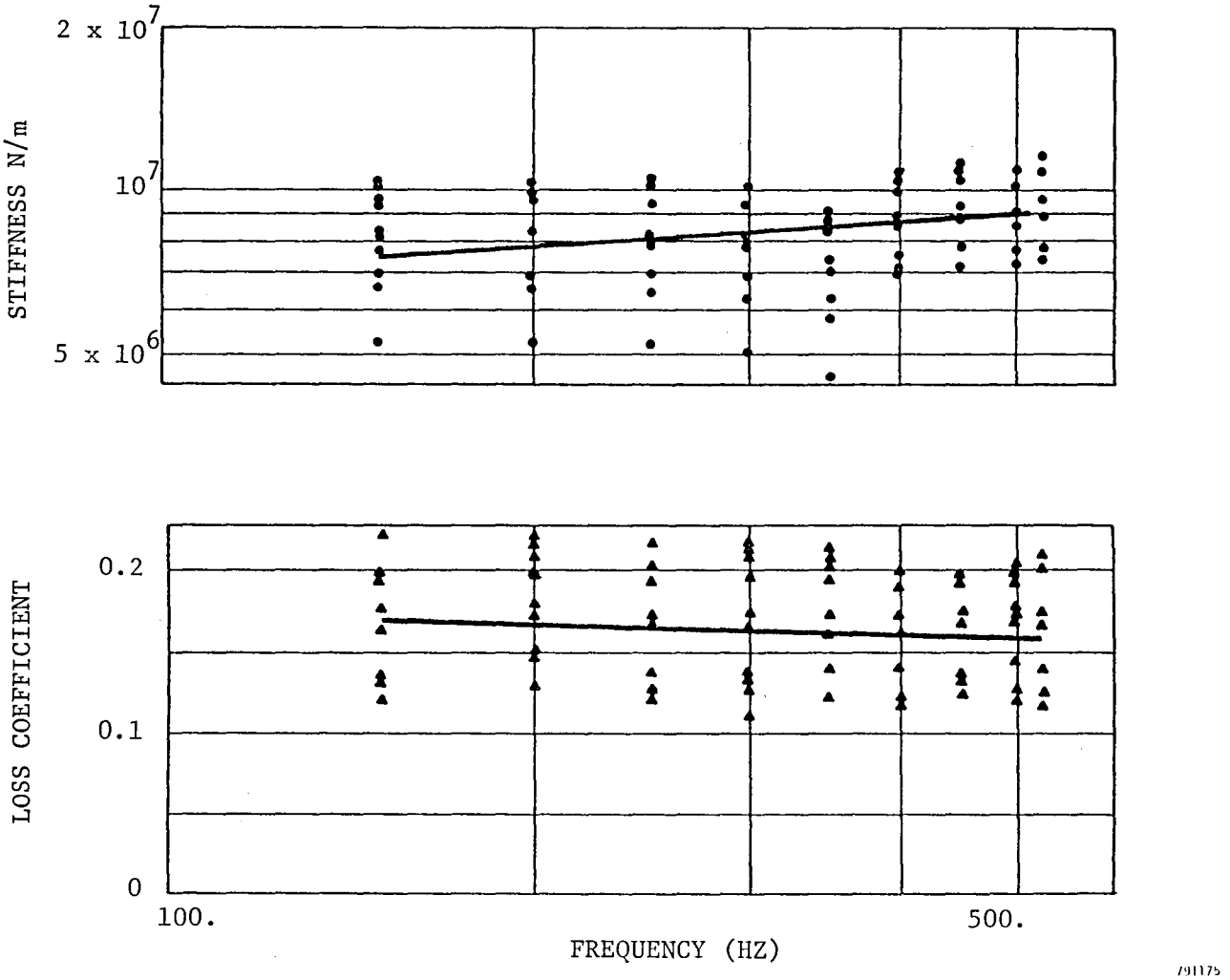

Fig. 18 Stiffness and Loss Coefficient vs. Frequency. Compression Specimen, 66°C.

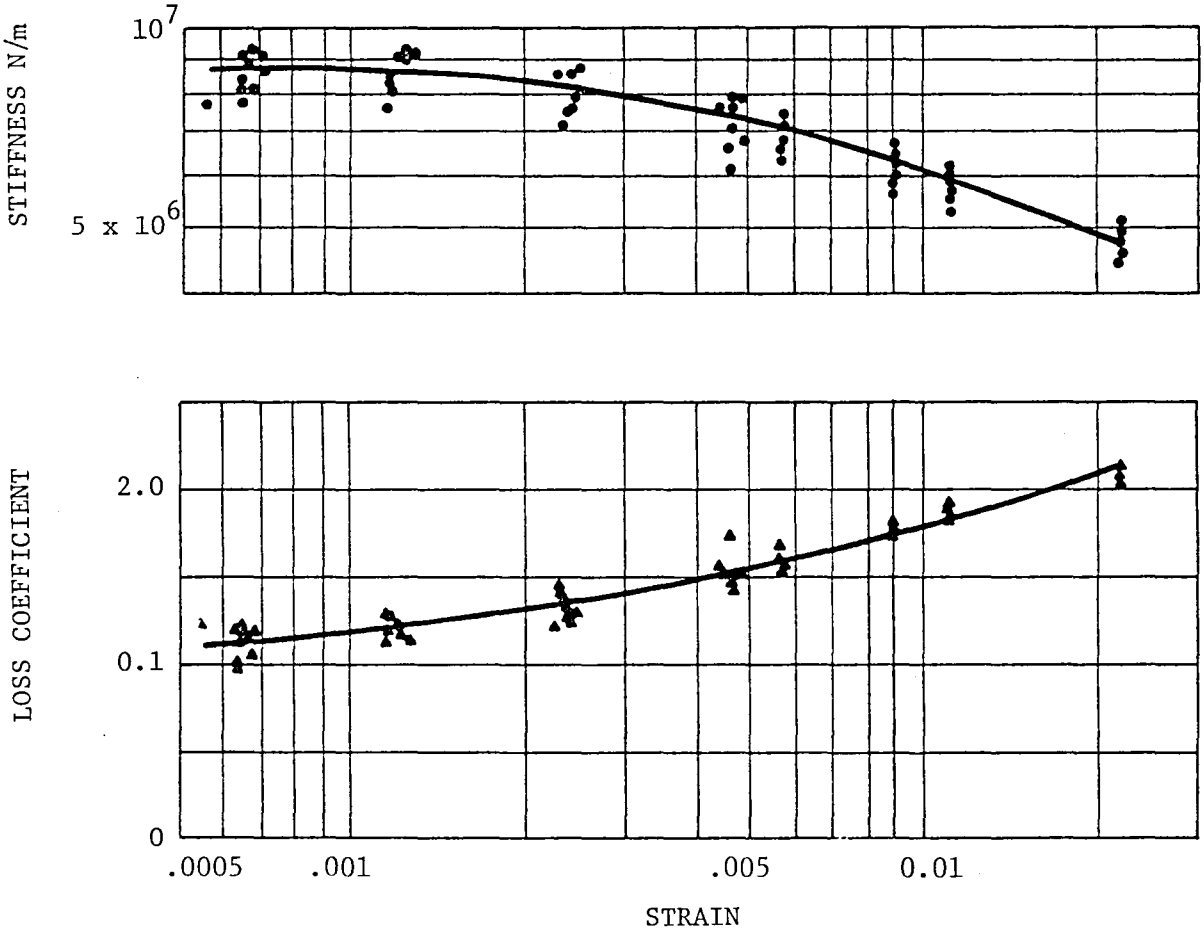

Fig. 19 Stiffness and Loss Coefficient vs. Strain.
Compression Specimen, 80°C

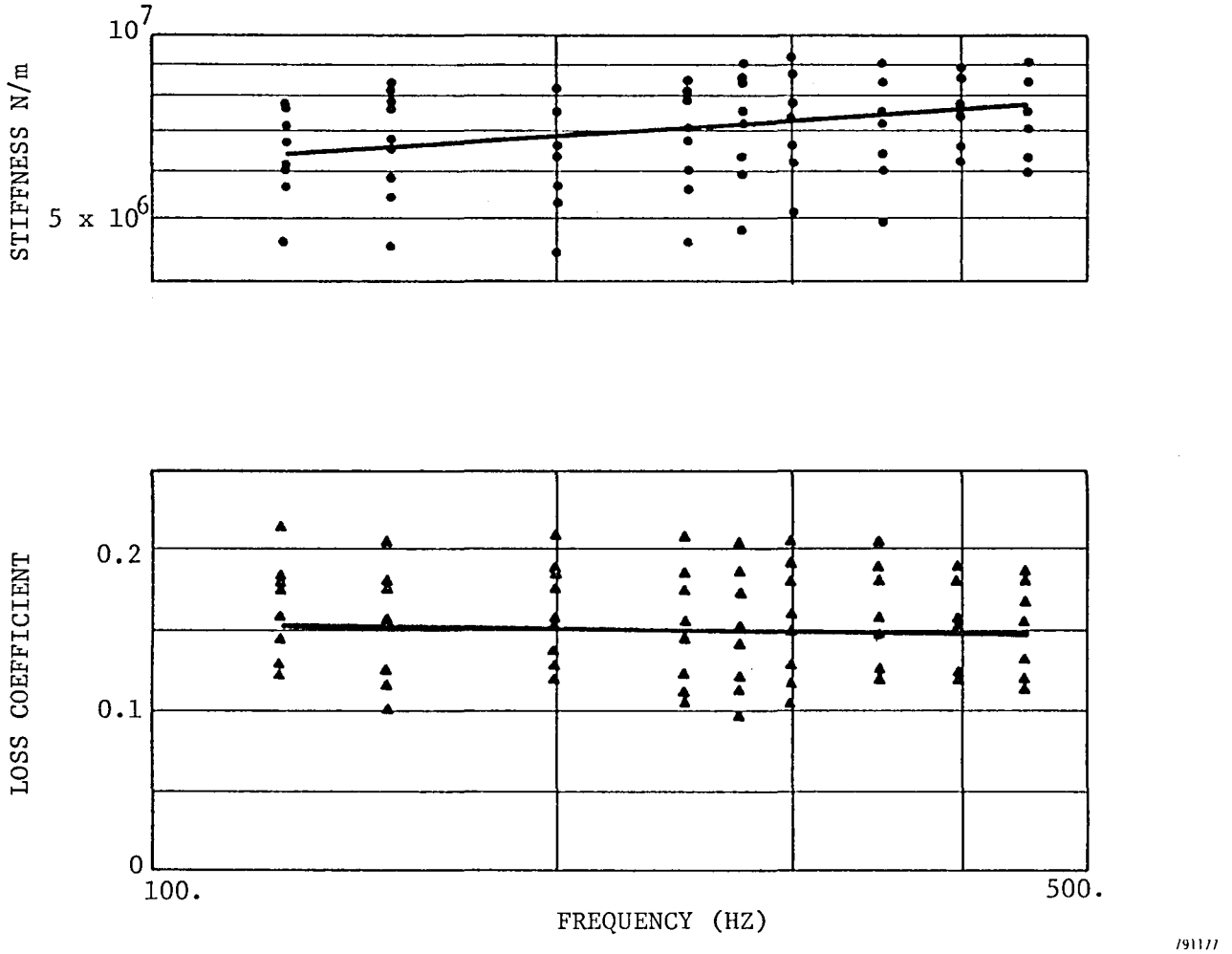

Fig. 20 Stiffness and Loss Coefficient vs. Frequency. Compression Specimen, 80°C.

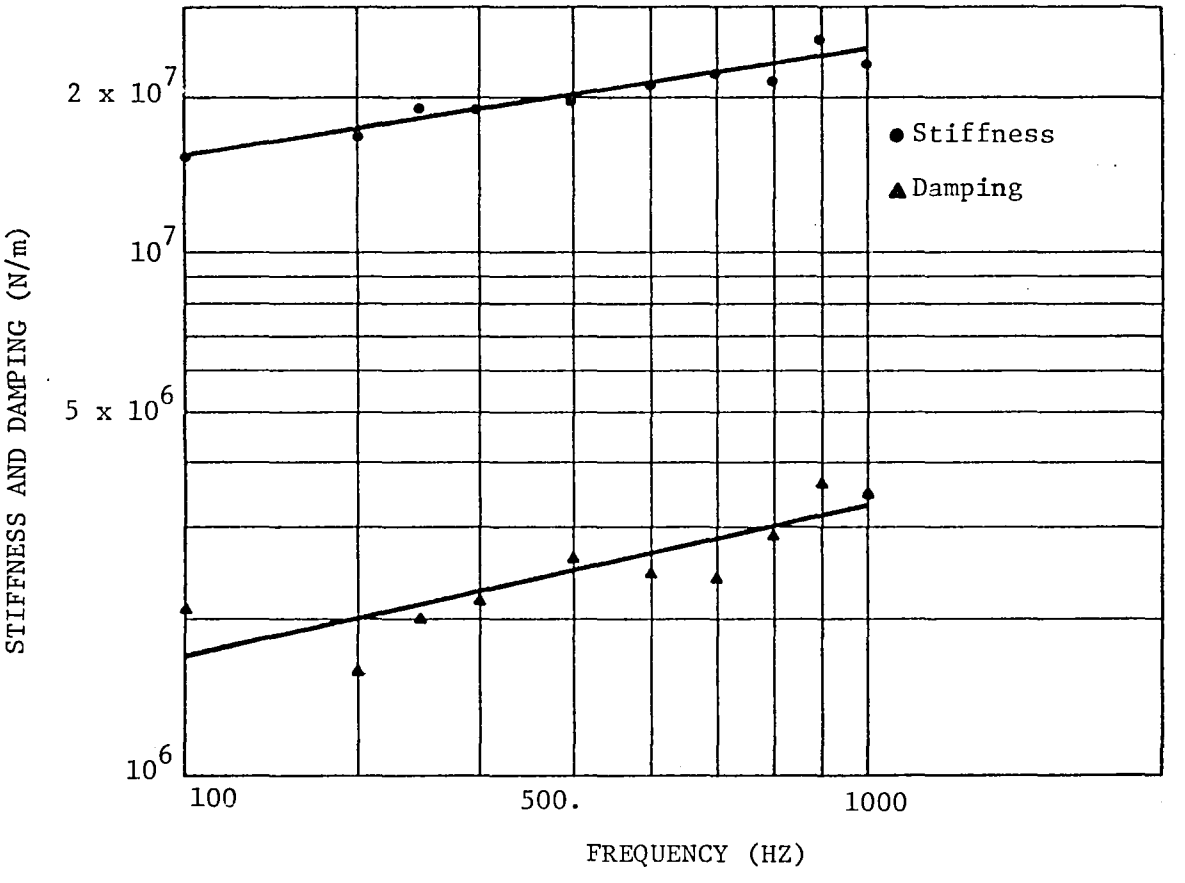

Fig. 21 Stiffness and Damping vs. Frequency. Low Strain ($\varepsilon \simeq .001$), Shear Specimen, 32°C.

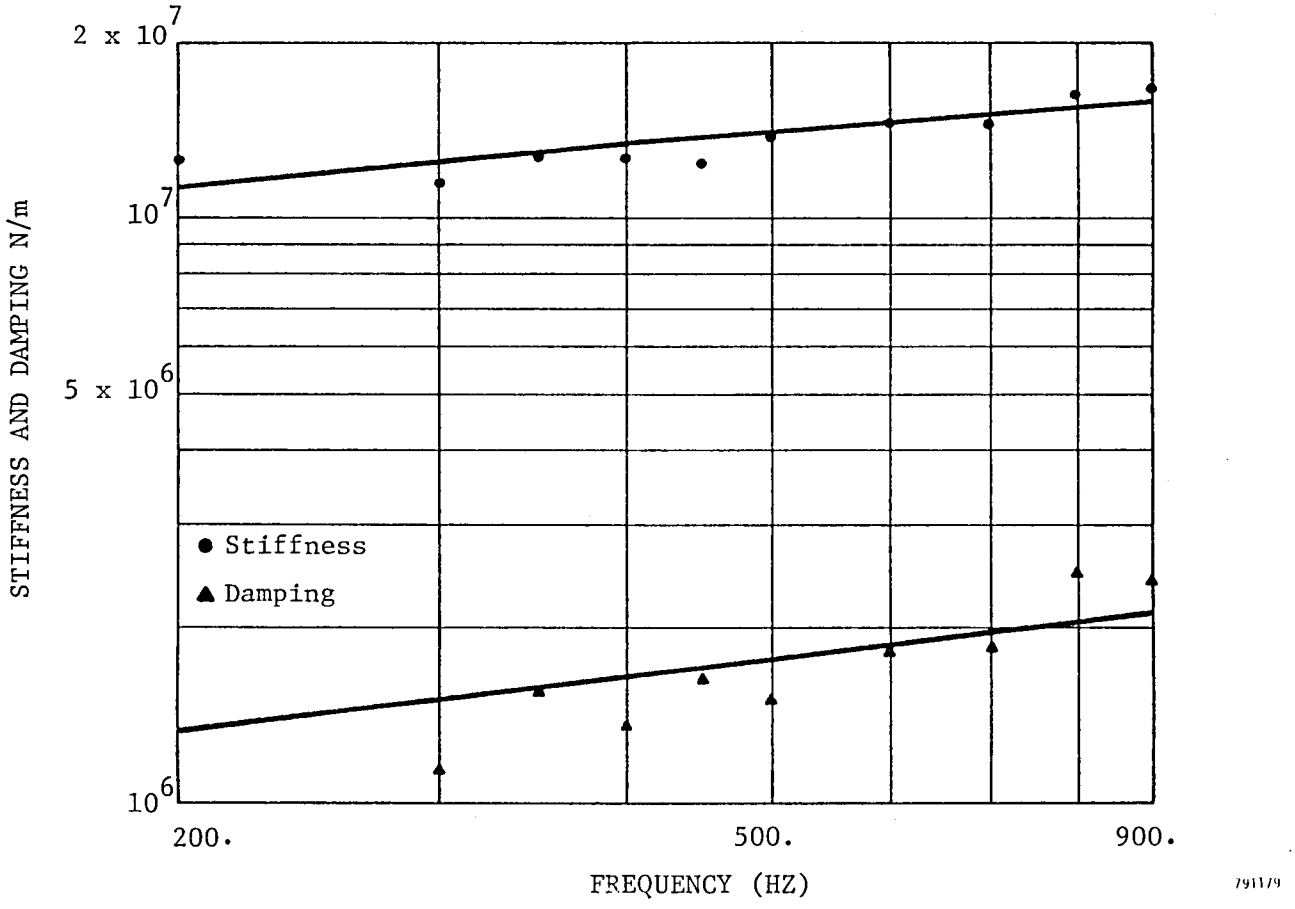

Fig. 22 Stiffness and Damping vs. Frequency. Low Strain ($\varepsilon \simeq .0008$), Shear Specimen, 66°C.

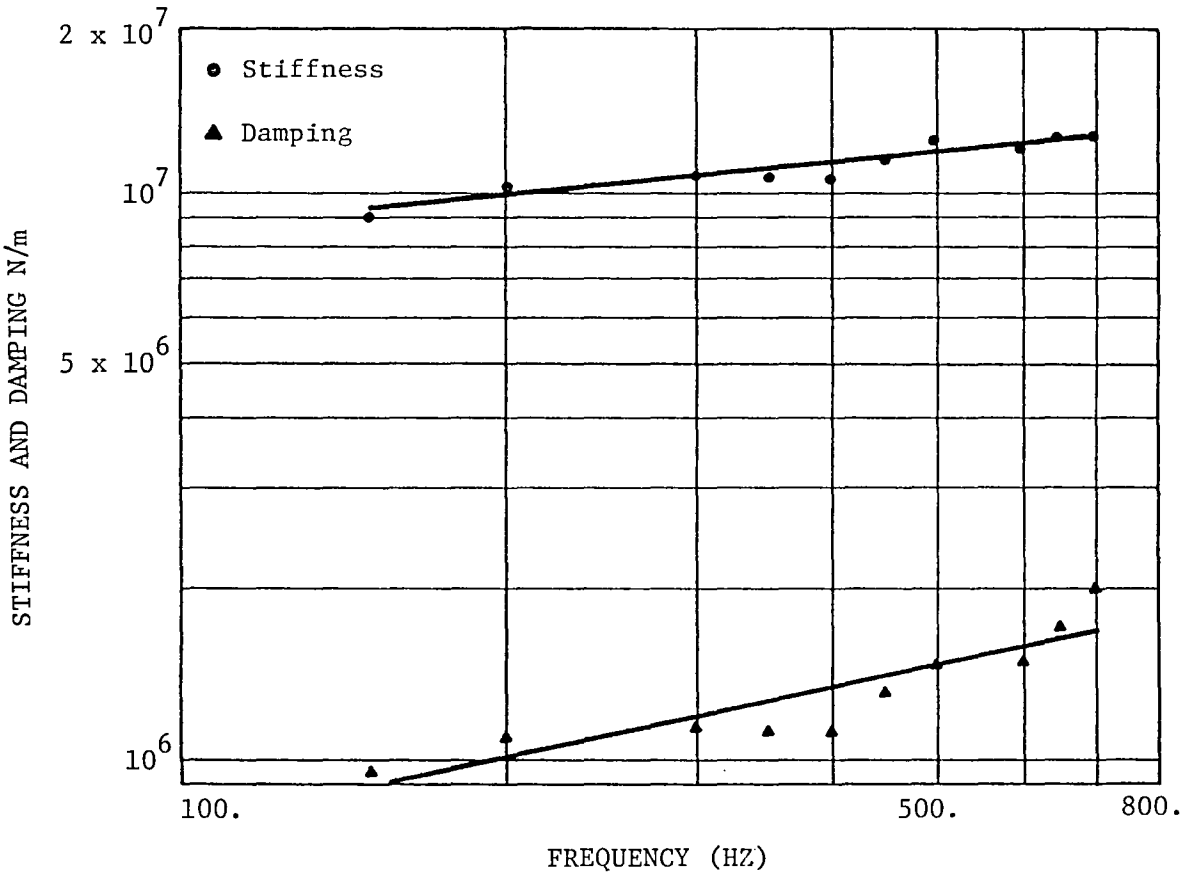

Fig. 23 Stiffness and Damping vs. Frequency. Low Strain ($\varepsilon \simeq .0008$), Shear Specimen, 80°C.

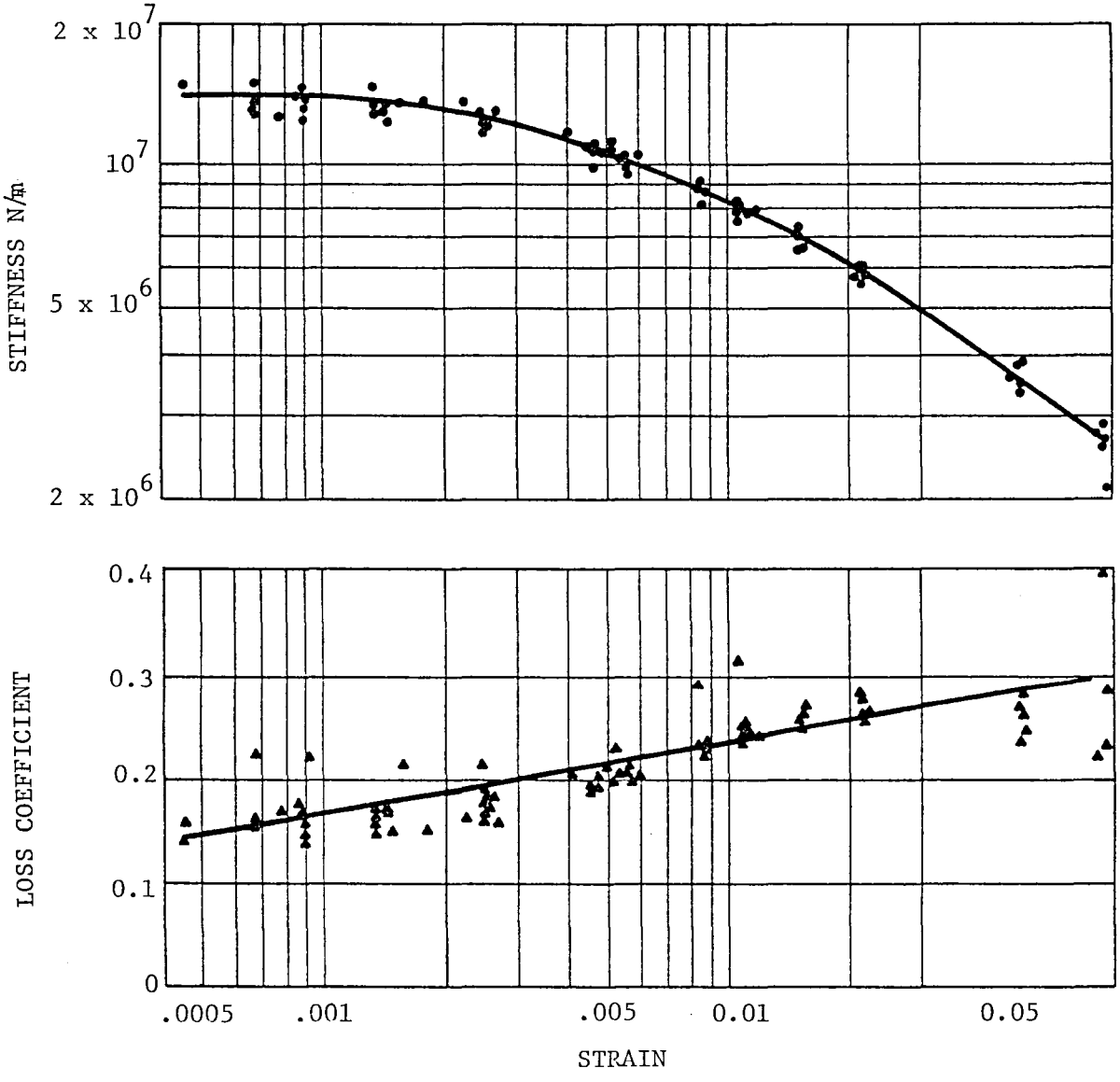

Fig. 24 Stiffness and Loss Coefficient vs. Strain. Temperature Instrumented Compression Specimen Test Results, 32°C.

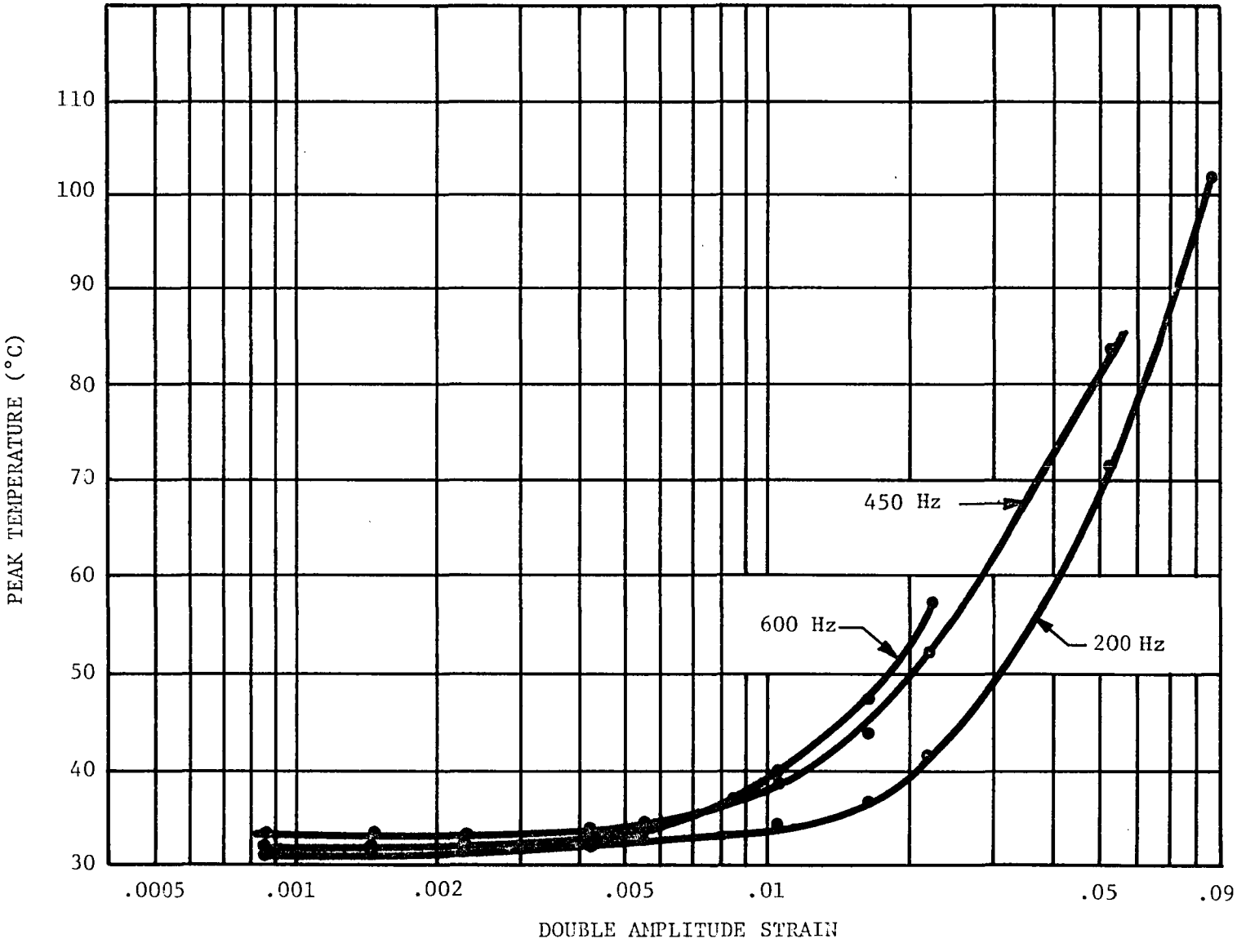

Fig. 25 Peak Temeprature vs. Strain. Compression Specimen.

791182

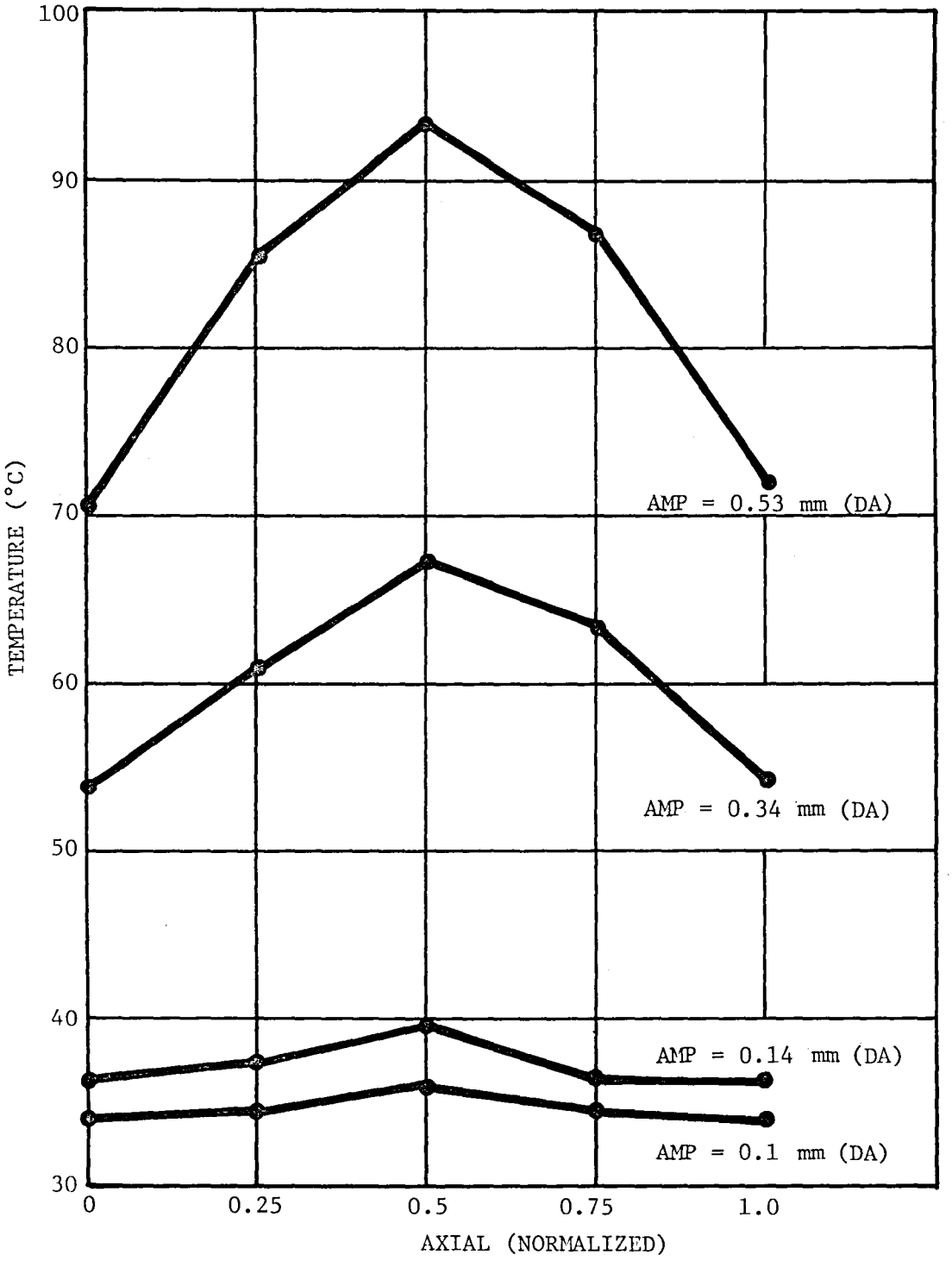

Fig. 26 Center Line Temperature Profiles. Compression Specimen, 200 Hz, 32°C Ambient Temperature

791183

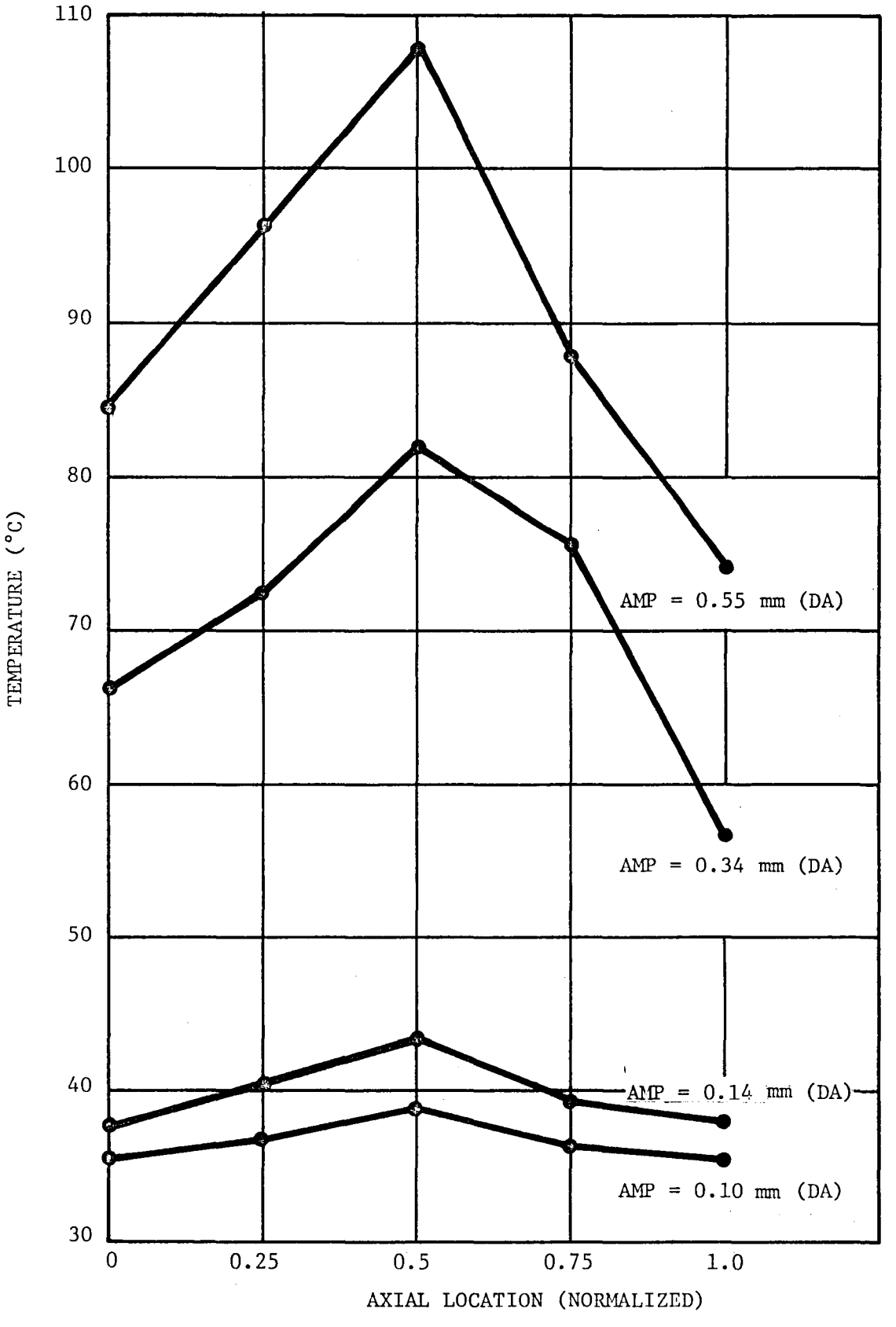

Fig. 27 Center Line Temperature Profiles. Compression Specimen, 300 Hz, 32°C Ambient Temperature.

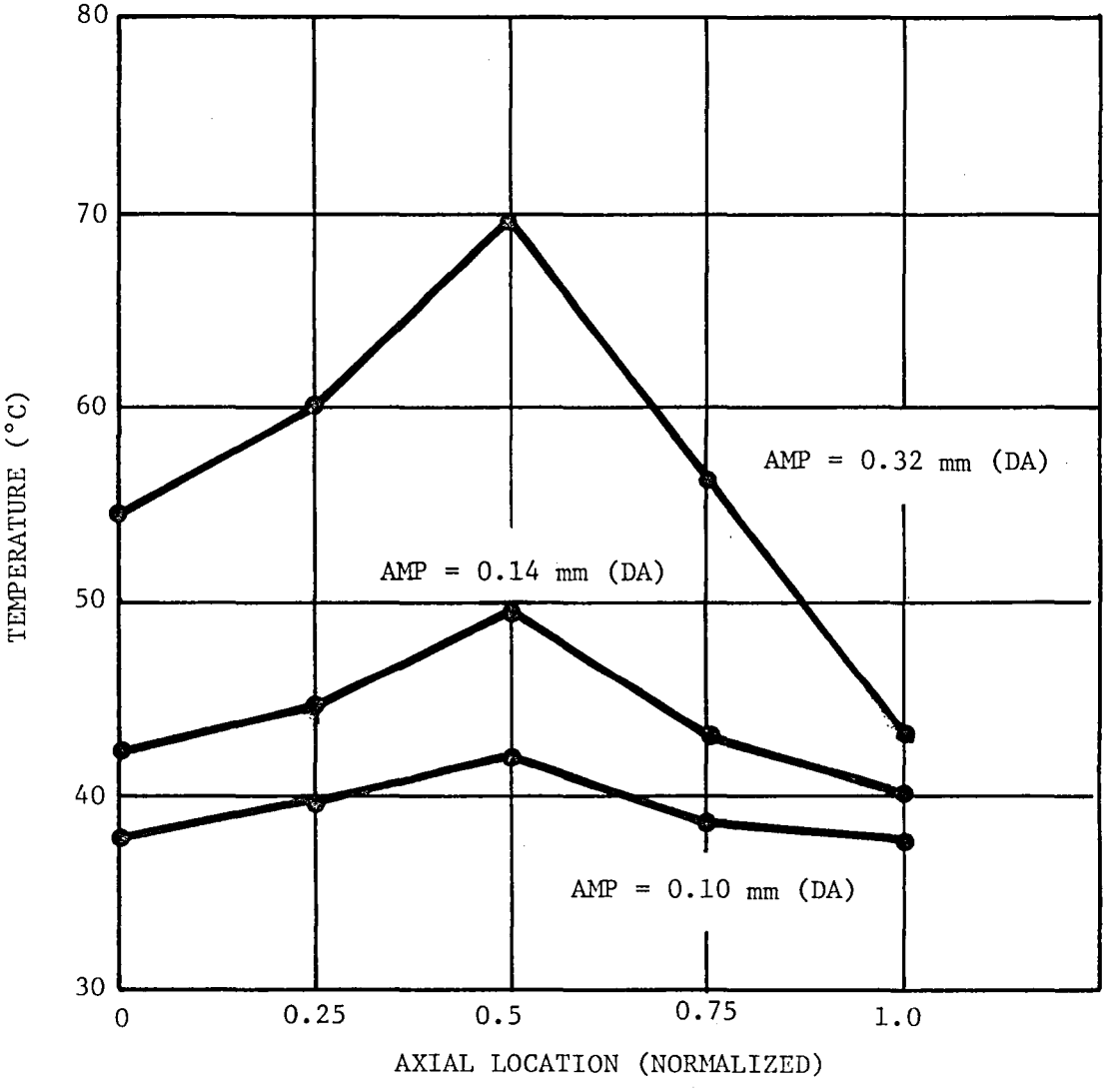

Fig. 28 Center Line Temperature Profiles. Compression Specimen, 450 Hz, 32°C Ambient Temperature

791185

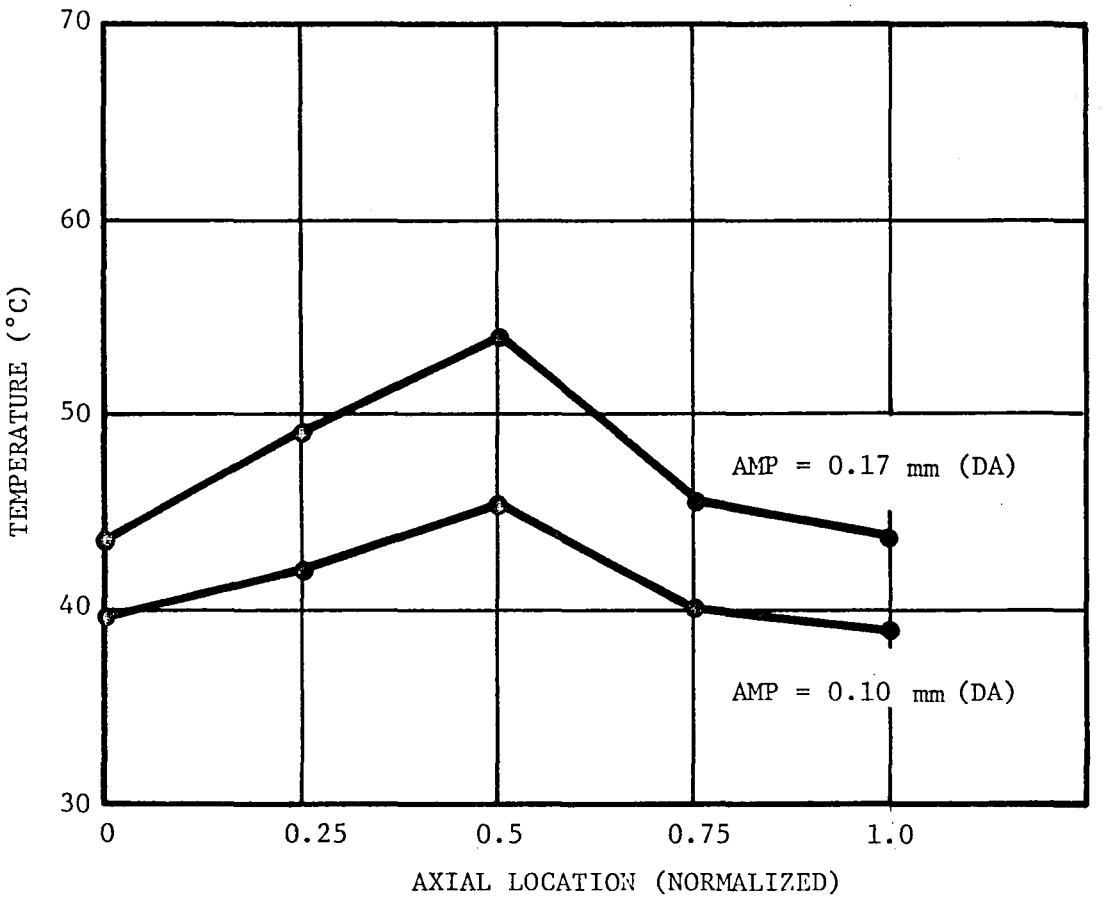

Fig. 29 Center Line Temperature Profiles. Compression Specimen, 600 Hz, 32°C Ambient Temperature

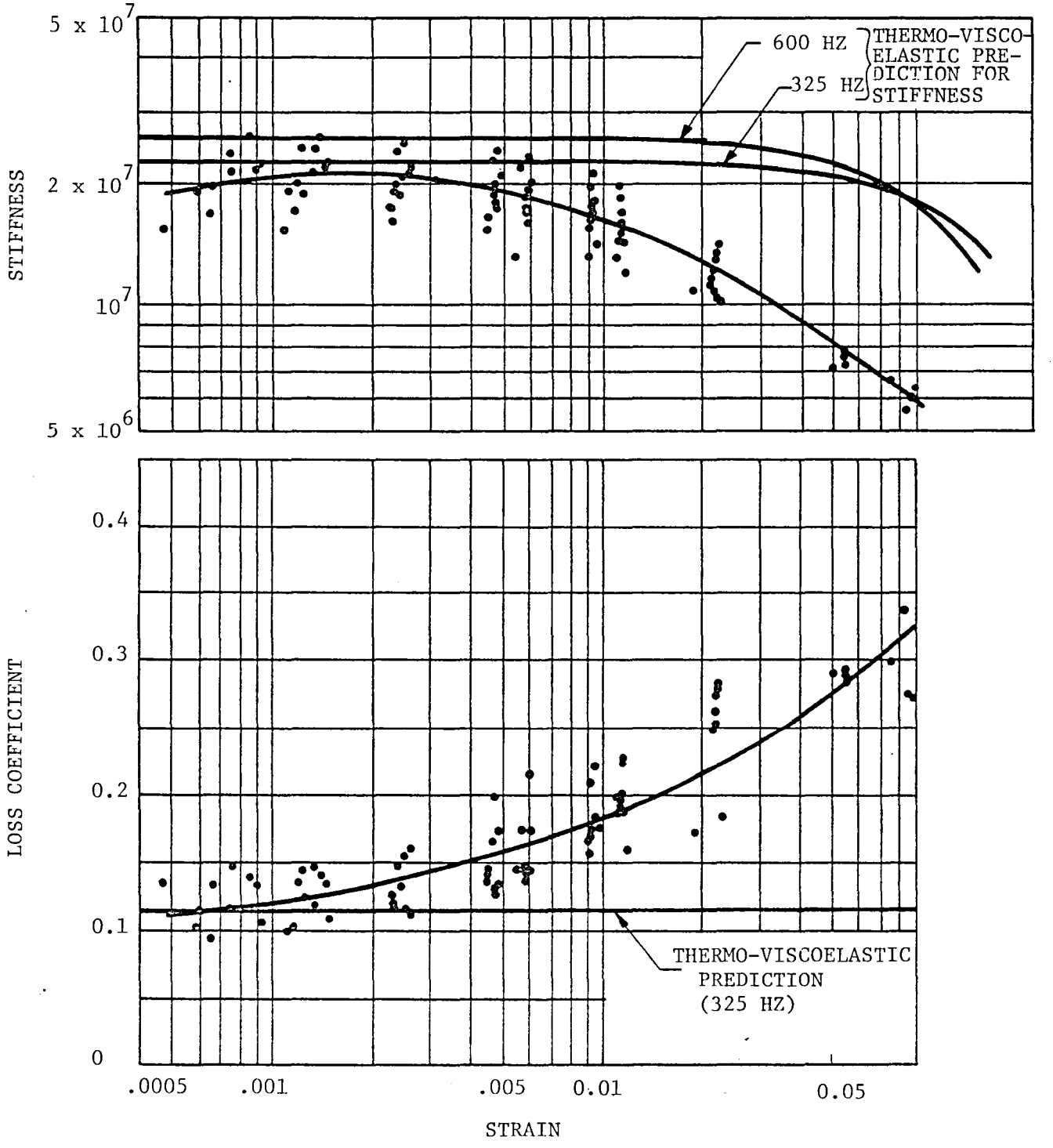

Fig. 30 Stiffness and Loss Coefficient vs. Strain. Comparison of Predicted and Measured Results, Shear Specimen.

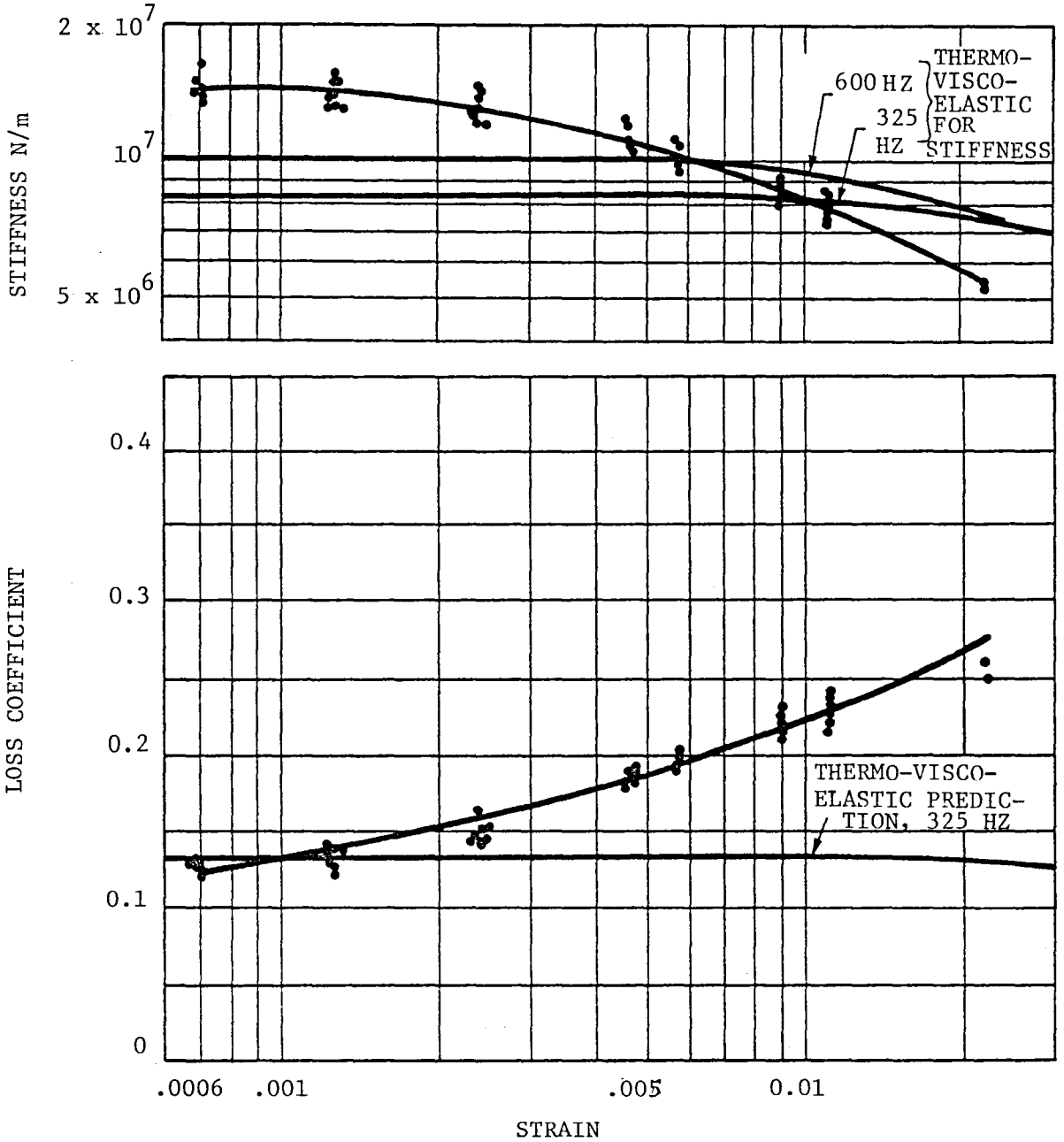

Fig. 31 Stiffness and Loss Coefficient vs. Strain. Comparison of Predicted and Measured Results, Compression Specimen, 32°C

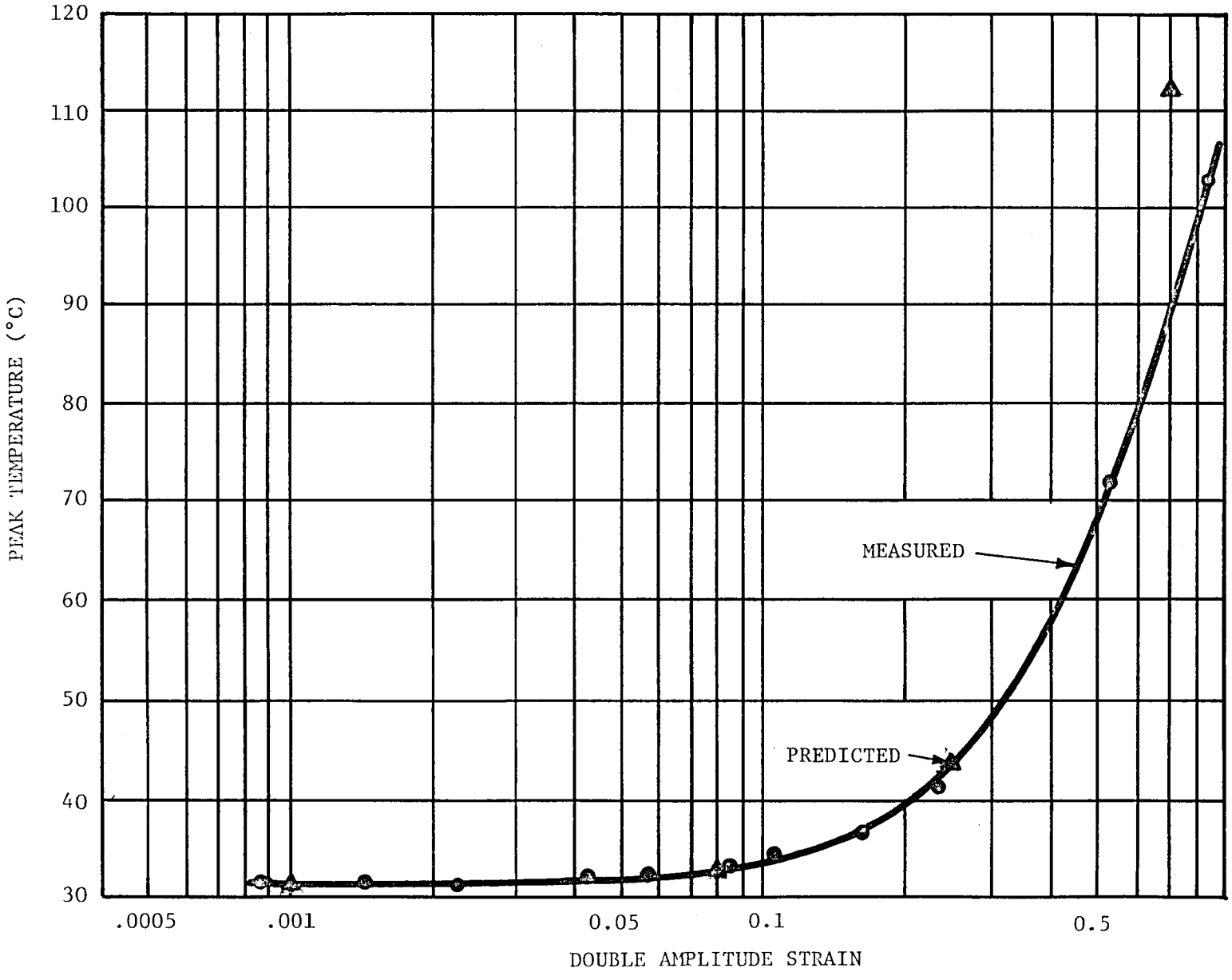

Fig. 32 Peak Temperature vs. Strain. Comparison of Prediction and Measurement Results, Compression Specimen, 200 Hz.

791191

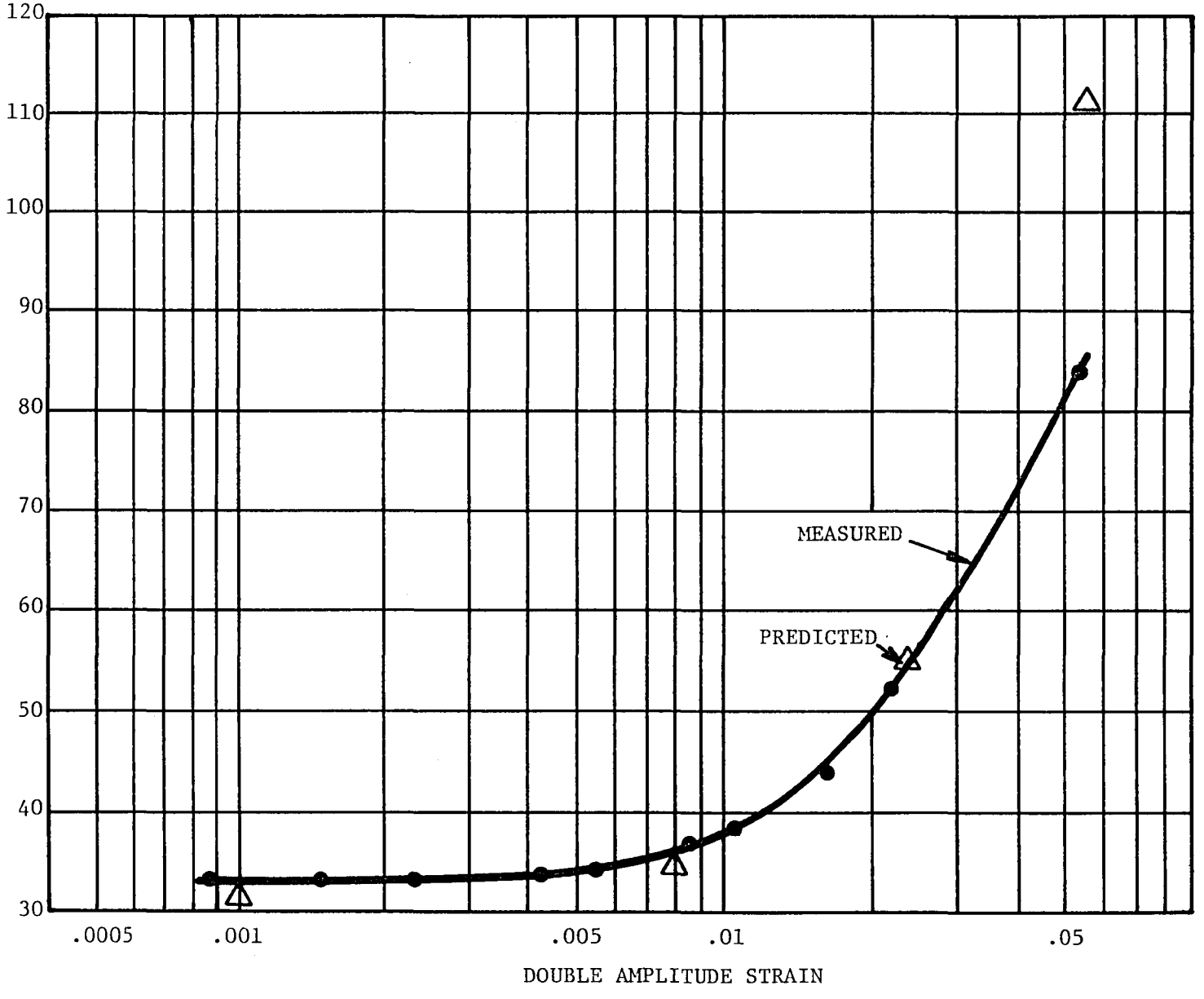

Fig. 33 Peak Temperature vs. Strain. Comparison of Prediction and Measurement Results, Compression Specimen, 450 Hz.

791192

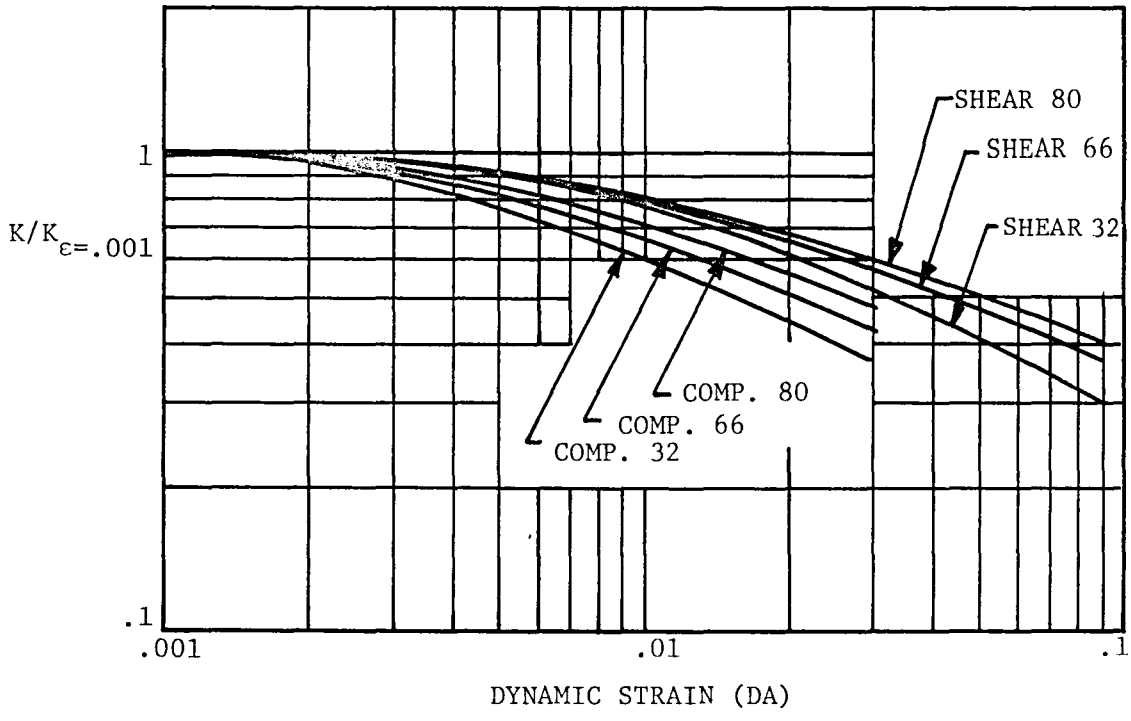

Fig. 34 Ratio of Stiffness at Finite Strain to Stiffness at .001 Strain as a Function of Dynamic Strain. Shear and Compression Specimens, 32°C, 66°C and 80°C

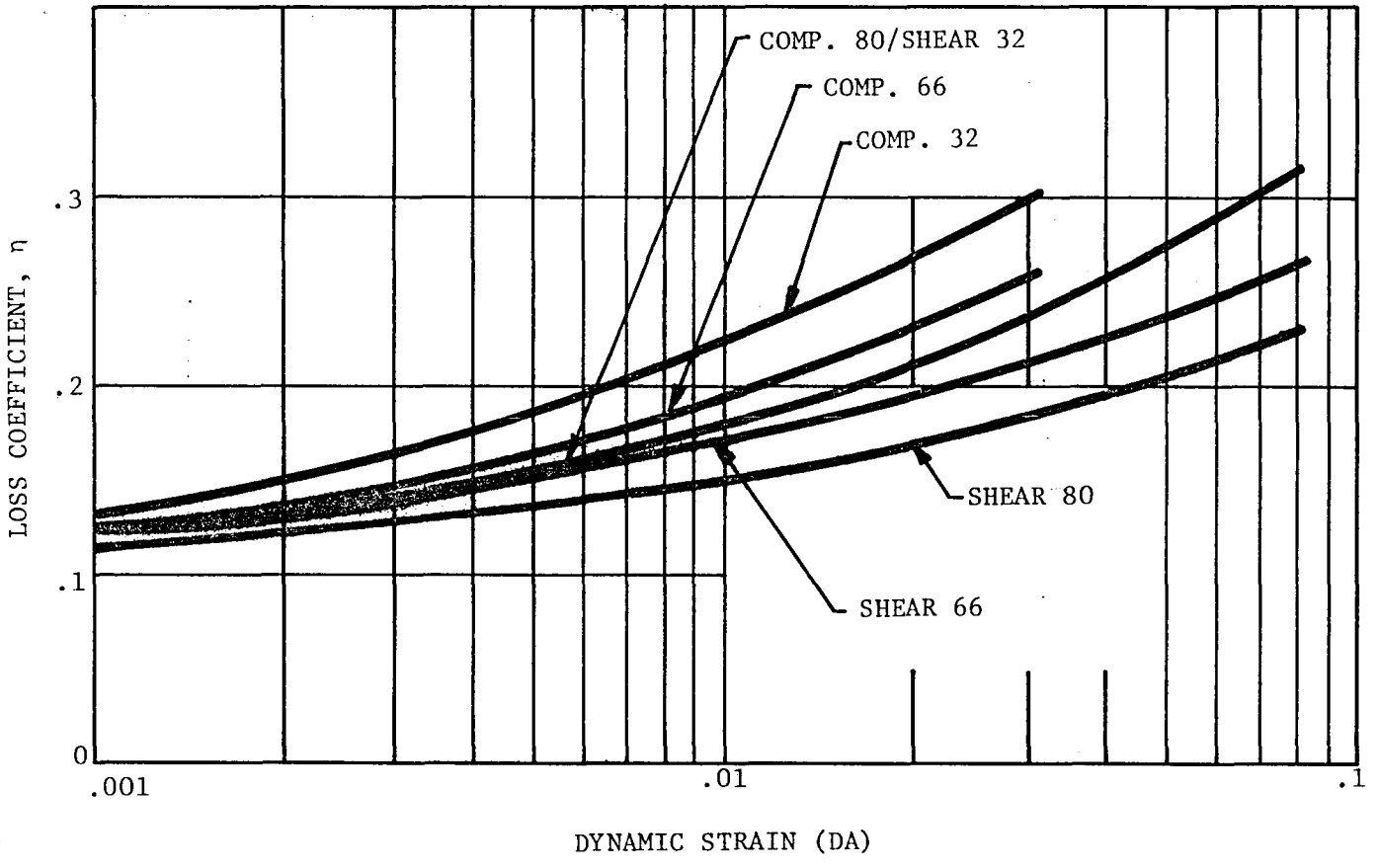

Fig. 35 Loss Coefficient vs. Dynamic Strain. Shear and Compression Specimens, 32°C, 66°C, and 80°C

791194

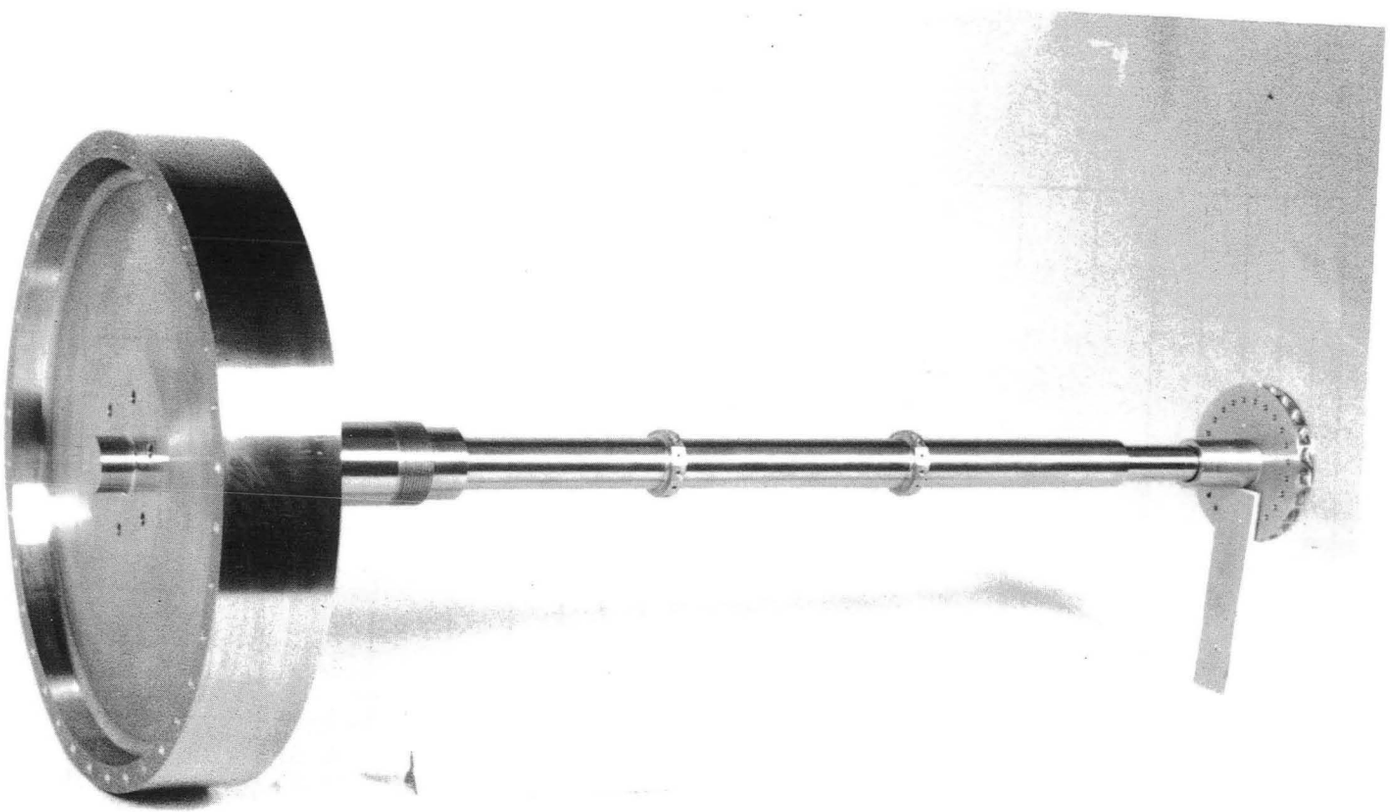

Fig. 36 Photo of Test Rotor During Assembly

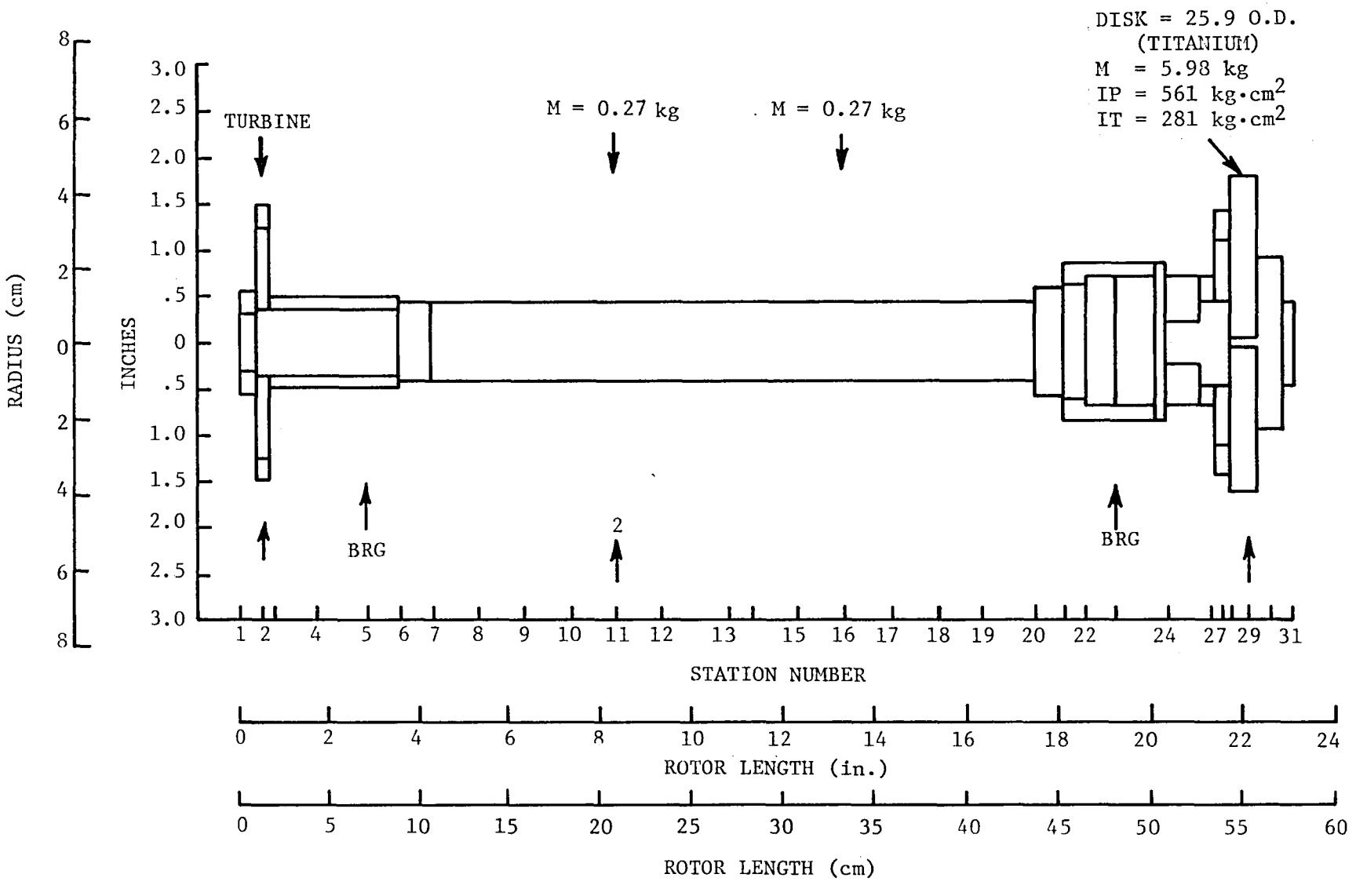

Fig. 37 Test Rotor Schematic Diagram

791206

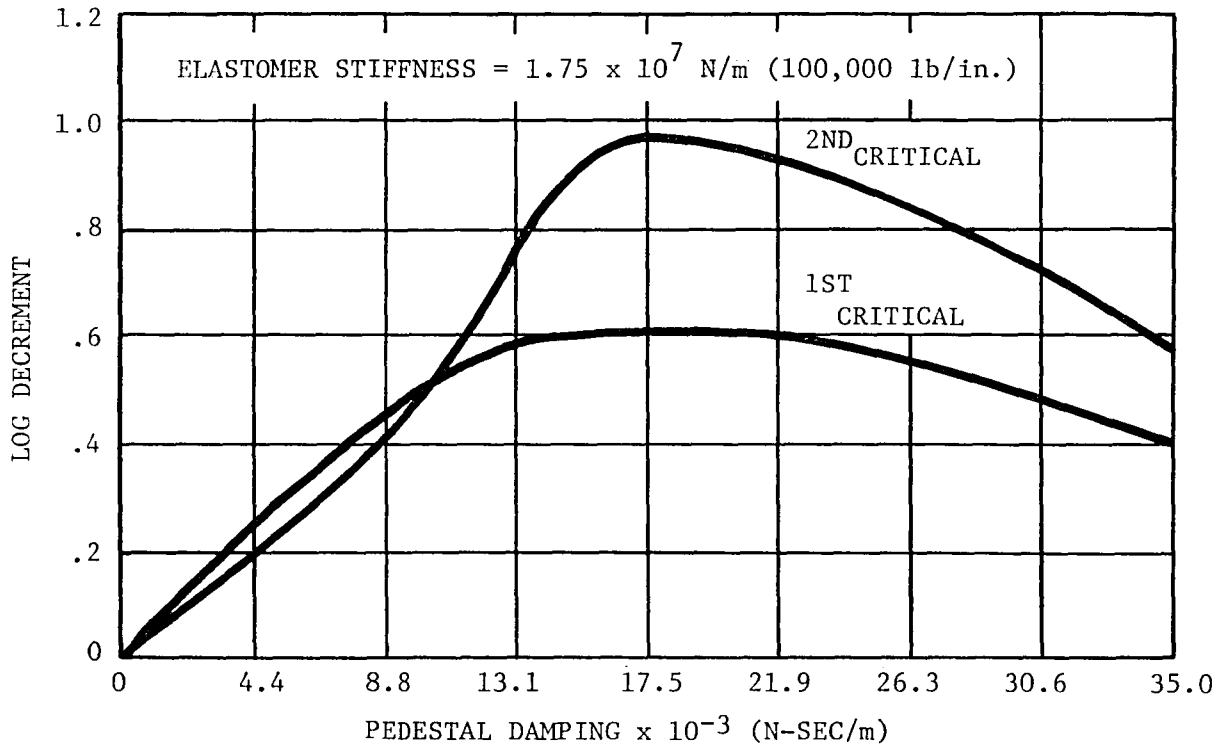

Fig. 38 Elastomer Damper Test Rig. Log Decrement as a Function of Elastomer Damping

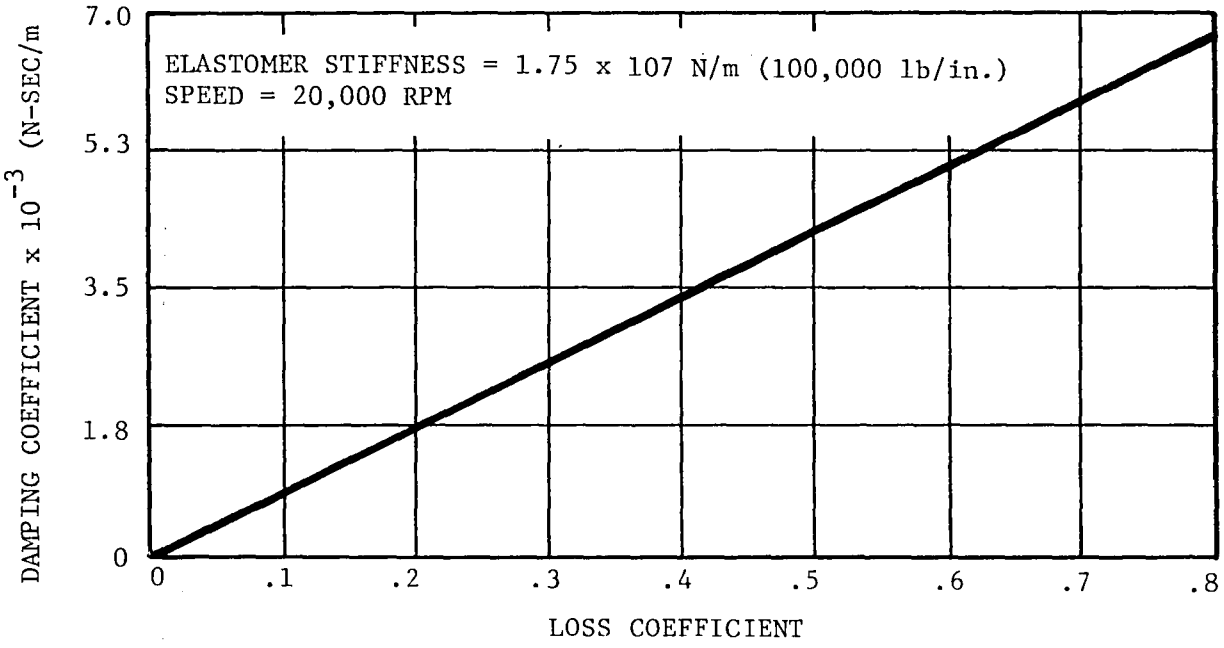

Fig. 39 Damping Coefficient as a Function of Loss Coefficient

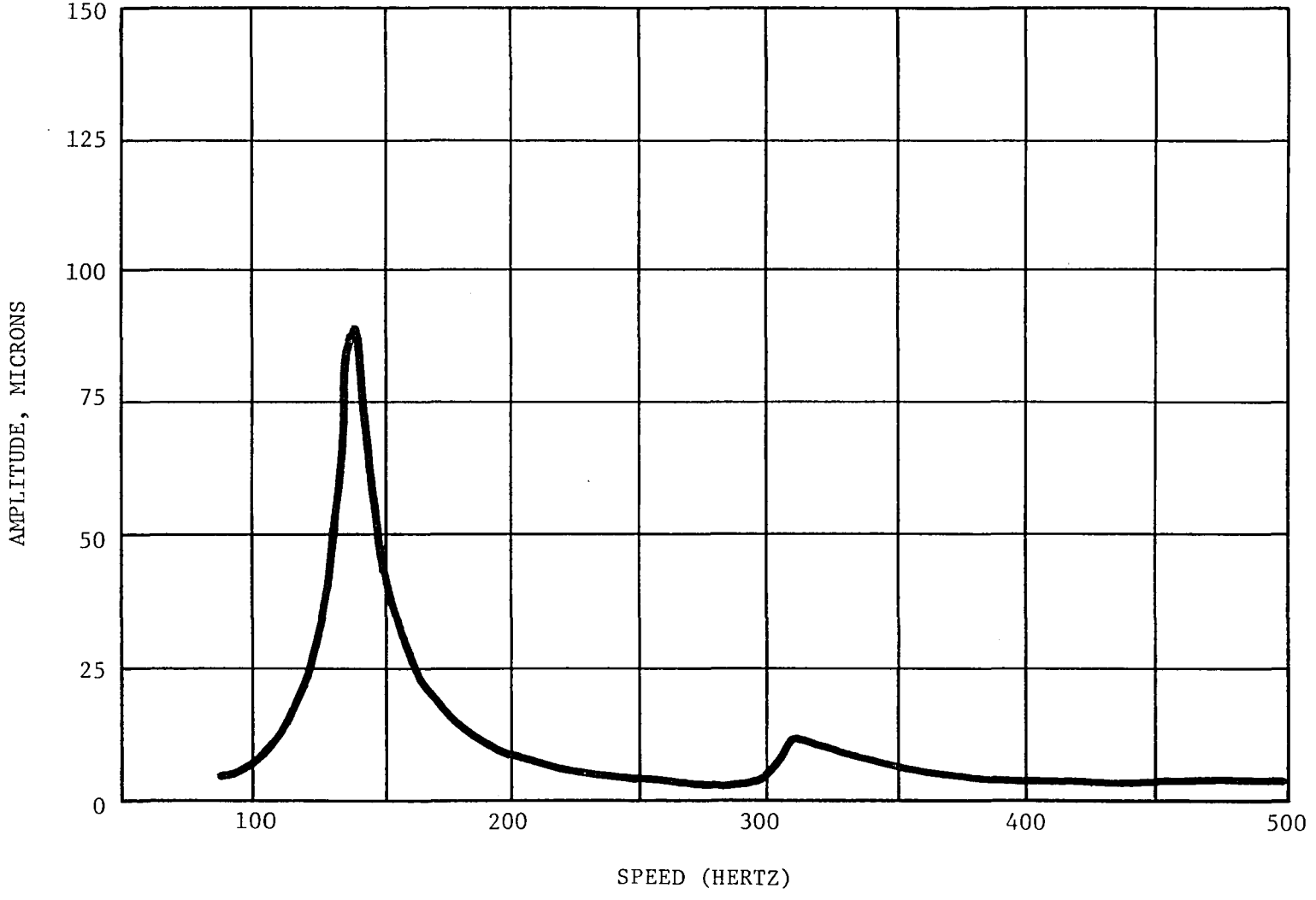

Fig. 40 Disc Unbalance. Sensitivity to Weight at Disc for Polybutadiene Mounts

791209

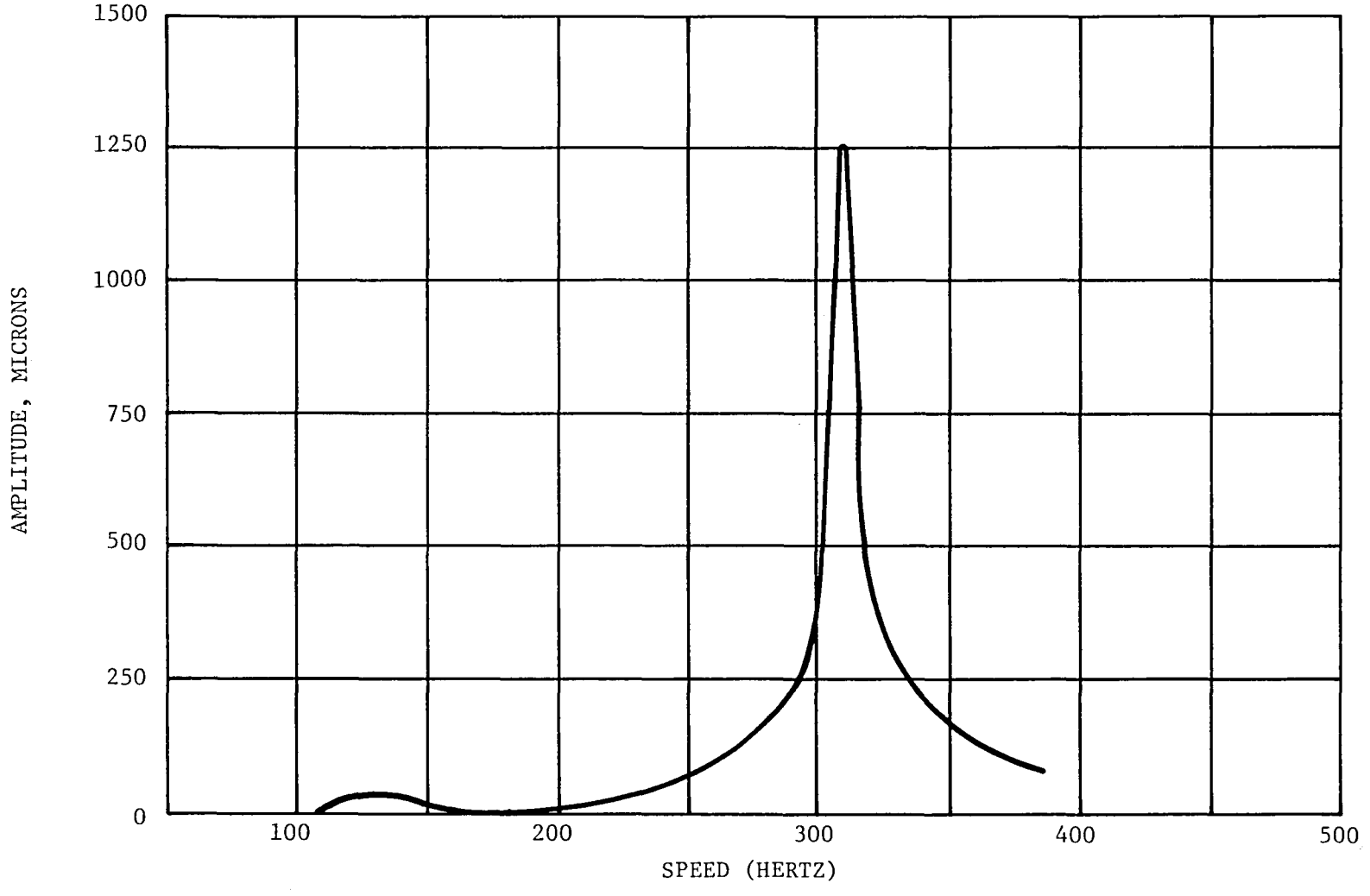

Fig. 41 Shaft Unbalance. Sensitivity to Weight at Shaft for Polybutadiene Mounts

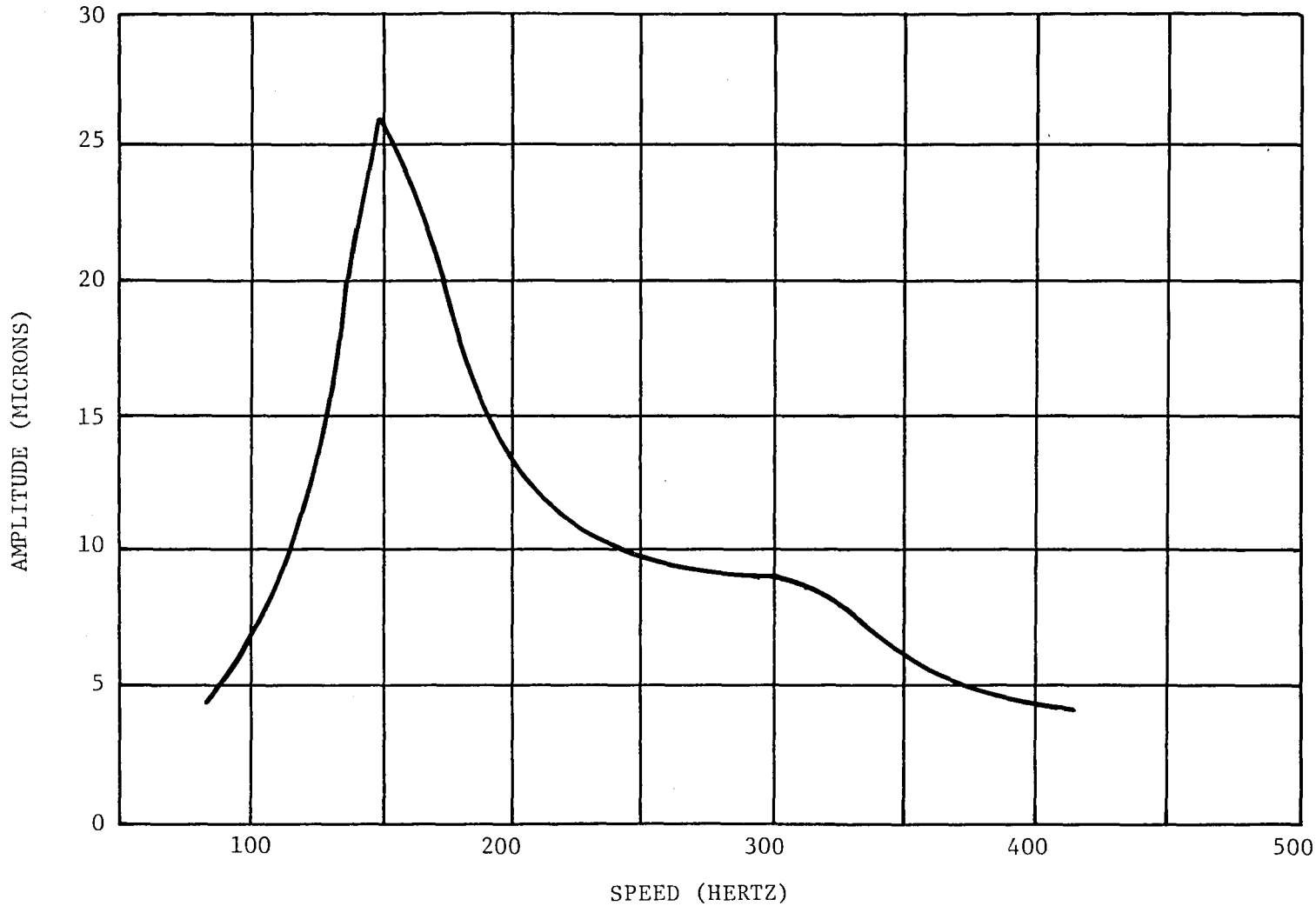

Fig. 42 Disc Unbalance. Sensitivity to Weight on Disc for Viton-70 Mounts

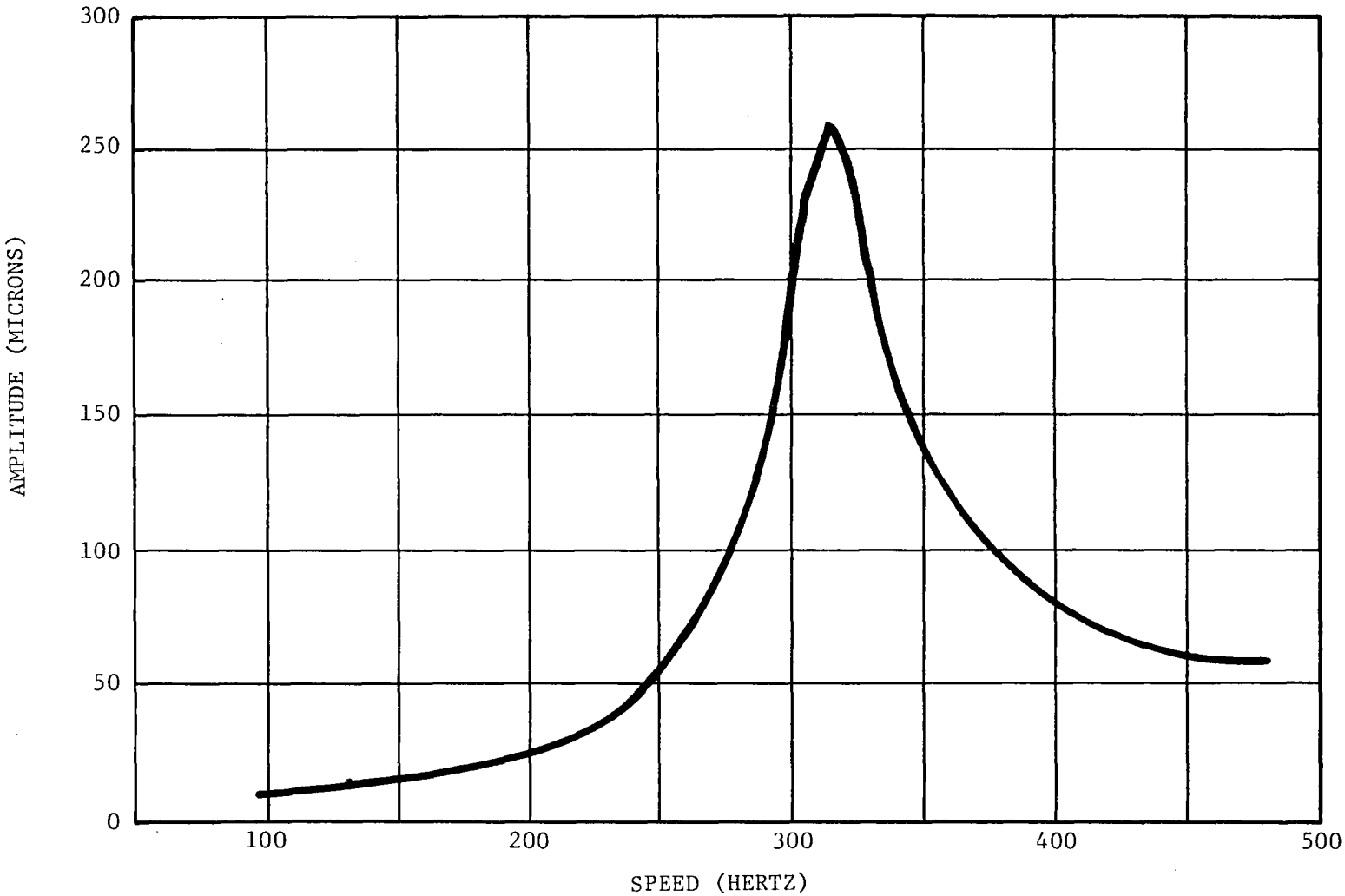

Fig. 43 Shaft Unbalance. Sensitivity to Weight on Shaft for Viton-70 Mounts

791212

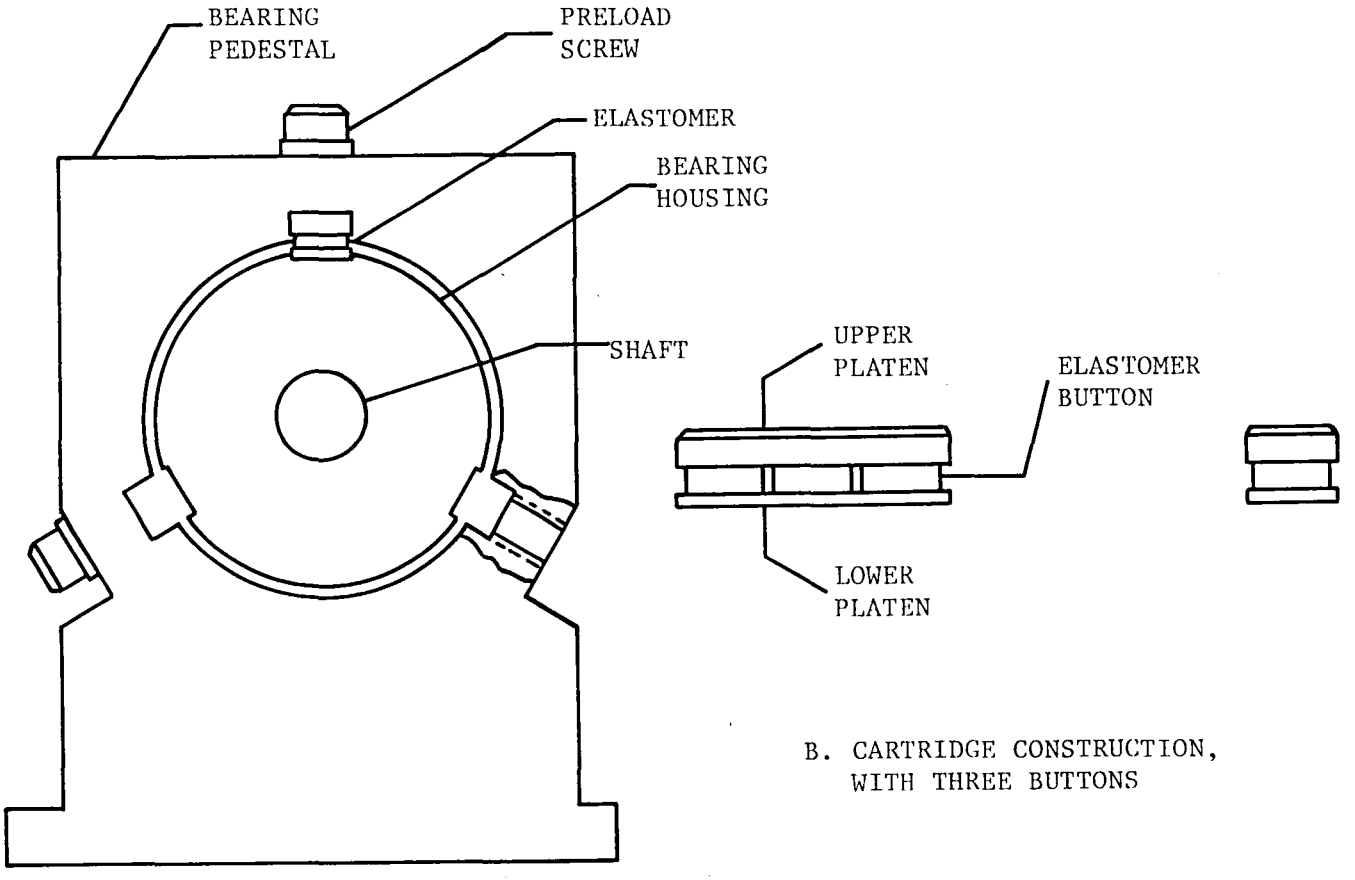

Fig. 44 Method of Supporting Test Rig Rotor on Elastomers

791213

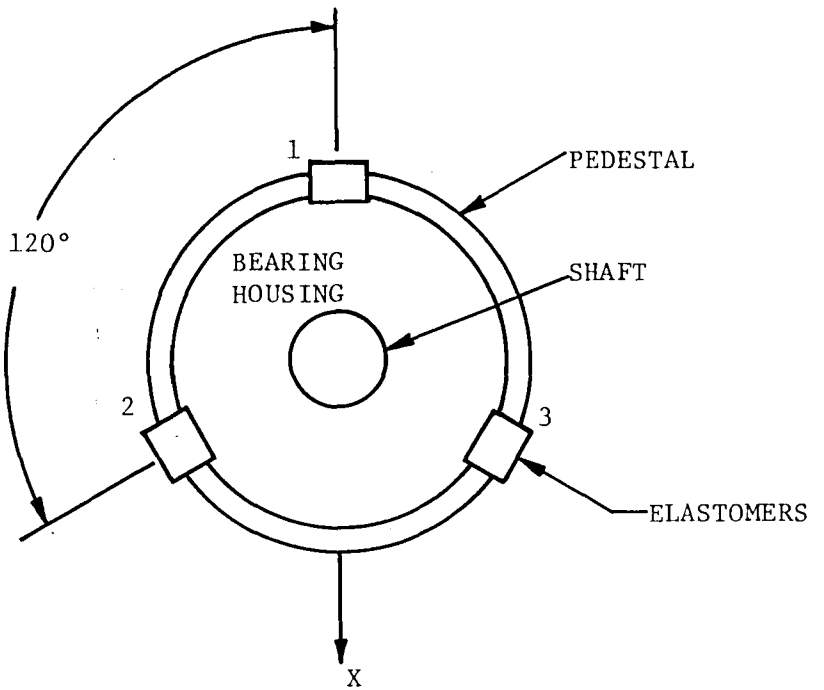

A. OVERALL SUPPORT GEOMETRY

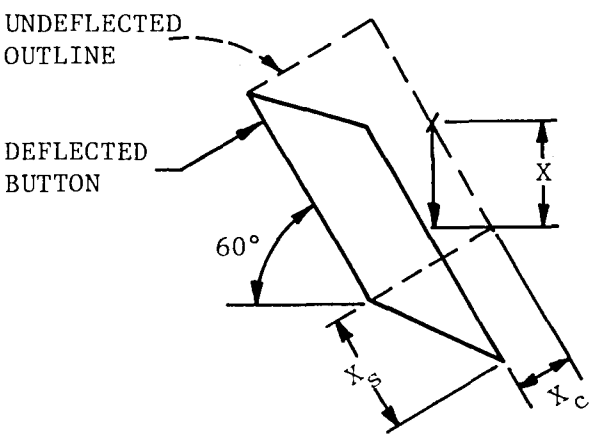

B. DETAIL OF INDIVIDUAL DEFLECTED BUTTON - NO. 2 (5 x SCALE OF VIEW A)

Fig. 45 Support Geometry and Button Deformation for Stiffness Calculations

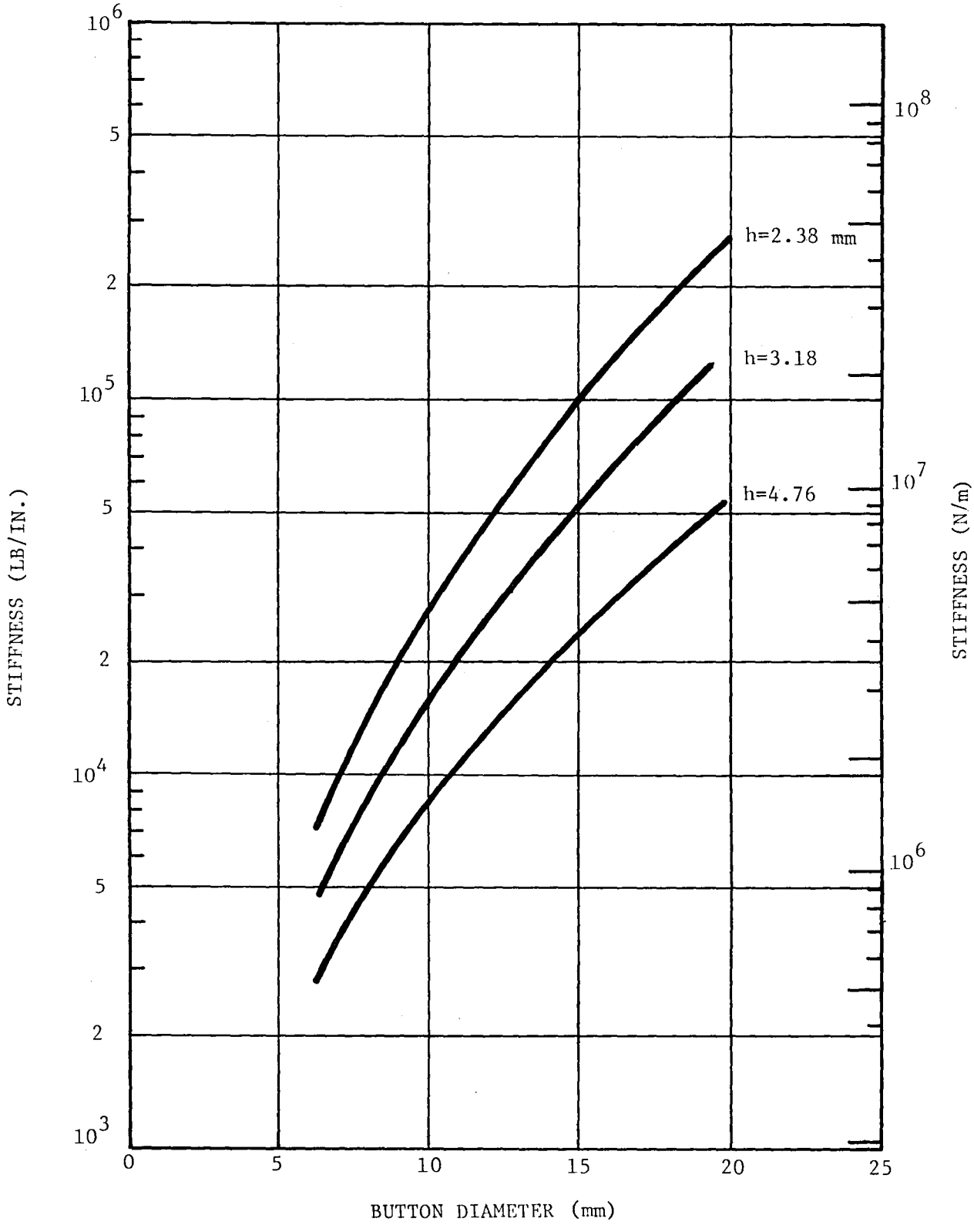

Fig. 46 Plot of Support Stiffness vs. Button Diameter for Viton-70 at 32°C

791215

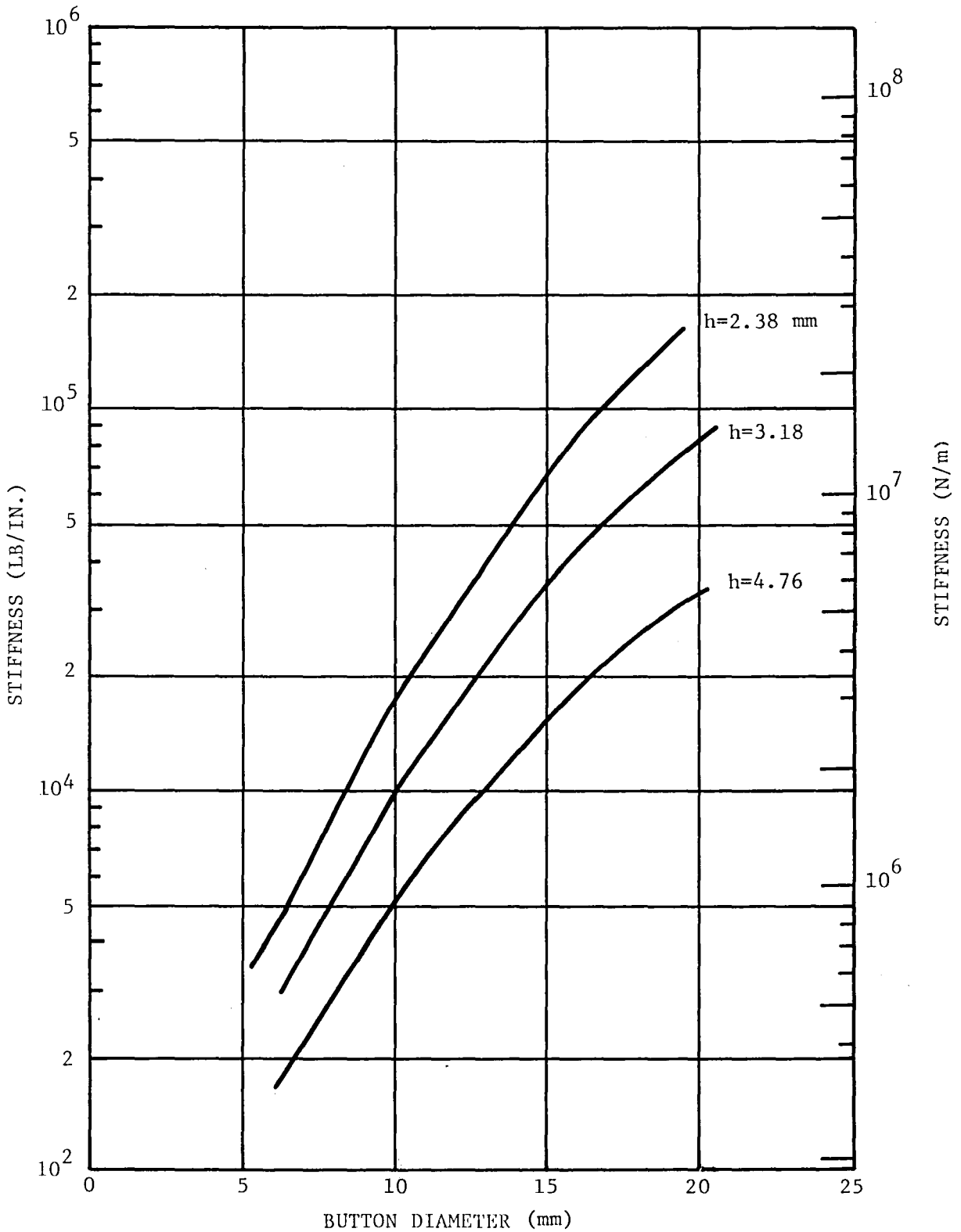

Fig. 47 Plot of Support Stiffness vs. Button Diameter for Viton at 50°C

791216

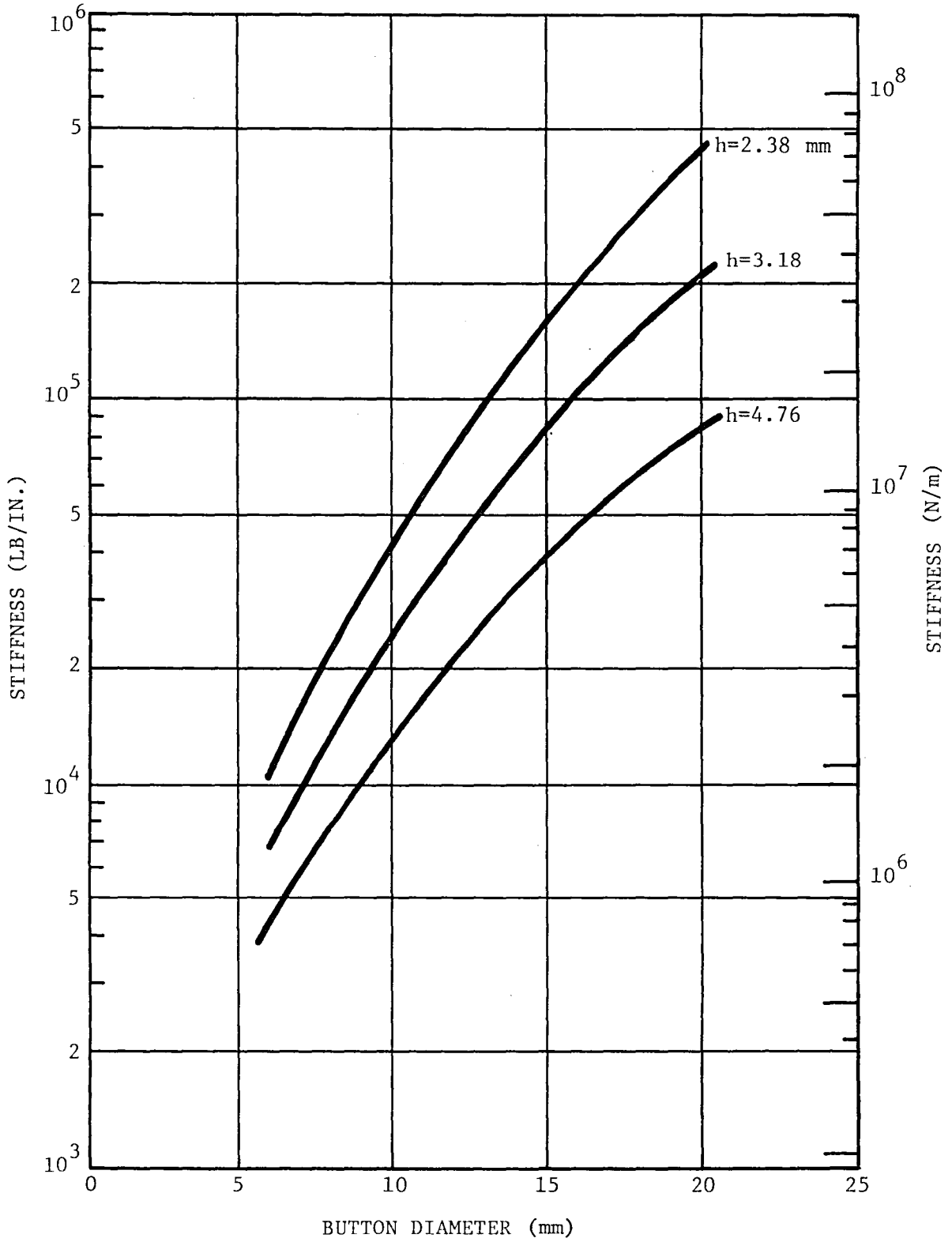

Fig. 48 Plot of Support Stiffness vs. Button Diameter for Polybutadiene at 32°C

791217

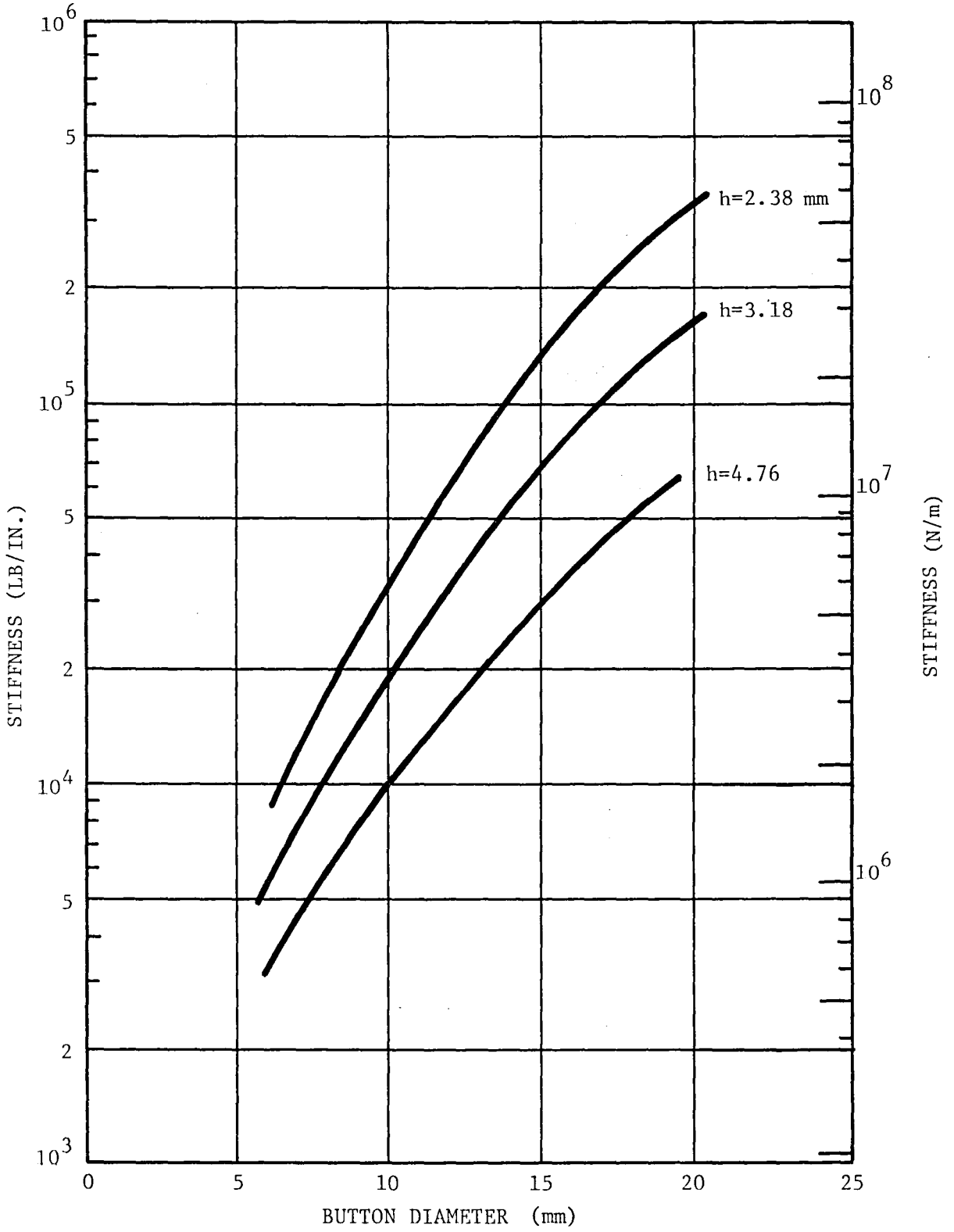

Fig. 49 Plot of Support Stiffness vs. Button Diameter for Polybutadiene at 50°C

791218

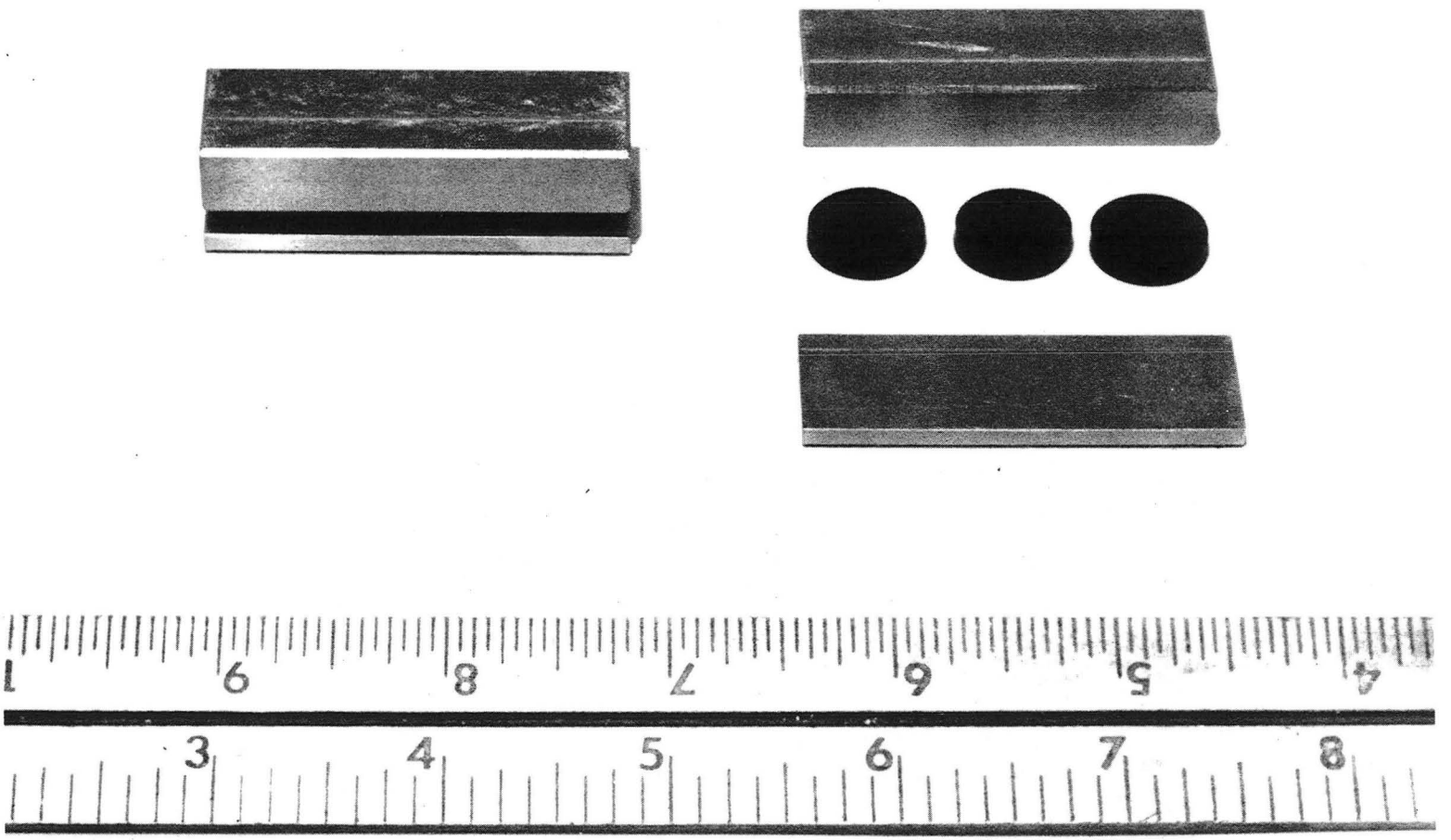

Fig. 50 Detail View of Elastomer Cartridge During Assembly

MTI-18367

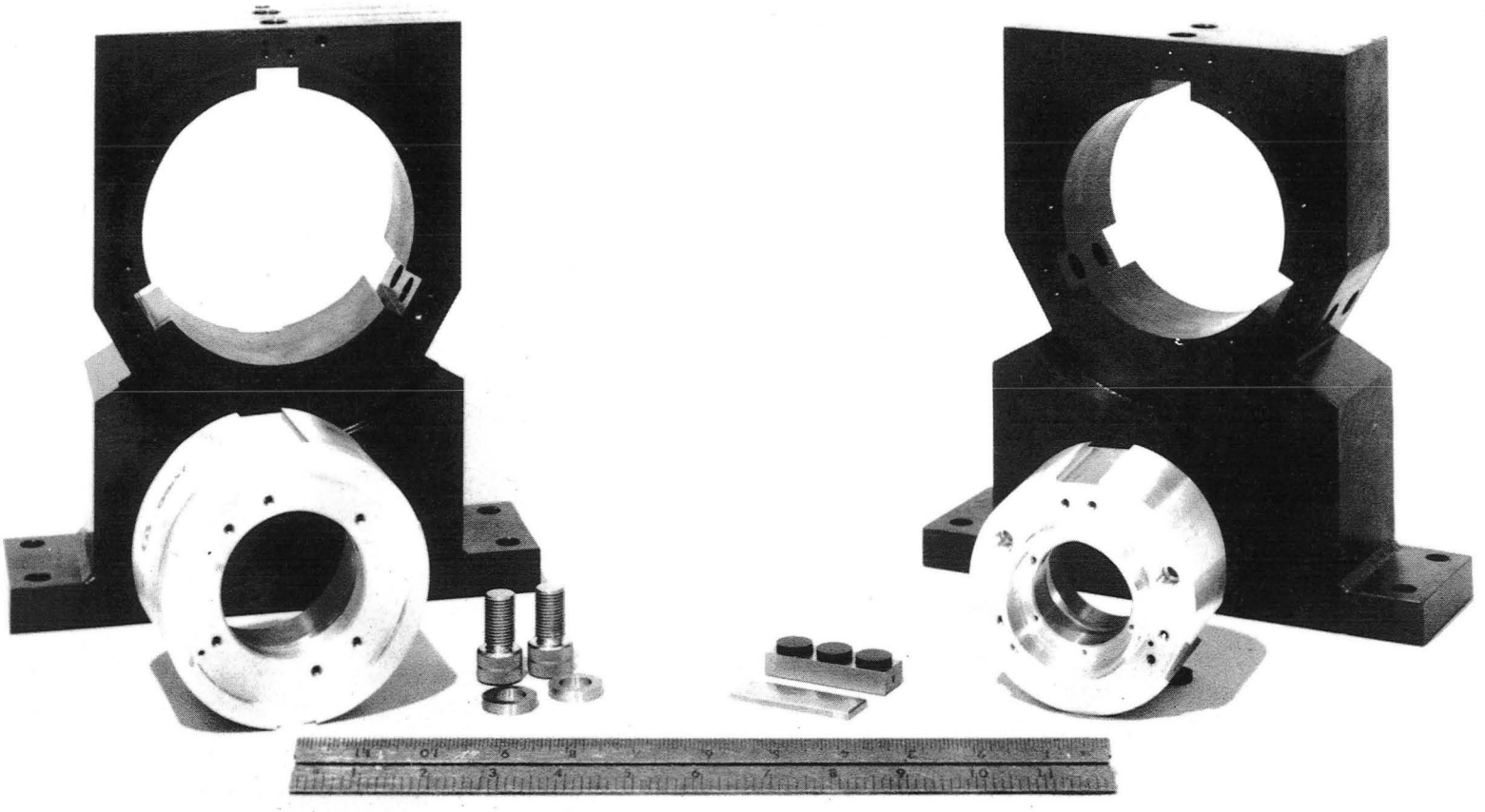

Fig. 51 Elastomer Damper Rig, Pedestals, and Bearing Housing

MTI-18371

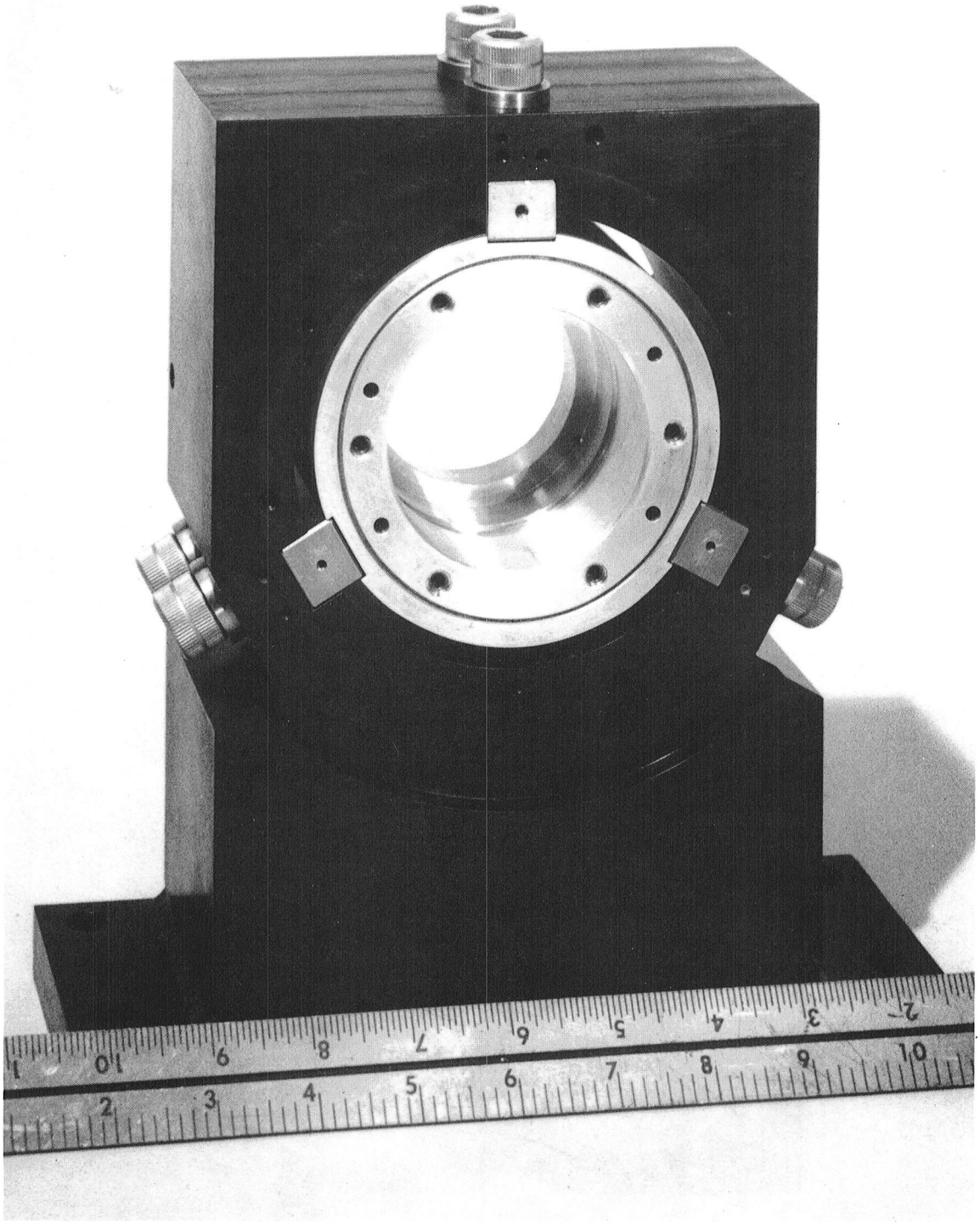

Fig. 52 Partially Assembled Disc, Bearing Housing and Pedestal

MTI-18369

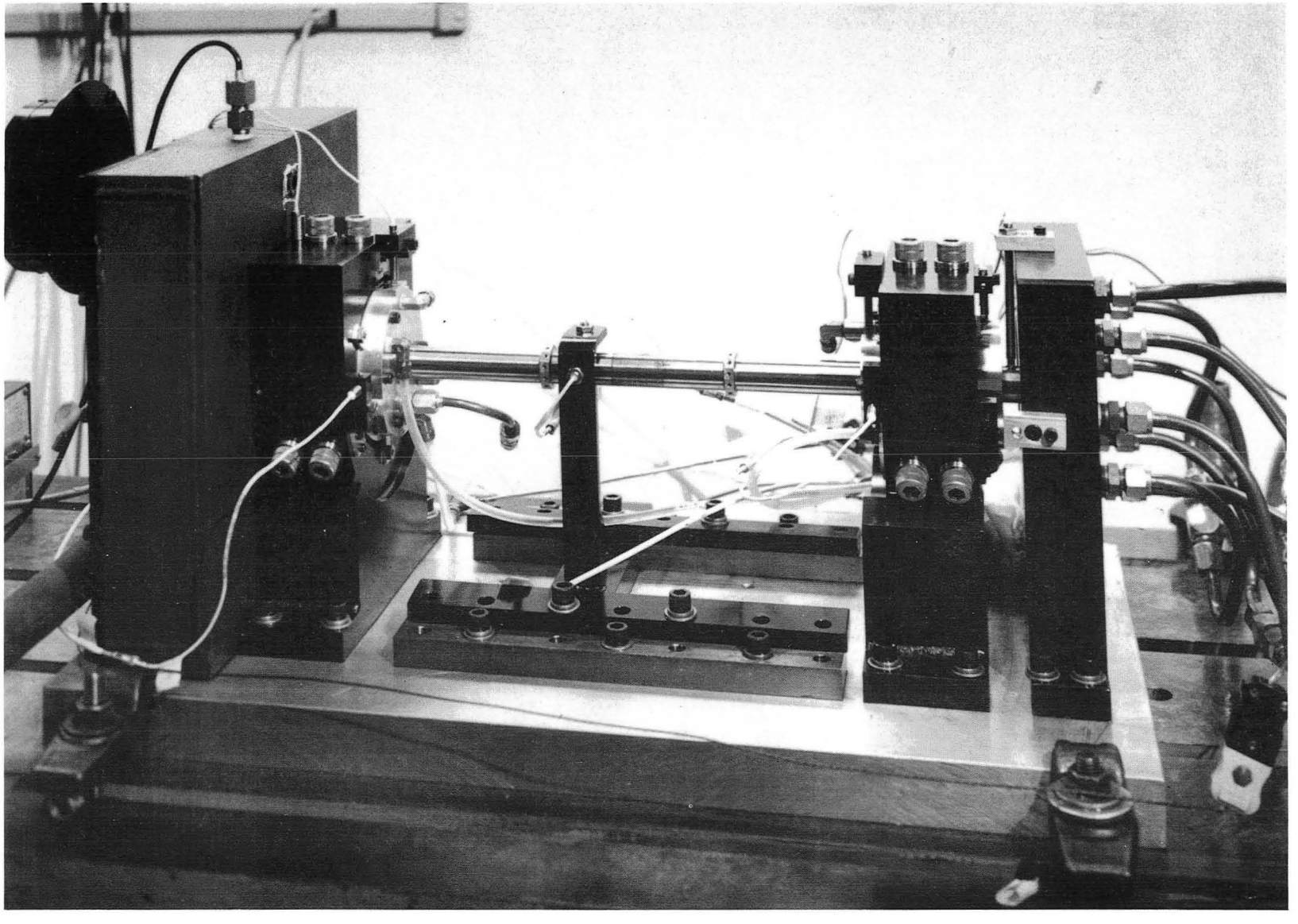

Fig. 53 Side View of Assembled Test Rig

MTI-18370

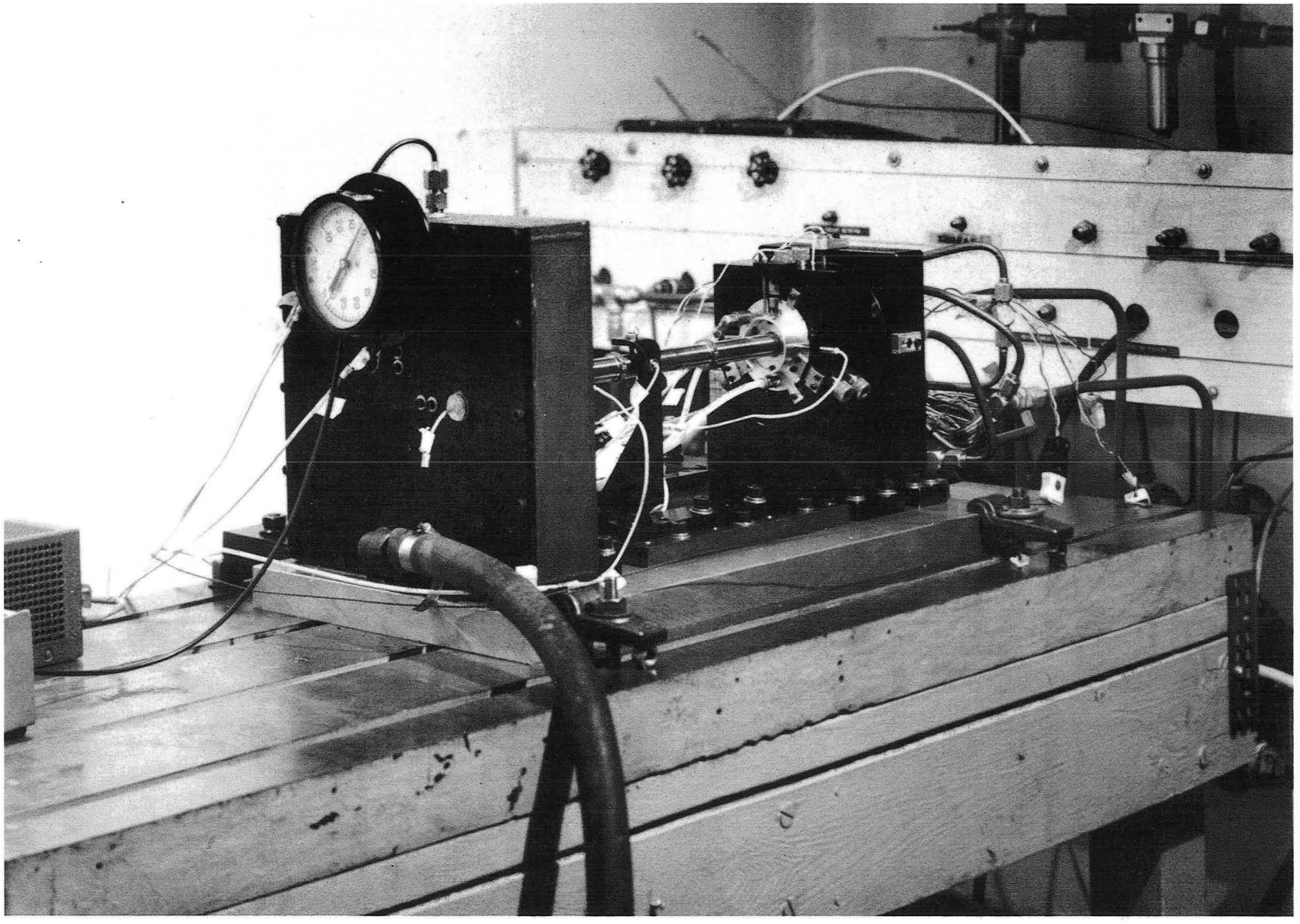

Fig. 54 Front View of Assembled Test Rig

MTI-18366

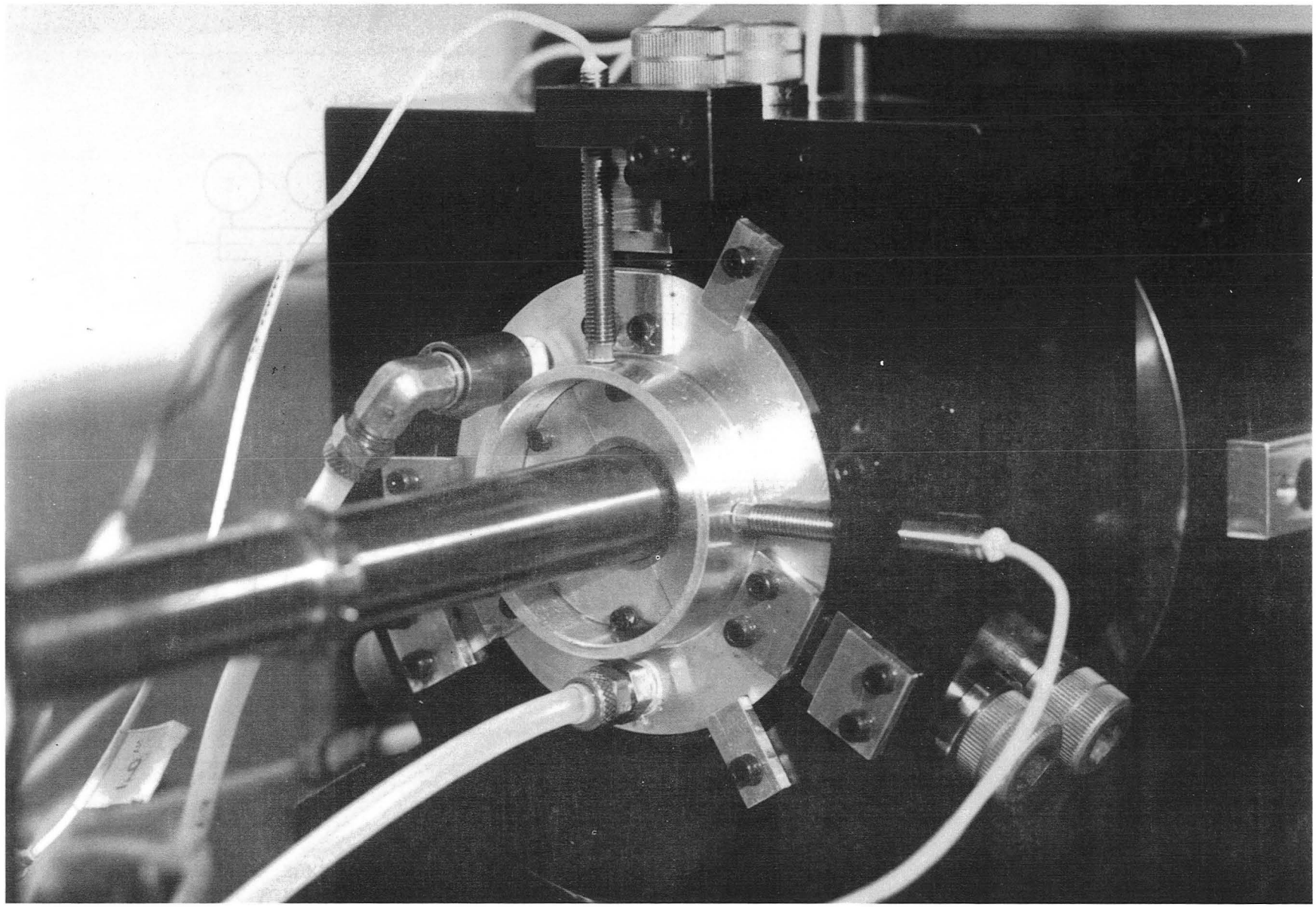

Fig. 55 Close-up of Turbine in Bearing Housing Showing Elastomer Cartridges at 12 noon and 4:00 Positions

MTI-18038

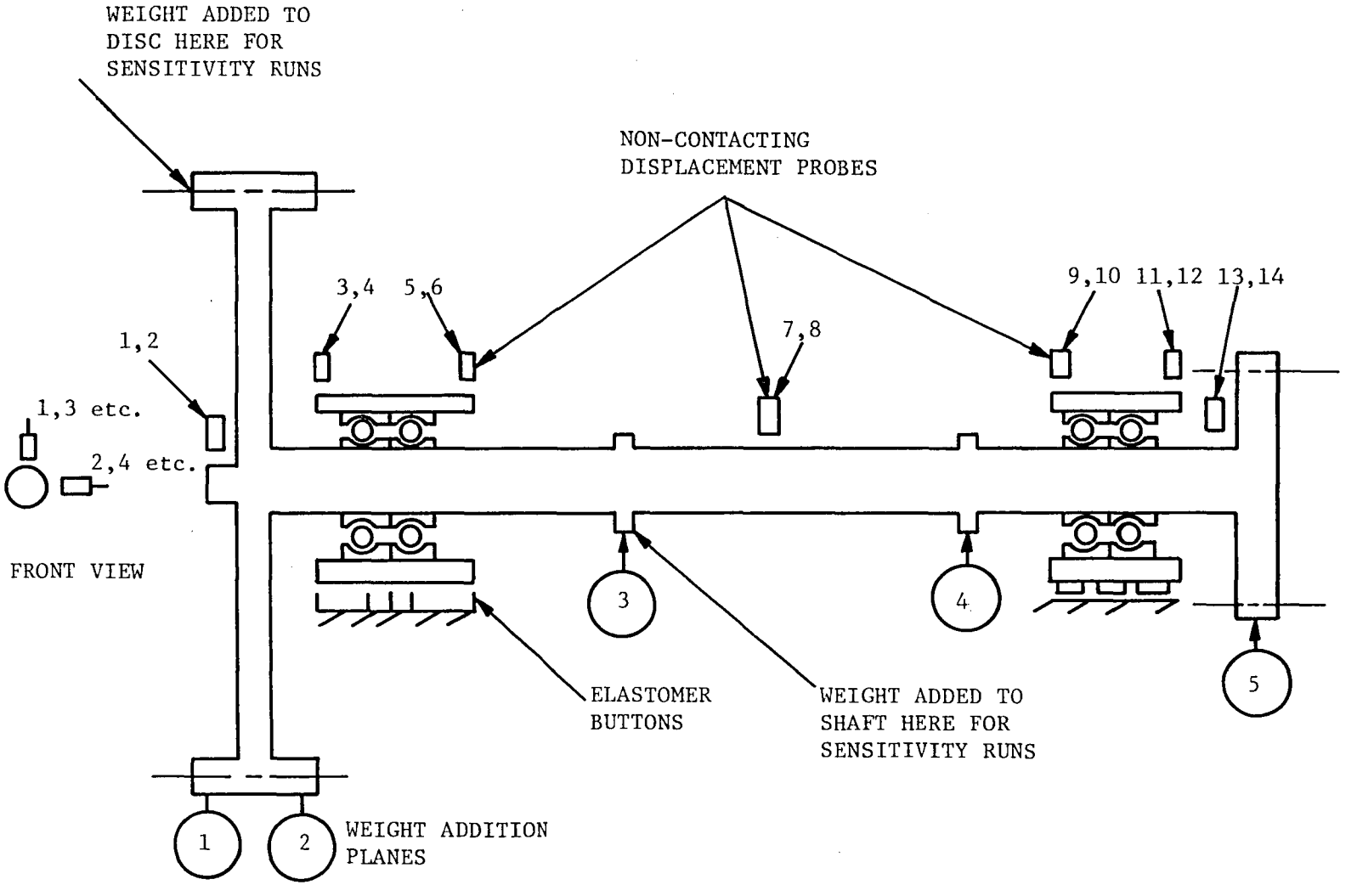

Fig. 56 Schematic Drawing of Rotor System Showing Weight Addition Planes and Displacement Probe Locations

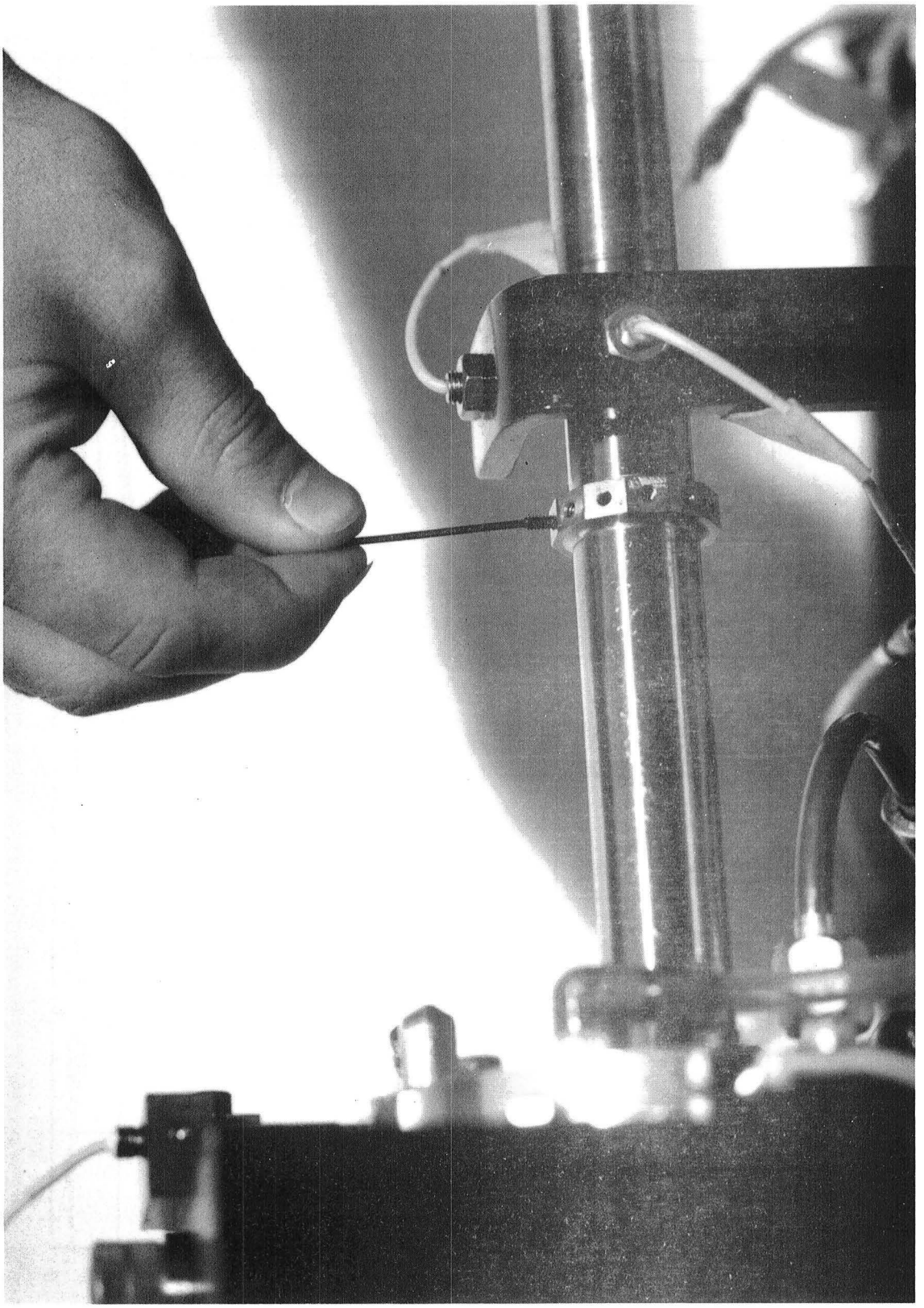

Fig. 57 Installation of Unbalance Weight on the Test Rig Shaft

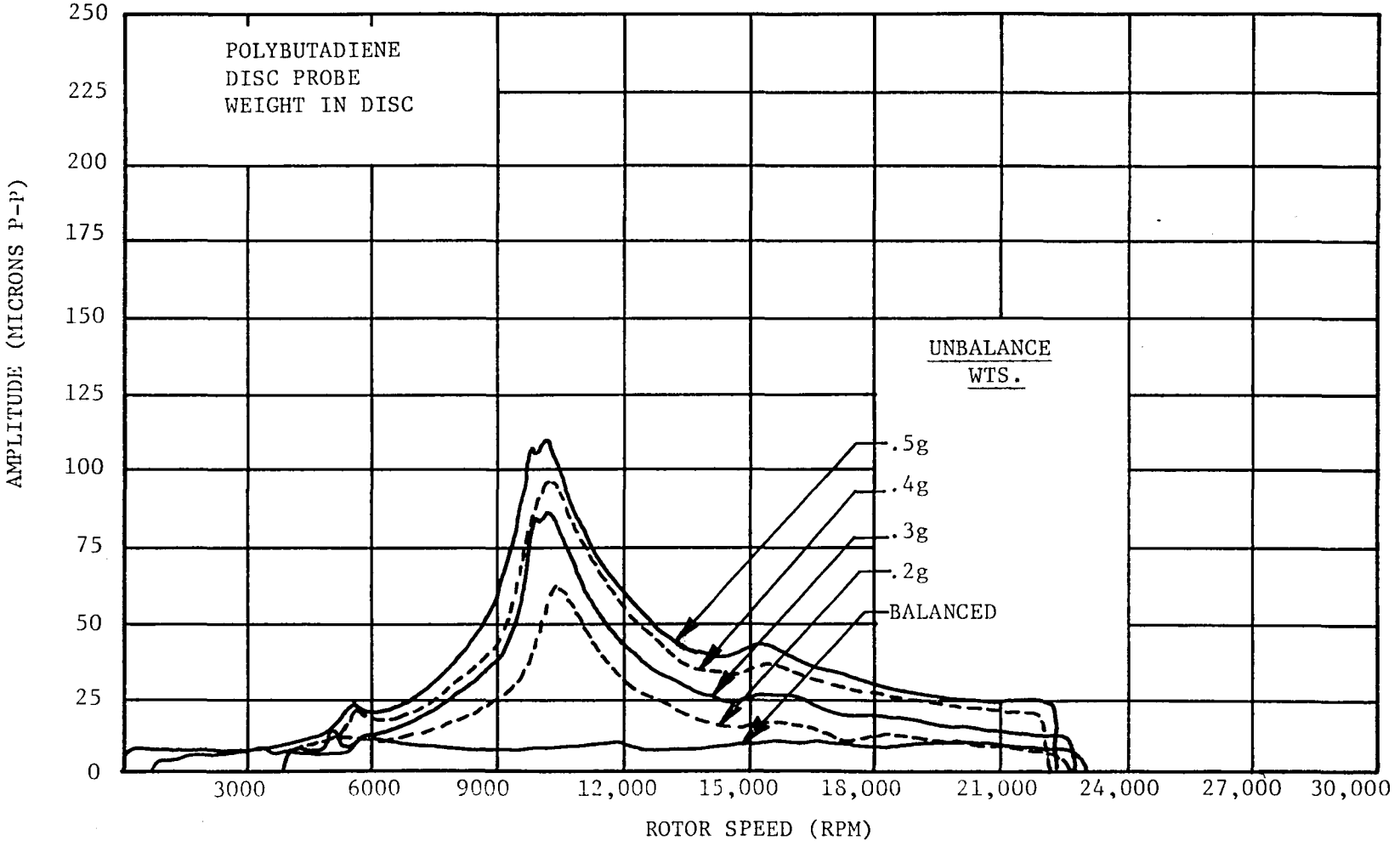

Fig. 58 Effect of Disc Unbalance With Polybutadiene Dampers

791196

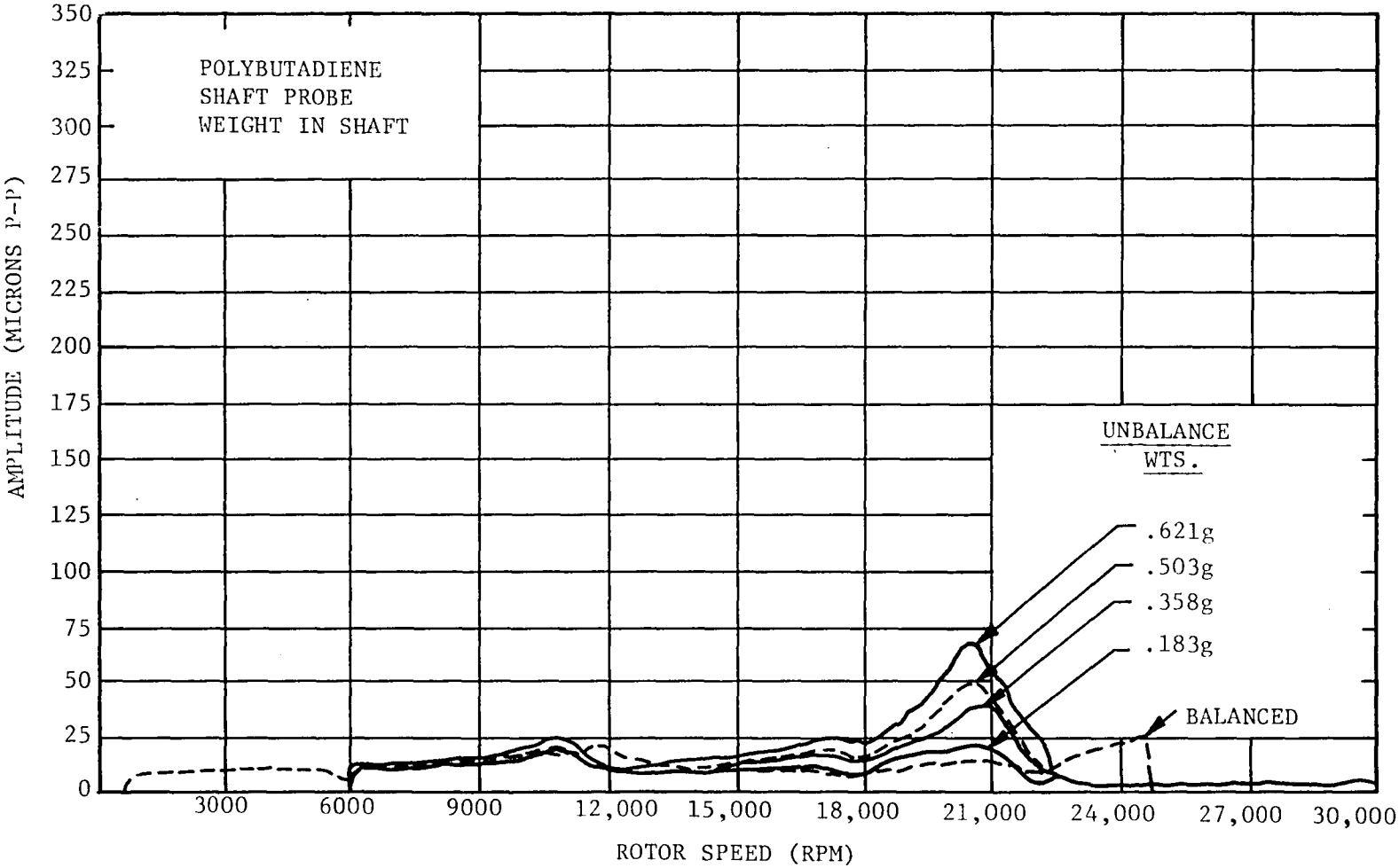

Fig. 59 Effect of Shaft Unbalance With Polybutadiene Dampers

791197

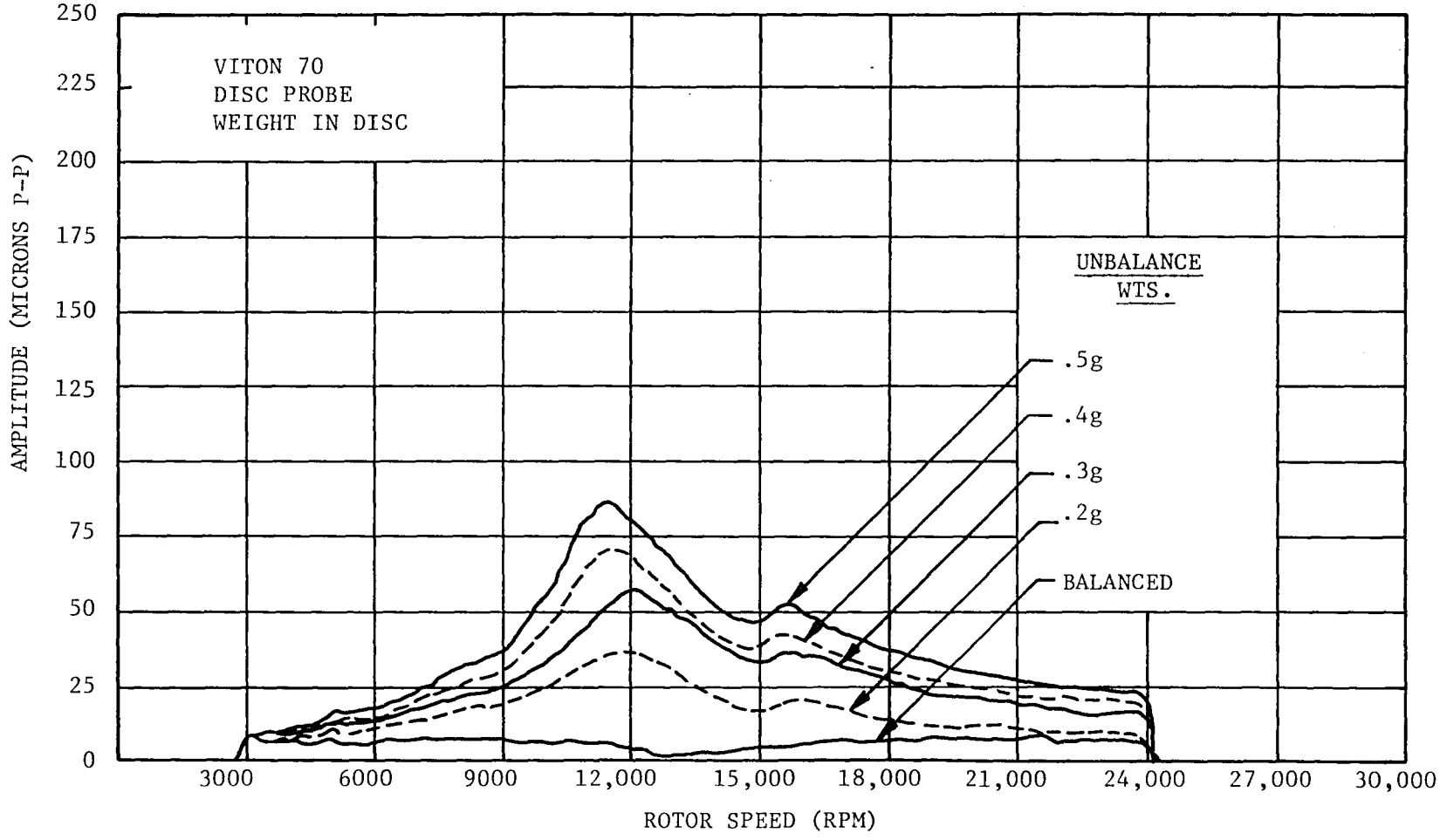

Fig. 60 Effect of Disc Unbalance With Viton Dampers

791198

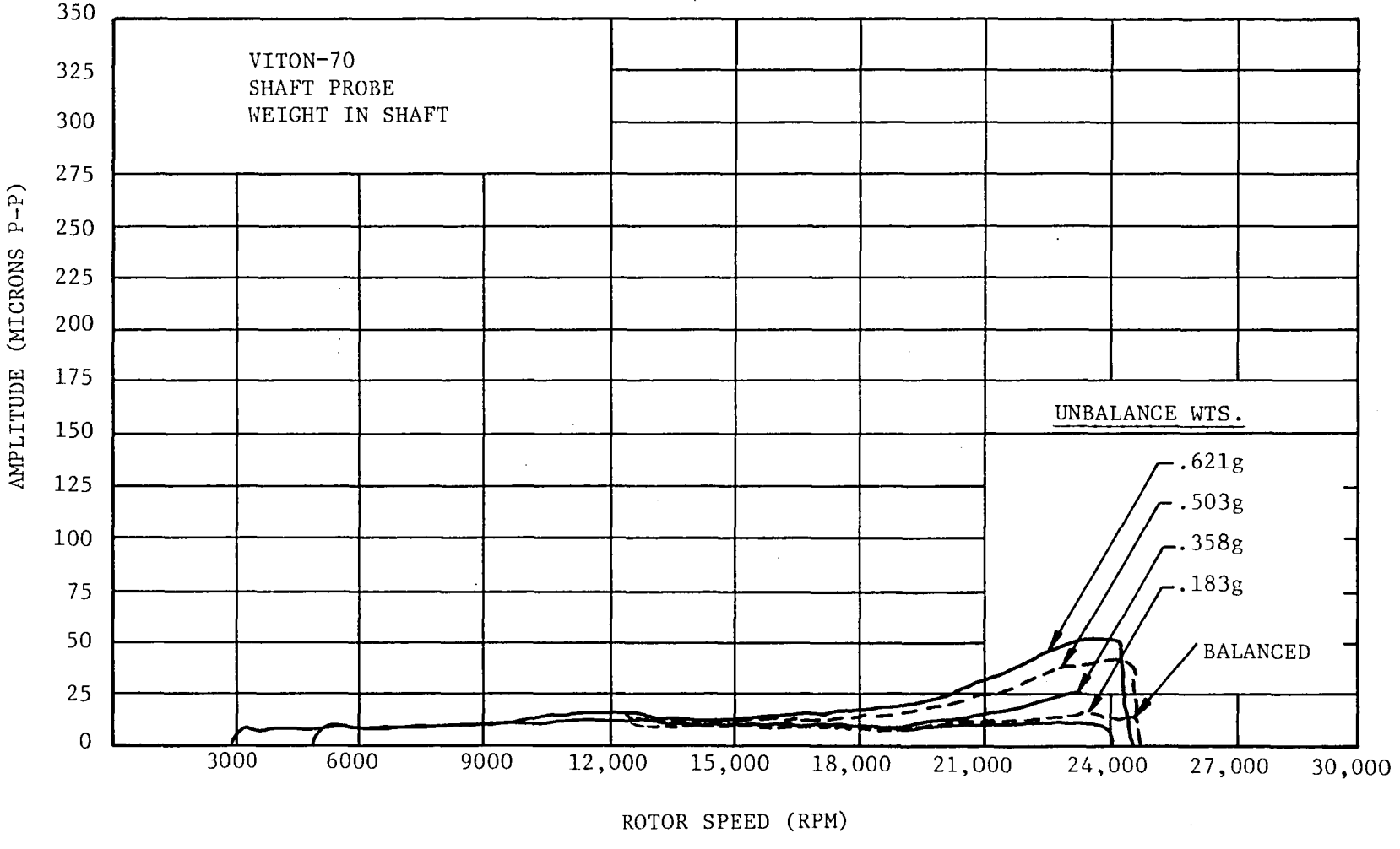

Fig. 61 Effect of Shaft Unbalance With Viton Dampers

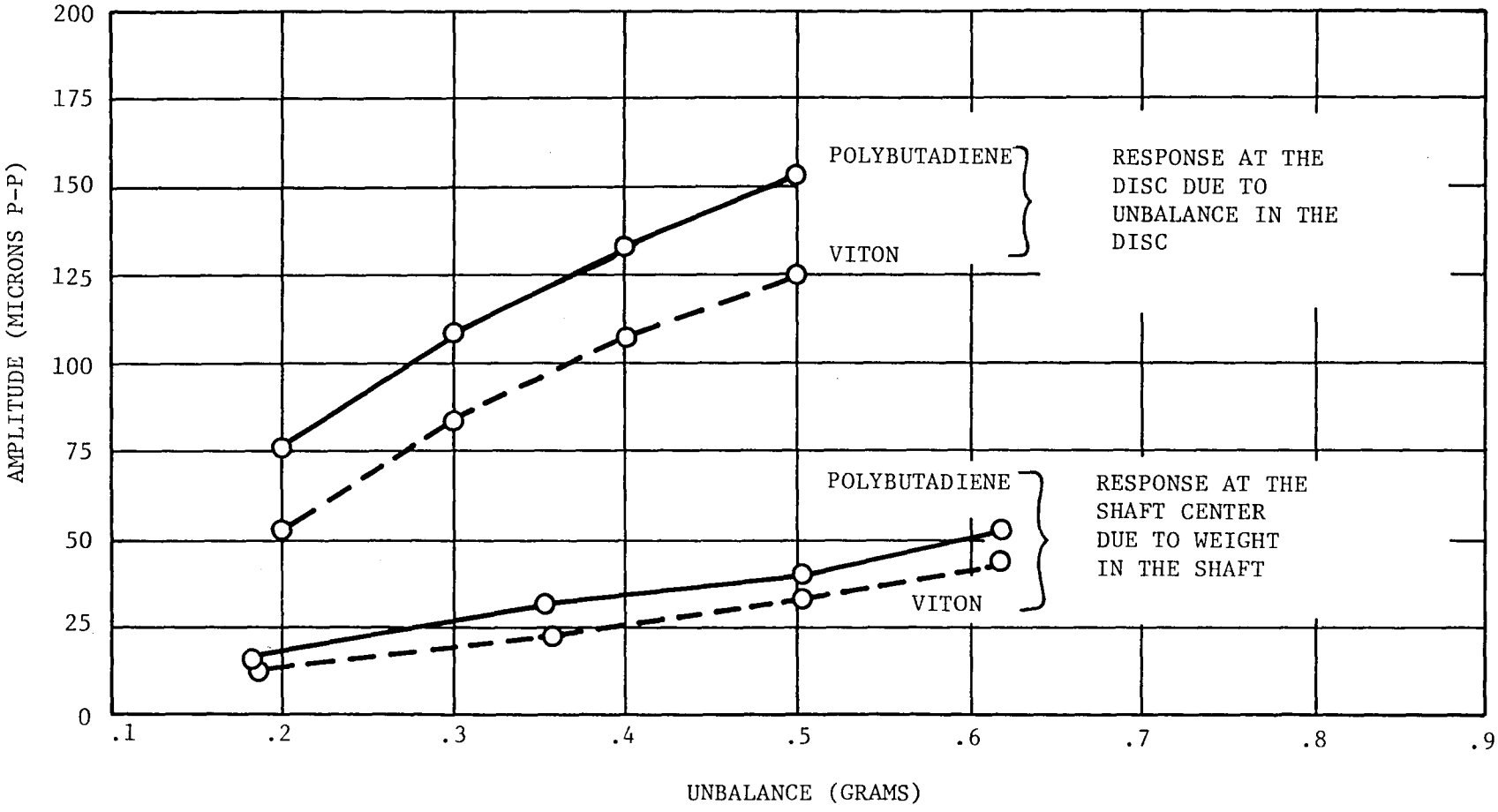

Fig. 62 Sensitivity of Test Rig to Unbalance

791200

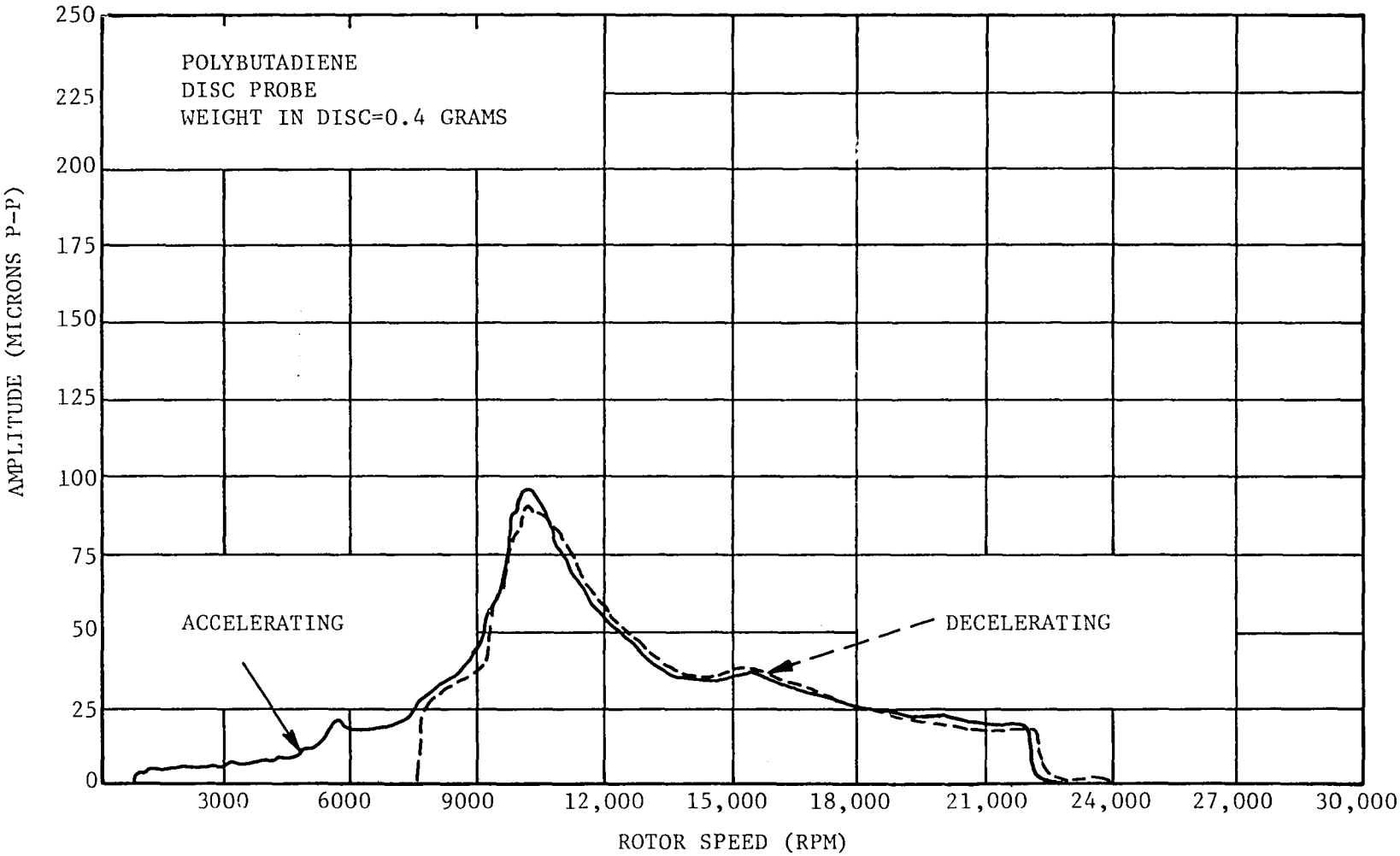

Fig. 63 Repeatability of Elastomer Mounted Rotor Running To and From Speed

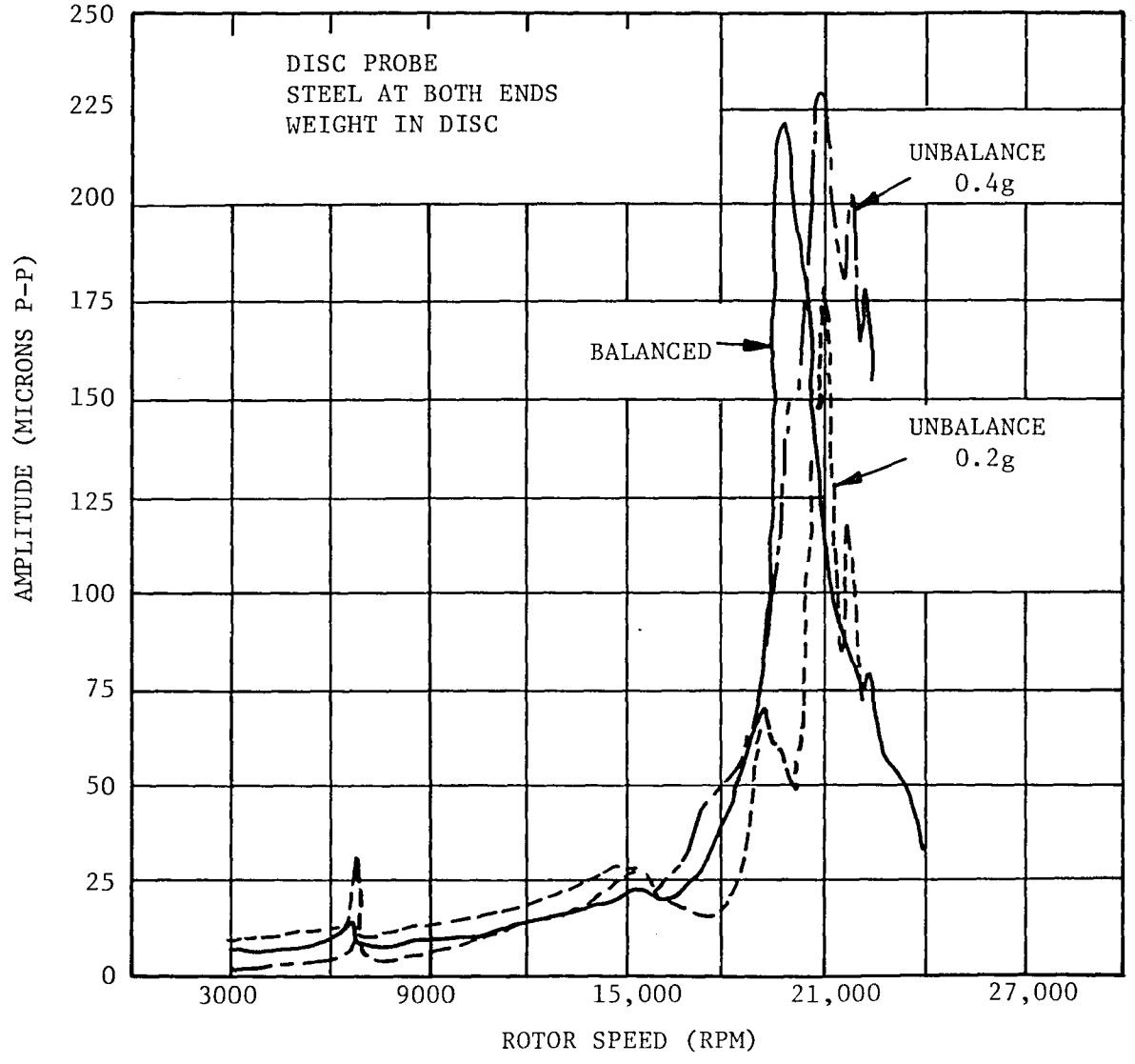

Fig. 64 Response at the Disc to Disc Unbalance for the Hard-Mounted Rotor

791205

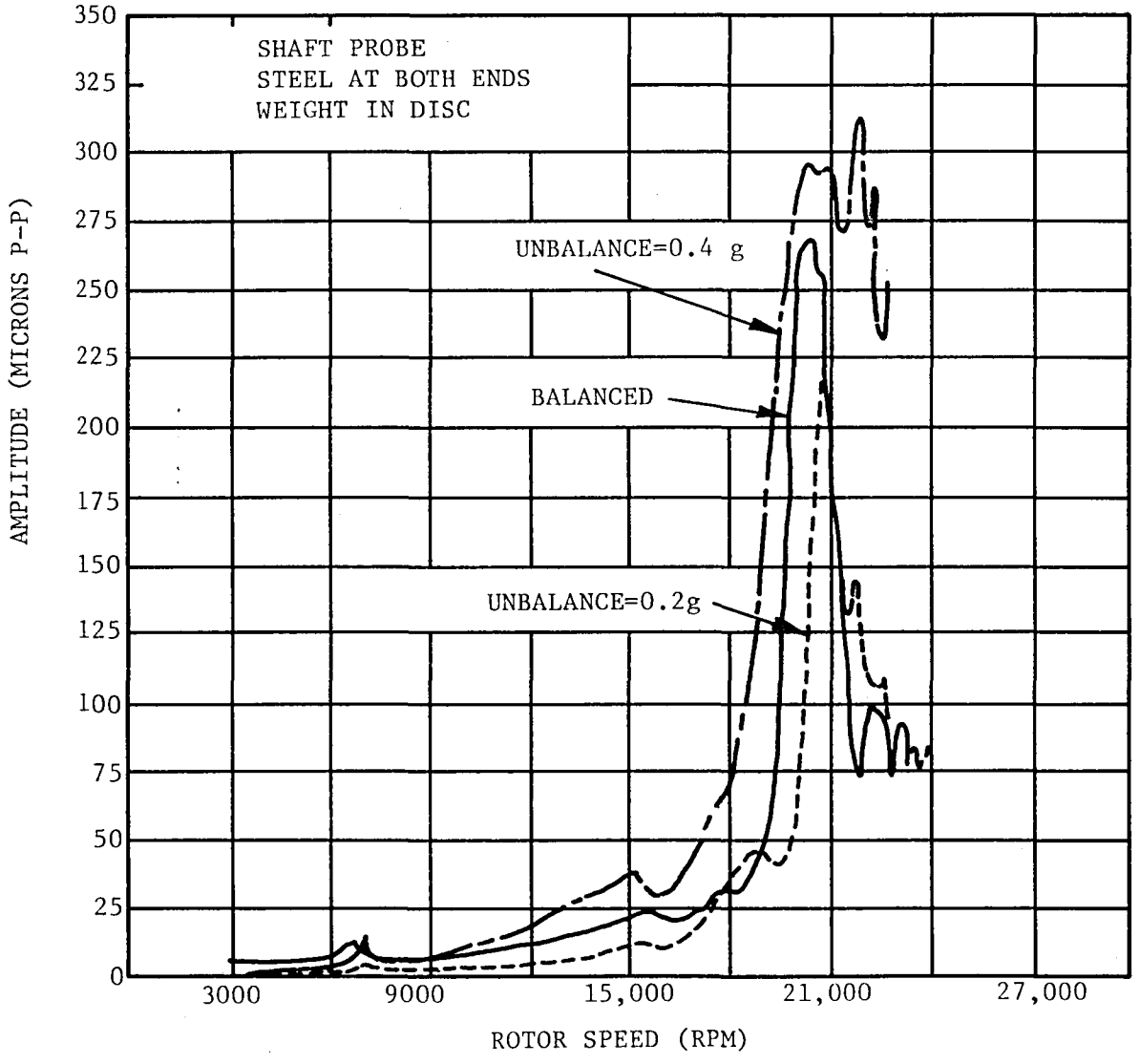

Fig. 65 Response at the Shaft to Disc Unbalance, for the Hard-Mounted Rotor

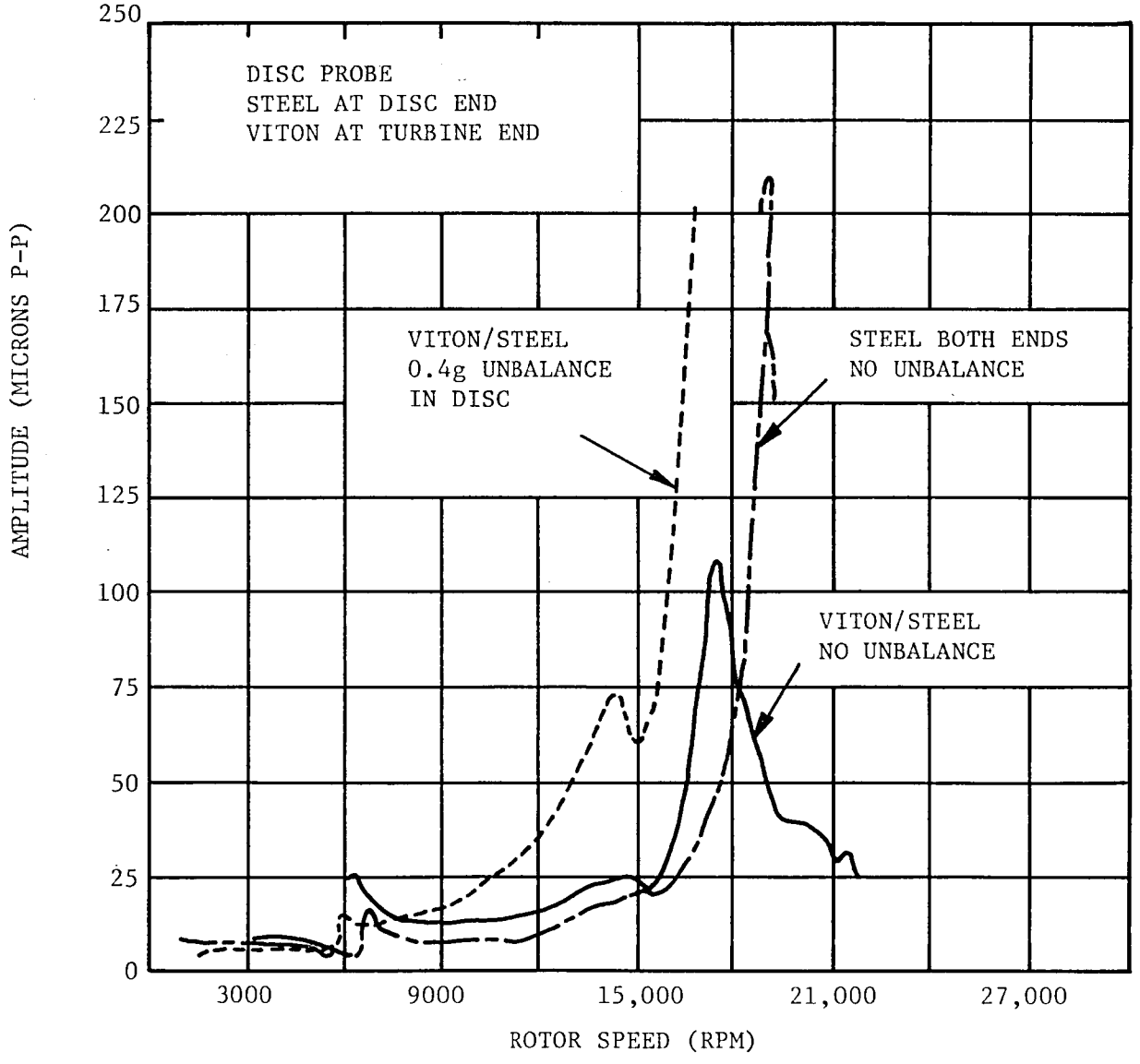

791203

Fig. 66 Effect of Using Viton Damper Cartridges at the Turbine End Only

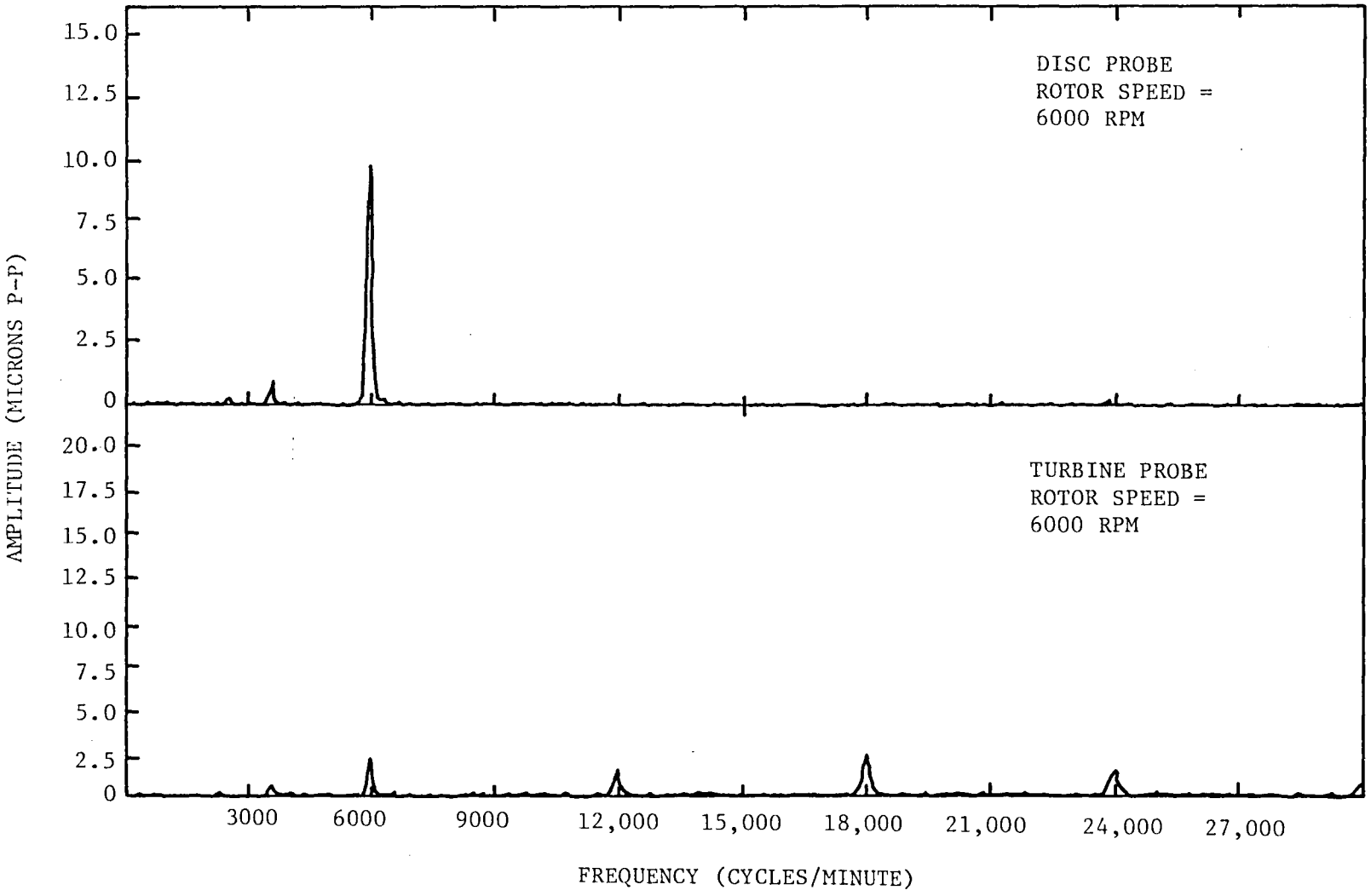

Fig. 67 Spectrum Analyses of Output From Disc and Turbine Probes

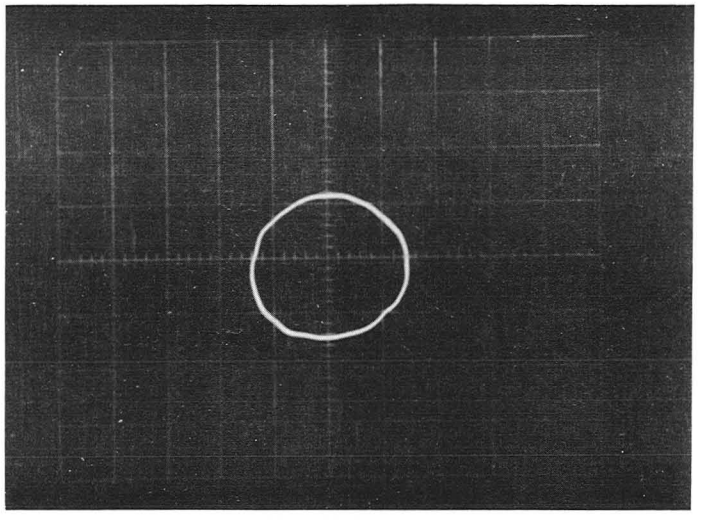

a) Below First Critical
9000 rpm

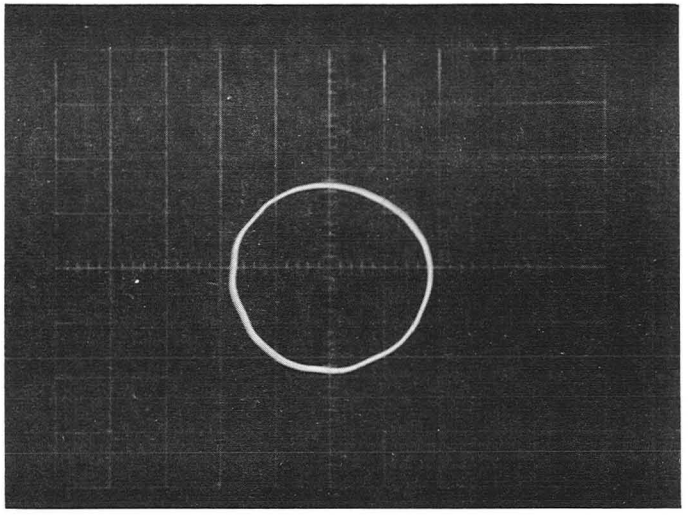

c) Above First Critical
12,000 rpm

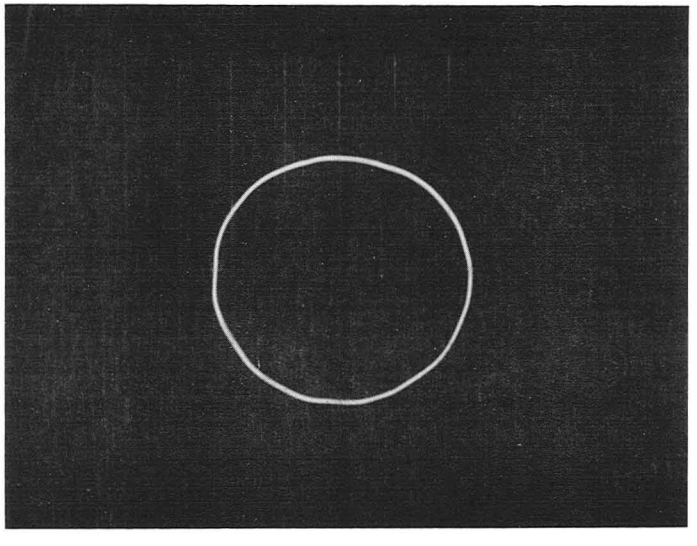

b) At First Critical 10,950 rpm

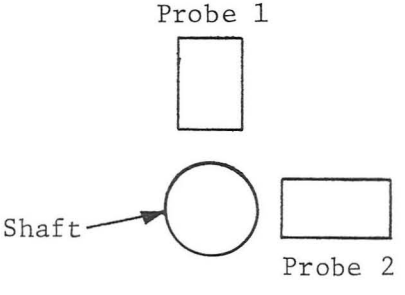

Fig. 68 Disc Orbit Photos Through First Critical With Unbalance in Disc

MTI-18740

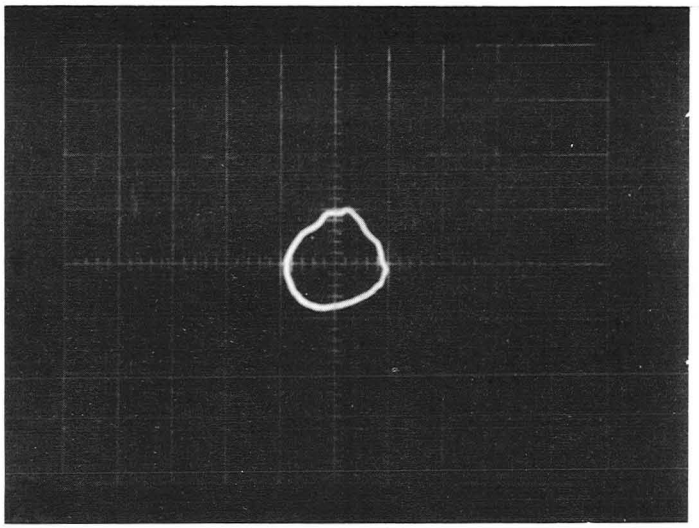

a) Below Second Critical
21,000 rpm

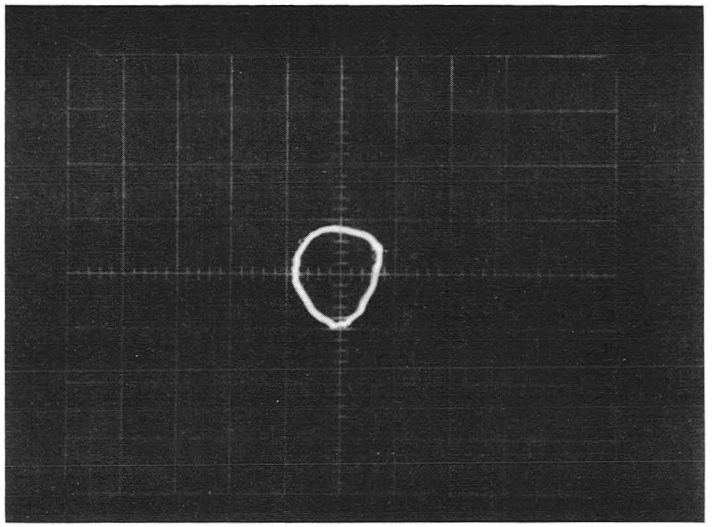

c) Above Second Critical
26,500 rpm

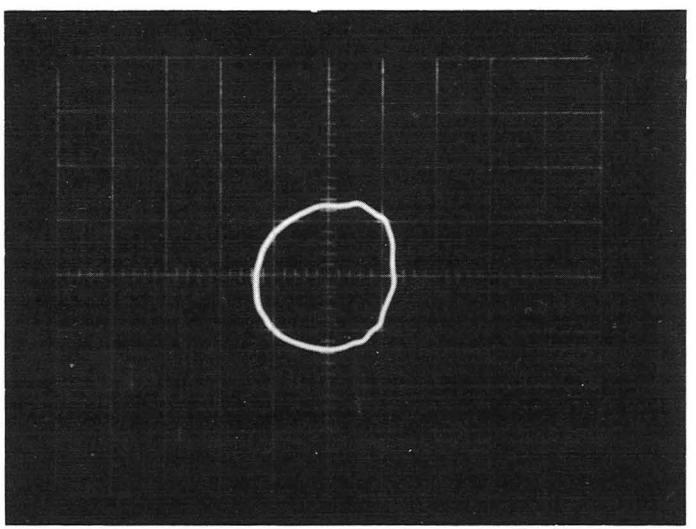

b) At Second Critical
23,000 rpm

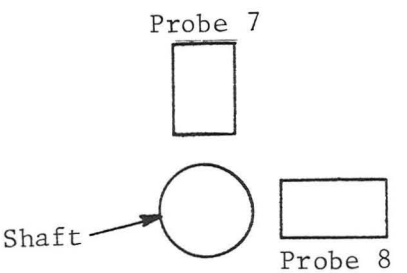

Fig. 69 Shaft Orbit Photos Through Second Critical With Unbalance in Shaft

MTI-18741

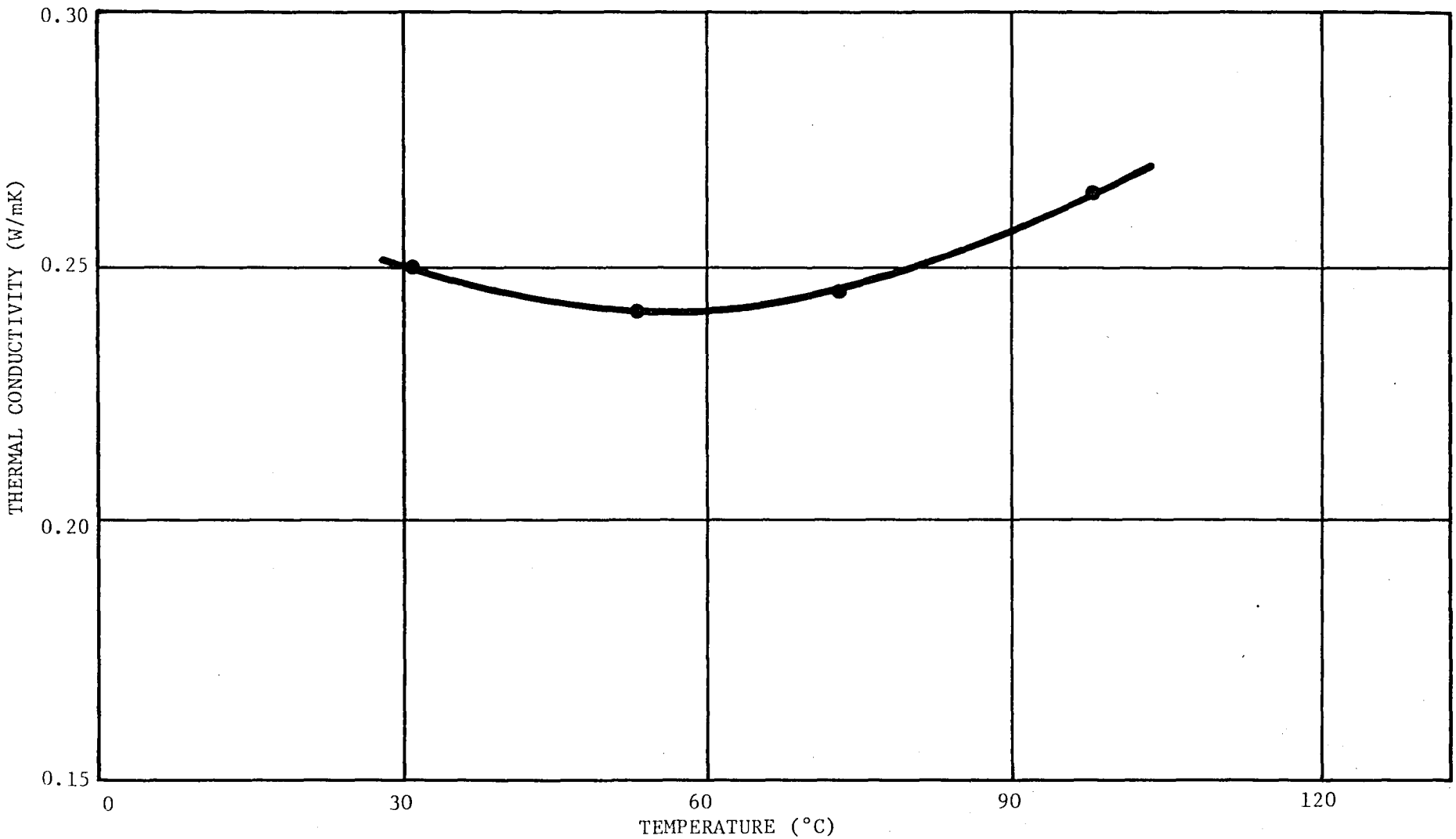

Fig. A-1 Thermal Conductivity Versus Temperature
Nicholls NEX 156G

791219

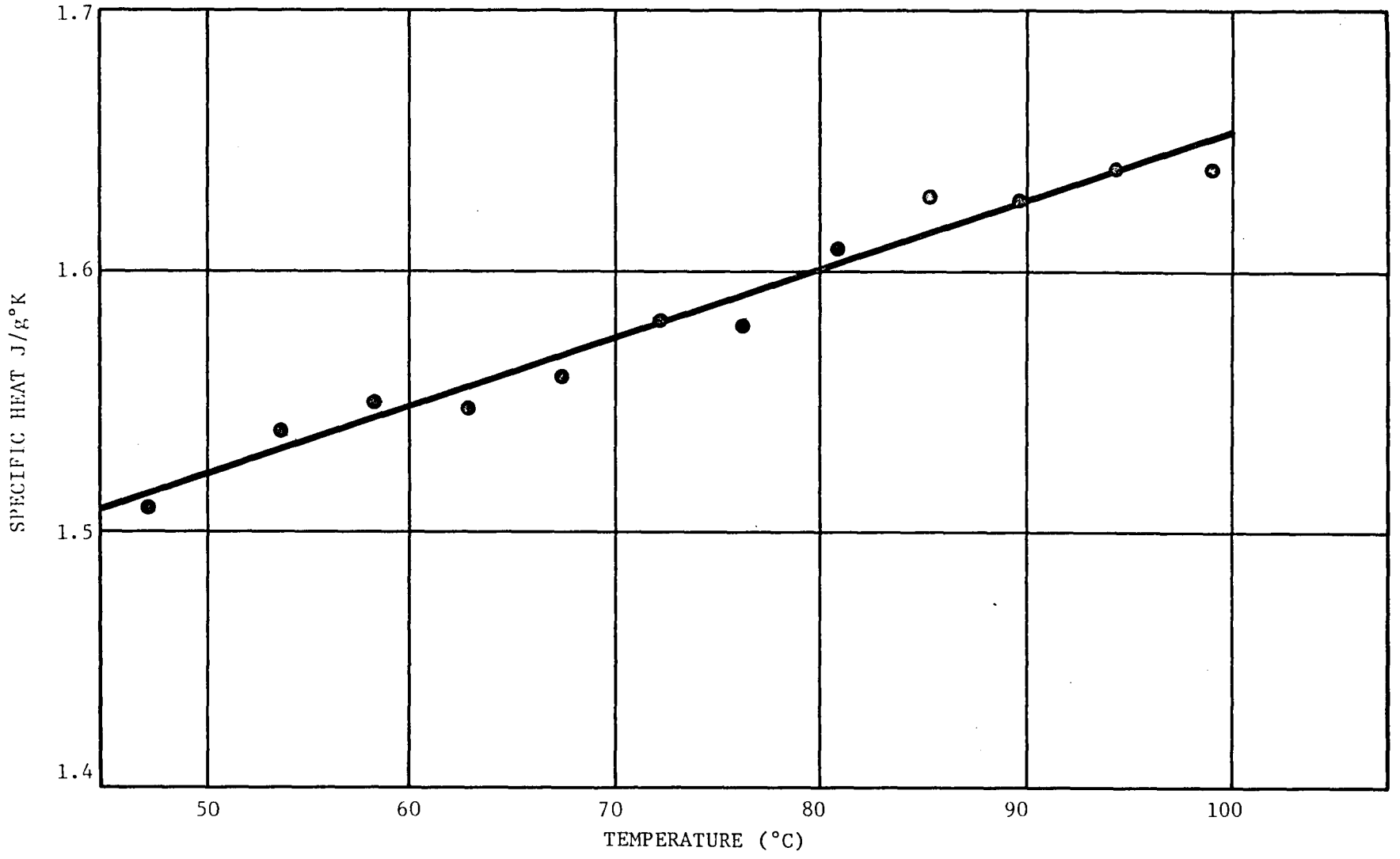

Fig. A-2 Specific Heat Versus Temperature
Nicholls NEX 156G D.S.C.

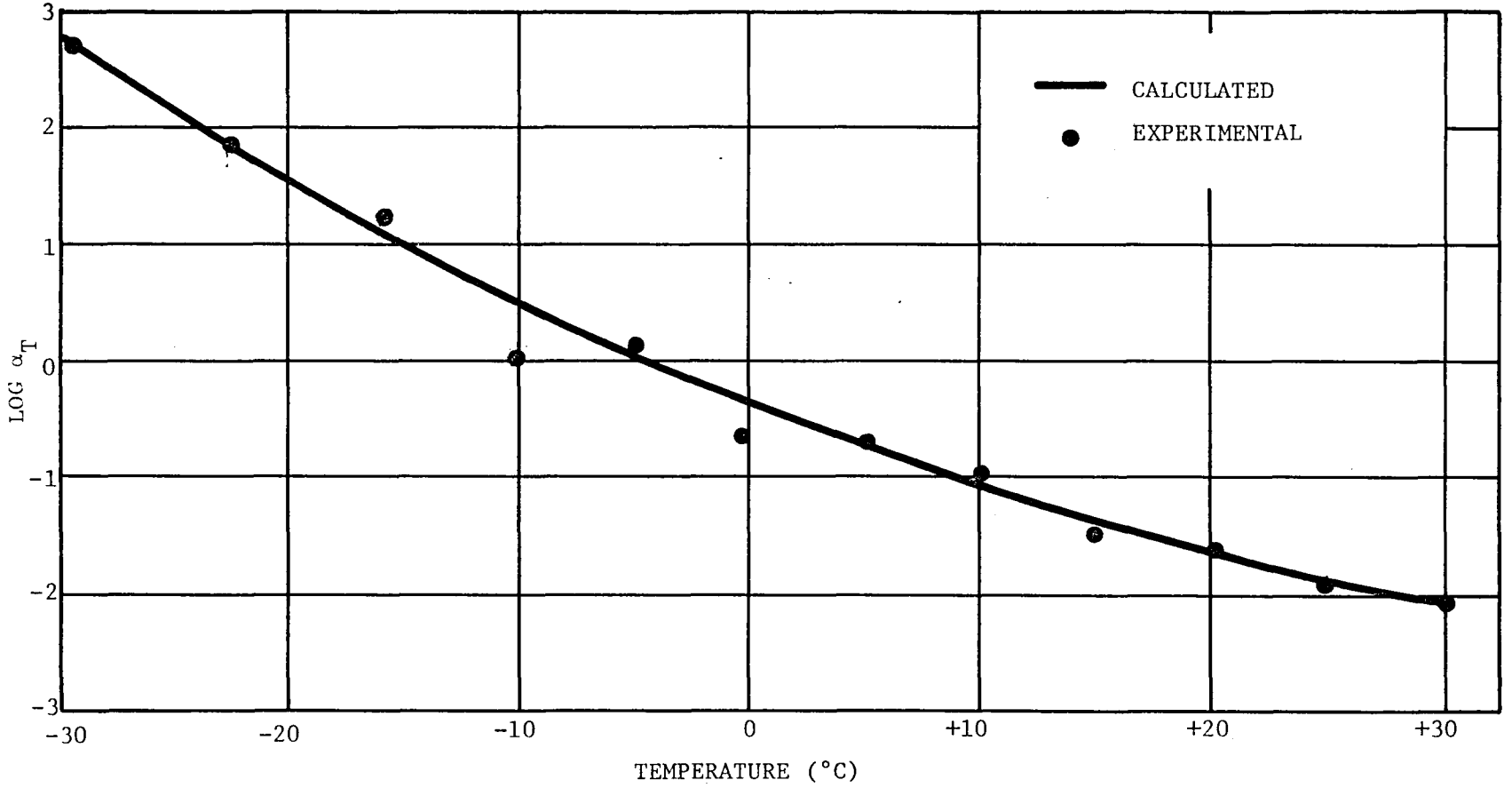

Fig. A-3 Log α_T Versus Temperature
Nicholls NEX 156G

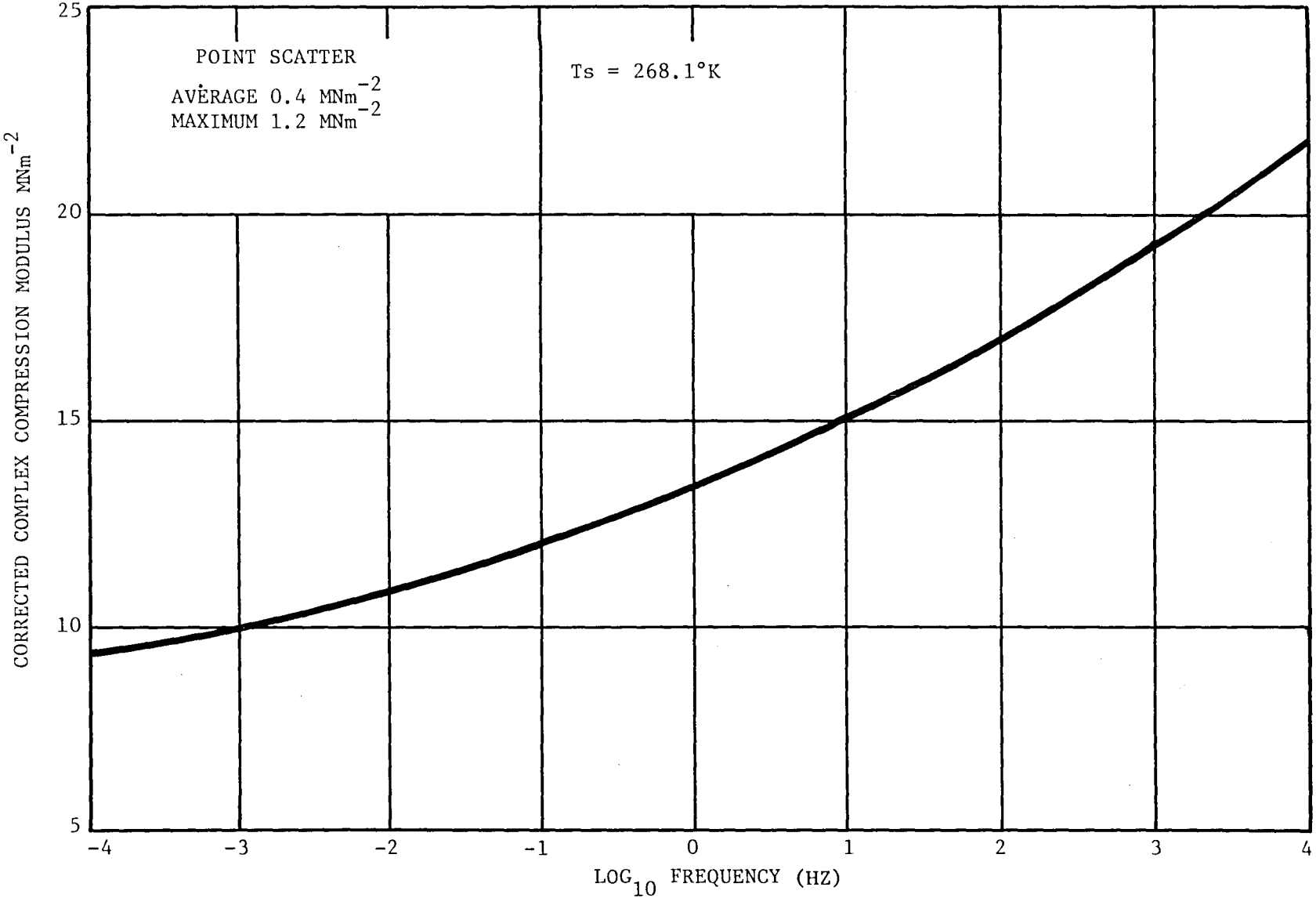

Fig. A-4 Corrected Complex Compression Modulus Versus Frequency. Master Curve, Nicholls NEX 156G

791222

DISTRIBUTION LIST
CR-159552 NAS3-18546

Recipient	Number of Copies
NASA/Lewis Research Center 21000 Brookpark Rd. Cleveland, OH 44135	
Attn: R. E. Cunningham, MS 6-1	(15 + reproducible)
M. J. Hartmann, MS 5-3	1
L. P. Ludwig, MS 23-2	1
W. L. Stewart, MS 3-5	1
D. Drier, MS 21-4	1
J. E. Dilley, MS 500-305	2
N. Musial, MS 500-311	1
Report Control Office, MS 5-5	1
Library, MS 60-3	2
Reliability & Quality Assurance Office, MS 500-211	1
Technology Utilization Office, MS 7-3	1
Resources Management Office, MS 3-10	1
NASA Scientific and Technical Information Facility P. O. Box 8757 Balt/Wash International Airport Maryland 21240	
Attn: Accessioning Department	10
NASA Headquarters Washington, DC 20546	
Attn: RTP-3/D. J. Miller	1
NASA/Ames Research Center Moffett Field, CA 94035	
Attn: Library	1
NASA/Hugh L. Dryden Research Center P. O. Box 273 Edwards, CA 93523	
Attn: Library	1
NASA/Goddard Space Flight Center Greenbelt, MD 20771	
Attn: Library	1
Jet Propulsion Laboratory 4800 Oak Grove Drive Pasadena, CA 91103	
Attn: Library	1

Recipient	No. of Copies
NASA/Langley Research Center Langley Station Hampton, VA 23365	
Attn: Library	1
NASA/Lyndon B. Johnson Space Center Houston, TX 77058	
Attn: Library	1
NASA/Marshall Space Flight Center Marshall Space Flight Center, AL 35812	
Attn: Library	1
NASA National Space Technology Laboratories NSTL Station, MS 39529	1
Aerospace Corporation P. O. Box 95085 Los Angeles, CA 91745	
Attn: Library	1
AiResearch Manufacturing Co. Phoenix, AZ 85034	
Attn: Library	1
AiResearch Manufacturing Co. 9851 Sepulveda Blvd. Los Angeles, CA 90009	
Attn: Library	1
Air Force Aero Propulsion Laboratory Wright Patterson AFB, OH 45433	1
Attn: H. F. Jones R. Dayton	
Battelle Columbus Labs 505 King Avenue Columbus, OH 43201	
Attn: Library	1
Bendix Research Labs Division Detroit, MI 48232	
Attn: Library	1
Boeing Co. Aerospace Division P. O. Box 3707 Seattle, WA 98124	
Attn: Library	1

Recipient	No. of Copies
Boeing Company Vertol Division P. O. Box 16858 Philadelphia, PA 19142 Attn: Library	1
Continental Aviation and Engineering Corp. 12700 Kercheval Ave. Detroit, MI 48215 Attn: Library	1
Curtiss Wright Corporation Wright Aero Division Main & Passaic Streets Woodridge, NJ 07075 Attn: Library	1
Fafnir Bearing Co. 37 Booth St. New Britain, CT 06050 Attn: R. J. Matt	1
General Electric Company Aircraft Engine Technical Division Bearings, Fuels and Lubricants Evendale, OH 45215 Attn: E. N. Bamberger	1
General Electric Co. Gas Turbine Division Bldg. 53-330 Schenectady, NY 12345 Attn: C. C. Moore	1
General Electric Company Mechanical Technology Laboratory R&D Center Schenectady, NY 12301 Attn: Library	1
General Motors Corporation Allison Division Indianapolis, IN 46206 Attn: Library	1

Recipient	No. of Copies
Hughes Aircraft Corporation Centinda & Teale Avenue Culver City, CA 90230 Attn: Library	1
Industrial Tectonics, Inc. 18301 Santa Fe Avenue Compton, CA 90024 Attn: H. Signer	1
Institute for Defense Analyses 400 Army-Navy Drive Arlington, VA 22202 Attn: Library	1
Lockheed Missiles & Space Co. P. O. Box 504 Sunnyvale, CA 94088 Attn: Library	1
Massachusetts Institute of Technology Cambridge, MA 02139 Attn: Library	1
Mechanical Technology, Inc. 968 Albany-Shaker Rd. Latham, NY 12110 Attn: Library	1
National Science Foundation Engineering Division 1800 G Street, NW Washington, DC 20540 Attn: Library	1
Naval Air Systems Command Washington, DC 20360 Attn: Library	1
Naval Ship Engineering Center Washington, DC 20360 Attn: W. C. Lindstrom (NSC 613D4B)	1
David W. Taylor Naval Ship R&D Center Annapolis Division Annapolis, MD 21402 Attn: Library	1

Recipient	No of Copies
Naval Ship Systems Command Washington, DC 20360 Attn: J. E. Dray SNHIP 6148	1
Rockwell International 6633 Canoga Ave. Canoga Park, CA 91304 Attn: Library	1
Office of Naval Research Arlington, VA 22217 Sttn: S. W. Doroff (Code 438)	1
SKF Industries, Inc. Engineering & Research Ctr. 1100 First Ave. King of Prussia, PA 19406 Attn: T. Tallian L. Sibley	1 1
Sundstrand, Denver 2480 W. 70 Avenue Denver, CO 80221 Attn: Library	1
TRW, Inc. 23555 Euclid Avenue Cleveland, OH 44117 Attn: Library	1
TRW Marlin Rockwell Division 402 Chandler St. Jamestown, NY 14701 Attn: Library	1
U. S. Army Engineering R&D Labs Gas Turbine Test Facility Fort Belvoir, VA 22060 Attn: W. Crim	1
Pratt & Whitney Aircraft Division 400 Main St. East Hartford, CT 06108 Attn: R. Shevchenko P. Brown Dr. F. C.Hsing Library	1 1 1 1

Recipient	No. of Copies
United Aircraft Corporation Sikorsky Aircraft Division Stratford, CT 06497 Attn: L. Burroughs	1
U. S. Army Research & Technology Labs Applied Technology Laboratory Fort Eustis, VA 23604 Attn: Library	1
Rensselaer Polytechnic Institute Mechanics Division Troy, NY 12181 Attn: F. F. Ling	1
Southwest Research Institute P. O. Drawer 28510 San Antonio, TX 78284 Attn: Library	1
Tribon Bearing Co. Division of Pure Carbon Co. 5581 W. 164th St. Brookpark, OH 44132 Attn: D. W. Moyer	1
Materials Science Corp. Blue Bell Office Campus Merion Towel Bldg. Blue Bell, PA 19422 Attn: Library	1
Shaker Research Corp. Northway 10 Executive Park Ballston Lake, NY 12019 Attn: Dr. C. H. T. Pan	1
General Electric Co. P. O. Box 8, Malta Site Schenectady, NY 12301 Attn: Dr. A. J. Martenson	1
Northwestern University Department of Mechanical Engineering & Astronautical Science Evanston, IL 60201 Attn: Dr. R. Burton Dr. H. S. Cheng	1 1

Recipient	No. of Copies
Thiokol Corporation P. O. Box 524 Brigham City, UT 84302 Attn: Bliss Law, MS 308	1
Teledyne CAE, Turbine Engines 1330 Laskey Rd. Toledo, OH 43697 Attn: R. Beck	1
Ingersoll-Rand Corp. Phillipsburg, NJ 08865 Attn: R. G. Kirk	1
Deposits & Composites, Inc. 318 Victory Dr. Herndon Industrial Park Herndon, VA 22070 Attn: R. E. Engdohl	1
Williams Research Corporation 2280 W. Maple Rd. Walled Lake, MI 48088 Attn: G. Rourk	1
University of Virginia School of Engineering & Applied Science Charlottesville, VA 22901 Attn: Dr. E. J. Gunter	1
Chalk River Nuclear Labs Chalk, Ontario, Canada KOJIJO Attn: Dr. R. Metcalf	1